

QUANTUM TRAJECTORY THEORY OF OPEN
CAVITY-QED SYSTEMS WITH A TIME DELAYED
COHERENT OPTICAL FEEDBACK

by

GAVIN CROWDER

A thesis submitted to the
Department of Physics, Engineering Physics & Astronomy
in conformity with the requirements for
the degree of Master of Science

Queen's University
Kingston, Ontario, Canada
May 2020

Copyright © Gavin Crowder, 2020

Abstract

The emergence of integrated (or solid state) photonic systems, including quantum dots, waveguides, and cavities, has provided a base to harness quantum optic phenomena for use in current and future quantum technologies. These systems also provide opportunities for exploring fundamentally new regimes in quantum optics. In order to fully realize the potential of these systems, many figures of merit need to be improved, for example by increasing the stability and coherent lifetimes of these systems. Following the notable improvements using measurement-based feedback, time-delayed coherent optical feedback has been proposed as one such method of stabilizing and improving these systems. Furthermore, modelling coherent feedback itself presents an interesting fundamental problem due to its non-Markovian nature. In this thesis, we use quantum trajectory (QT) theory to derive two models for simulating cavity quantum electrodynamic (cavity-QED) systems with time-delayed coherent feedback. First, an explanation of QT theory is given and the related time discretized waveguide (TDW) model is derived. Next we present a model for feedback using the frequency modes of the waveguide and results are presented in the “one photon in the loop” approximation. We demonstrate how the photon lifetime can be improved in typical cavity-QED with coherent feedback and we explore some nonlinear effects. We then expand the system to allow for two photons in the feedback loop which requires us to use the TDW model. Lastly, this new approach is used to model two two-level systems coupled via a waveguide and connected to a feedback loop. These findings have implications on improving quantum optic systems by creating a new degree of control, as well as for modelling non-Markovian features in quantum optics.

Statement of Co-Authorship

This thesis contains a published manuscript including theoretical and computational results, produced by myself and written with editorial feedback from Dr. Stephen Hughes and Dr. Howard Carmichael. In addition, Chapter 3 contains work that built upon the initial theory of Dr. Carmichael, and the time-domain modelling of the feedback loops in Chapter 4 was an implementation of the recent method described in S. J. Whalen 2019. All computer codes were written by myself.

Acknowledgements

First of all I would like to thank my supervisor, Dr. Stephen Hughes, for introducing me to the field of quantum optics, and setting me on the path that I have taken. Throughout my master's, his advice and feedback have helped me grow as a physicist and as a professional, and I am very thankful for the time he has spent guiding me.

I would also like to thank Dr. Howard Carmichael for passing on his notes to us about the problem of coherent feedback, which started this entire line of research. Furthermore, our many discussions on this topic were very helpful for further refining the model, and placing it on a strong analytic foundation.

Lastly, I would like to thank my friends and family for their support throughout my master's. Especially to my girlfriend, Karen, and my dog, Argo, for dealing with me while I paced around the house, muttering to myself about quantum trajectories and proper conditioning in the presence of feedback.

This work was funded by the Natural Sciences and Engineering Research Council of Canada (NSERC).

Refereed Publications and Presentations

Published Journal Paper:

- G. Crowder, H. Carmichael, and S. Hughes, “Quantum trajectory theory of few-photon cavity-QED systems with a time-delayed coherent feedback”, [Phys. Rev. A **101**, 023807 \(2020\)](#) [**Chapter 3**].

Conference Contributions:

- G. Crowder and S. Hughes, “Quantum Trajectory Theory Applied to Cavity-QED Systems with Coherent Optical Feedback”, Talk at Photonics North 2018, Montreal, Quebec, Canada.
- G. Crowder, H. Carmichael, and S. Hughes, “Quantum Trajectory Theory of Few Photon Cavity-QED Systems with Coherent Feedback”, Poster session at the Rochester Conference on Coherence and Quantum Optics, 2019, Rochester, New York, USA.

Contents

Abstract	i
Statement of Co-Authorship	ii
Acknowledgements	iii
Refereed Publications and Presentations	iv
Contents	v
List of Figures	vii
Common Acronyms	0
Chapter 1: Introduction	1
1.1 Photonic Systems	3
1.2 Time-Delayed Feedback as a Non-Markovian Dynamic	5
1.3 Layout of the Thesis	9
Chapter 2: Theory and Methods	11
2.1 Evolving Open Quantum Systems with Master Equations	11
2.2 Quantum Trajectory Theory	16
2.2.1 Example System Dynamics Solved Using QT Theory	20
2.2.2 Equivalence of QT Theory to the Master Equation	22
2.2.3 Generalized Conditioning of the Quantum Trajectories	23
2.3 Time-Discretized Waveguide Model	25
2.4 Computational Methods	30
Chapter 3: Quantum trajectory theory of few photon cavity-QED systems with a time-delayed coherent feedback	32
3.1 Introduction	33
3.2 Model and Hamiltonian	36
3.3 Quantum Trajectory Theory	38
3.3.1 Decoupling $R_{\mu,n}$ in the $N = 1$ Case	41

3.3.2	Solving the Dynamical Evolution Equations in the $N = 1$ Case	42
3.3.3	Calculating the Probability for a Quantum Jump	43
3.3.4	Applying the Quantum Jump Operator	45
3.3.5	Conditioning in the Presence of Feedback	47
3.4	Numerical Implementation	49
3.5	Results	50
3.5.1	Replication of Previous Results and Quantum Trajectory Insights	50
3.5.2	Investigation of the Effect of the Feedback Loop on Excitation Trapping	54
3.5.3	Nonlinear Cavity-QED Effects	56
3.6	Conclusions	59
3.7	Acknowledgements	60
3.8	Appendices	60
3.8.1	Appendix A: Deriving the Feedback Coupling Term	60
3.8.2	Appendix B: Deriving (3.11)	61
3.8.3	Appendix C: Deriving (3.14) and (3.15)	63
3.8.4	Appendix D: Optimized Technique for Simulating Quantum Trajectories with No Drive	65
Chapter 4:	Extending Beyond One Photon in the Feedback Loop	67
4.1	QT Theory with Two Photons in the Loop	67
4.2	TDW Model with a Single TLS	72
4.2.1	Results in the One Photon in the Loop Limit	74
4.2.2	Results in the Two Photon in the Loop Limit	79
4.3	Computational Performance of the Models	84
Chapter 5:	Coupling Two TLS's via a Waveguide with Coherent Feedback	87
5.1	Embedding Two TLS's in the Feedback Loop Using the TDW Model	87
5.2	Results	91
5.2.1	System Dynamics Without a Feedback Loop	91
5.2.2	Introducing Feedback to the System	94
Chapter 6:	Conclusions and Recommendations	100
6.1	Summary and Conclusions	100
6.2	Suggestions for Future Work	101
Bibliography		102

List of Figures

1.1	Examples of experimental realizations of photonic waveguides.	4
1.2	An experimental realization of a qubit gate using quantum dots. . . .	5
1.3	Schematic example implementations of coherent time-delayed feedback. .	6
2.1	Model of an open quantum system.	12
2.2	Schematic of a QT time step.	18
2.3	Example system dynamics highlighting the features of QT theory. . . .	21
2.4	Schematic of the TDW model for an open waveguide with an integrated QO system.	29
3.1	Flowchart of a time step in the QT algorithm.	36
3.2	Schematic of the cavity-TLS coupled to the feedback waveguide. . . .	37
3.3	Vacuum Rabi oscillations and decaying Rabi oscillations without feedback.	51
3.4	Using feedback to produce population trapping or enhanced emission. . . .	52
3.5	Sample QTs and their average for two population trapping examples. . . .	52
3.6	Population dynamics for a very short and a very long delay time. . . .	53
3.7	Effects of varying the phase of the returning feedback on the system population at multiple loop lengths.	55
3.8	Population dynamics of the system at selected loop length and phases. . . .	56
3.9	Effect of varying the loop length of the system on the system population. . . .	57
3.10	Cavity photoluminescence spectrum with and without feedback.	58
3.11	The effect of properly conditioning the TLS population when feedback is present.	59
4.1	Schematic of the TDW Model with a TLS embedded in the feedback loop.	73
4.2	Dynamics of an excited, undriven TLS coupled to the feedback loop. . . .	75
4.3	Using feedback to stabilize TLS Rabi oscillations or enhance their decoherence in the one photon in the loop limit.	77
4.4	TLS population dynamics in the two photon in the loop limit using the TDW model.	80
4.5	Enhancement of the cavity photoluminescence spectrum by using a stronger pump in the two photon in the loop limit.	82

4.6	TLS photoluminescence spectrum with and without feedback for the single TLS coupled to a feedback loop setup.	83
5.1	Schematic of the system with two TLS's embedded in the feedback loop using the TDW model.	88
5.2	System dynamics of the undriven two-TLS setup without feedback when one TLS is initially excited and the other is in the ground state.	92
5.3	Examples of sub-radiance and super-radiance for the two-TLS setup.	93
5.4	Population dynamics for the two-TLS setup when feedback is present.	95
5.5	Trapped population for the two-TLS setup when the delay time between TLS's is increased.	96
5.6	Effect of feedback on a sub-radiant state for the two-TLS setup.	97
5.7	Effect of feedback on a super-radiant state for the two-TLS setup.	98
5.8	Population dynamics with and without feedback for an initial biexciton state.	99

Common Acronyms

CW Continuous Wave

DDE Delay Differential Equation

FMR Frequency Mode Representation

ME Master Equation

MPS Matrix Product States

ODE Ordinary Differential Equation

PC Photonic Crystal

QD Quantum Dot

QED Quantum Electrodynamics

QO Quantum Optic

QT Quantum Trajectory

RK Runge-Kutta

TDW Time Discretized Waveguide

TLS Two-Level System

Chapter 1

Introduction

It has been less than 100 years since the first full theory of quantum mechanics was proposed in the early 1920s. Since then, the field has influenced society in countless areas of research and development. Beginning with Planck's work on the quantization of radiation (Planck 1900) and the description of the Hydrogen atom by Bohr (Bohr 1913), quantum mechanics has given physicists a way to model the behaviour of the fundamental components of matter. However, as is typical in mathematical physics, the theory significantly outpaced the experimental capability and predictions were made which could not be verified until decades later. Indeed, one of the first industrial applications of quantum mechanics harnessed the phenomena of stimulated emission first proposed by Einstein 1917. It took 34 more years for the concept to be actualized in the "maser" (Gordon et al. 1954). This was just the early forerunner to the optical maser invented in 1960 (Maiman 1960), better known as the laser, one of the most important inventions in the modern era.

The introduction of lasers quickly had a deep impact in a broad spectrum of scientific fields. Just 19 months after its invention, the first laser was used to destroy a retinal tumor in surgery (M. R. Hogan and H. Hogan 2020). Since then lasers have become essential in fields such as communication (fiber optics and data storage), infrastructure (high energy laser welding and cutting), medicine (precision cuts and imaging), and mapping (LIDAR), to name a few. The entire field of photonics has grown out of the laser's ability to produce a high precision and high energy source of

coherent photons.

In physics research, the laser has allowed for experimentation on the quantum level with techniques such as optical trapping (Ashkin 1970), laser cooling (Chu et al. 1985), and atomic imaging with AFM microscopes (Binnig et al. 1986). With these successful experiments and further improvements in nano-scale engineering, the field of quantum optics has expanded rapidly. Many emerging quantum technologies make use of quantum optic systems to harness the coherence of light for use as a resource in their systems (Streltsov et al. 2017). The recent paper from Arute et al. 2019, researchers with Google, on the supremacy of quantum computing and the paper by Yin et al. 2017, demonstrating entanglement between particles 1200 km away, highlight the billions of dollars being injected into the field by companies and governments. These examples are just the beginning, as more technologies will begin to rely on the fundamental features of quantum mechanics such as superposition and coherence on the platform of photonic systems.

Photonic integrated circuits combine many different nanophotonic systems in order to achieve the goals of these quantum technologies. For example, photonic computing uses the long time coherence of light to form the basis of photonic computing chips (Mohammadi Estakhri et al. 2019). There is also a large demand for single-photon sources (Knill et al. 2001) and entangled-photon sources (Orioux et al. 2017) for use in quantum computing applications and quantum cryptography. Beyond industrial applications of these quantum technologies, they have also been used to research fundamental physics questions. For example, entangled qubits have been used by Zhong et al. 2019 to demonstrate violations of Bell’s inequality, supporting the fundamental theories of quantum mechanics. Furthermore, Mineev et al. 2019 has used nanophotonic systems to reverse the flight of a “quantum jump;” by monitoring the population of an adjacent energy level, they could demonstrably prevent a quantum jump from completing. However, in order for these quantum technologies to be fully realized, there is still much work to do in improving the stability and coherent lifetime of current photonic systems. Quantum feedback, coherently returning system output via an optical feedback loop after a time delay, has been proposed as a possible

avenue for improving these systems (Lloyd 2000; Hein, Schulze, et al. 2014; Droenner et al. 2019).

In this thesis, we present theoretical techniques to investigate the effects of time-delayed coherent feedback on quantum optical systems. By introducing a time-delayed feedback, the behaviour of these systems can be more precisely controlled and allow for stability far beyond the dynamics of the system without feedback. Specifically, this thesis employs quantum trajectory theory to model quantum two-level systems and optical cavities coupled to waveguides which are engineered to coherently return the output of these systems. The response of the coupled systems with and without feedback is investigated for multiple setups and parameter spaces.

1.1 Photonic Systems

A photonic system can come in a wide variety of forms; it could be a laser, or a photodetector, or a fibre-optic cable. Anything harnessing the interaction of light emitters with their photonic environments is a photonic system. Thus, we will narrow our focus to photonic waveguides and cavity quantum electrodynamic (cavity-QED) systems.

Photonic waveguides enable the control of the path of photons between different locations on an optical chip because of their ability to propagate photons with negligible loss over long distances. One of the most intriguing systems used to build an integrated waveguide is a photonic crystal. This material system is a periodic dielectric structure which has a band structure designed to either allow or forbid photons in certain frequency ranges (Maka et al. 2003). One such way to build a photonic crystal is to drill holes periodically in a two-dimensional dielectric slab (through electron-beam lithography) which creates a band gap that can prevent the propagation of photons within a certain frequency band. Then, for example, by removing one row of these holes, photons are able to propagate only down this row and a so-called “W1 photonic crystal waveguide” has been produced. An example is shown in Fig. 1.1 along with a photonic nanowire and a plasmonic nanowire, two other types

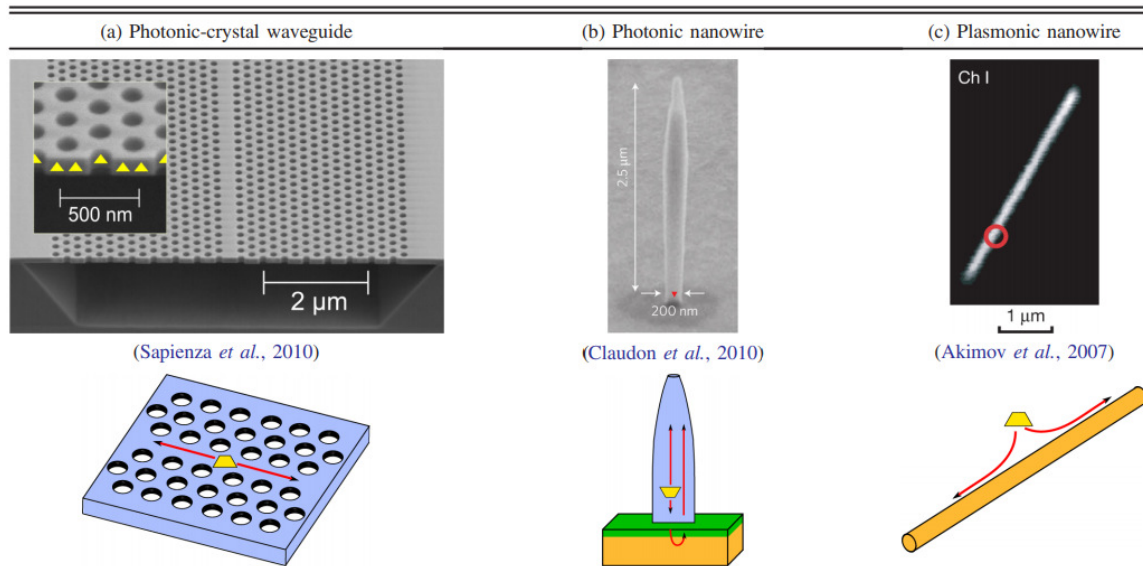


Figure 1.1: Examples of photonic waveguides reproduced from Lodahl, Mahmoodian, and Stobbe 2015. Each example contains a scanning electron micrograph of the device along with a schematic. The devices are: (a) a photonic crystal waveguide produced by Sapienza et al. 2010, (b) a photonic nanowire produced by Claudon et al. 2010, and (c) a plasmonic nanowire produced by Akimov et al. 2007.

of photonic waveguides that support integration. The modes of the waveguide allow for broadband coupling to quantum optic systems adjacent to the waveguide (Hughes 2007). Thus, multiple photonic systems can work in tandem to form larger devices which can be used to achieve the goals of quantum technologies.

The field of cavity-QED began with the discovery by Purcell in 1946 that the spontaneous emission rate of an atom was dependent on the (photonic) density of states of the environment rather than a fundamental constant from the atom (Purcell 1946). However, it was not until the 1980s that this area of research began to heat up experimentally when the Purcell-enhanced spontaneous emission rates of single sodium atoms was first observed (Goy et al. 1983). Since then, experiments coupling cavities with two-level systems (TLS's), such as atoms or quantum dots, have shown results such as strong coupling (a non-perturbative cavity-QED effect) between the TLS and cavity (Kaluzny et al. 1983; Meschede et al. 1985), squeezing of the emitted light waves (G. Milburn and Walls 1981), and super- and sub-radiant light emission

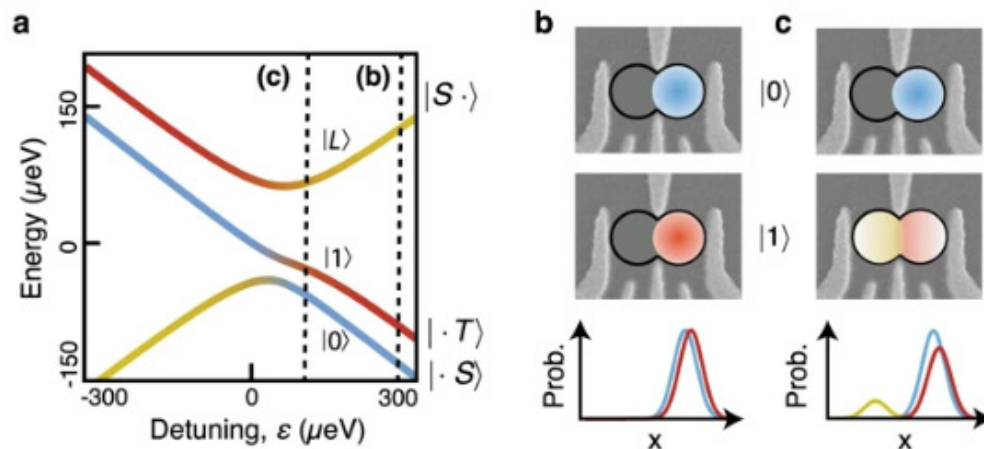


Figure 1.2: An implementation of a controlled-Z gate using capacitively coupled quantum dot hybrid qubits reproduced from Frees et al. 2019. (a) The energy dispersion of the quantum dot hybrid qubit as a function of detuning showing the two lower energy states forming the qubit levels. (b) and (c) charge distribution of an electron between the two qubits for (b) a large detuning and for (c) a smaller detuning near to the charge transition.

(Billinghurst et al. 2013) to name a few. More recently, these cavity-QED systems have been coupled to waveguides in order to produce “on demand” single-photon sources (Somaschi et al. 2016), entangled-photon pairs (Huber et al. 2018), and qubits (Zhang et al. 2018; Hensen et al. 2020), an essential component to achieve quantum computing.

Currently, there is research interest in improving the figures of merit of these systems in order to achieve standards high enough for use in future quantum technologies. For example, qubits can be built from a variety of photonic systems, such as electron spin in quantum dots (Nowack et al. 2011) or photonic circuit setups (Du et al. 2010); an example system from Frees et al. 2019 is shown in Fig. 1.2. However, for use in quantum computing longer coherence times are needed (Lloyd 2000), coherent optical feedback has been suggested as one avenue of improvement.

1.2 Time-Delayed Feedback as a Non-Markovian Dynamic

Coherent optical feedback is generally achieved by coupling a cavity-QED system to an optical feedback loop which coherently returns the photon output after a time

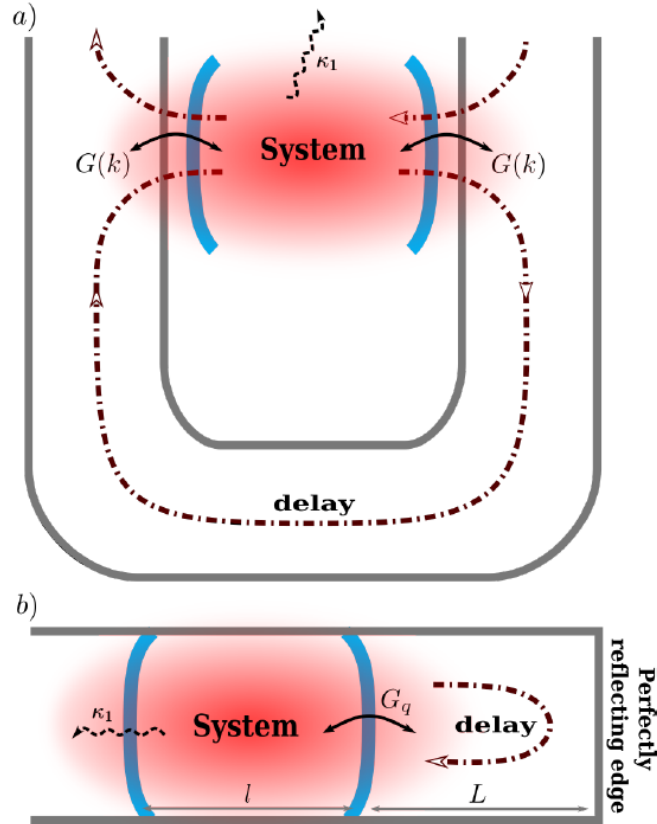


Figure 1.3: Schematic examples of coherent time-delayed feedback reproduced from N emet, Carmele, et al. 2019. (a) The cavity-QED system is coupled to a waveguide loop at two different spatial points, this leads to a feedback of continuous-modes. (b) The cavity-QED couples to a waveguide at a single point which is then reflected by a perfect mirror at the end of the waveguide, this leads to a feedback of discrete-modes.

delay. The feedback loop is typically either a circular waveguide or a waveguide that terminates in a mirror which sends back the photons; a few schematic examples of feedback setups from N emet, Carmele, et al. 2019 are shown in Fig. 1.3. One of the main applications of coherent feedback is to increase stability in cavity-QED, but other proposed applications include enhancement of photon entanglement (Hein, Carmele, et al. 2016) and squeezing (Kraft et al. 2016; N emet and Parkins 2016), enhanced photon bunching and antibunching (Lu et al. 2017), improved photon distributing in cavity-QED emitters (Droenner et al. 2019) and stabilization in optomechanics (L. N. Naumann et al. 2016).

The motivation for applying coherent feedback to the systems of interest has its genesis in the success of measurement-based feedback in a variety of mediums. This type of feedback takes a measurement on the output of the system and then applies forces on the system to control it (Wiseman and G. J. Milburn 2002). Indeed the quantum trajectory theory which is the backbone of modelling coherent feedback in this thesis, uses a stochastic measurement-based approach to infer the state of the system via “quantum jumps” (Tian and Carmichael 1992). This type of feedback has been shown to have strong results in adjacent fields such as laser stabilization (Hjelme et al. 1991), systems biology (Cosentino and Bates 2011), and mechanical systems (Franklin et al. 2014); in addition to controlling quantum optical systems (Kubanek et al. 2009; Gillett et al. 2010; Brandes 2010). However, it is limited by a number of factors such as measurement efficiency and processing delay (Balouchi and Jacobs 2017) which coherent feedback is free of.

The challenge with modelling a quantum optic system with coherent feedback is that it has a non-Markovian dynamic. A Markovian dynamic means that the system evolution depends only on the present system state at the local time only, while a non-Markovian dynamic does not, it can draw on information from the past. Mathematically, for a system to have a Markovian dynamic means that, at any time, knowing the equations of motion governing the behaviour of the system, and the initial conditions for the system at that time, allows one to solve completely for the state of the system at any time in the future. A non-Markovian dynamic on the other hand, can call on past states of the system in the differential equations governing the system evolution. If the state of the system is given by $|\psi(t)\rangle$, then the differential equations might need to evaluate $|\psi(t - \tau)\rangle$ where τ is some time delay. Therefore, simply knowing the initial conditions of a system is not enough to evolve it with a non-Markovian dynamic, the system state must be known as far back as the longest time delay in the system.

Systems with an underlying time delay are studied in mathematics under the field of delay differential equations (DDEs). These problems belong to the class of functional differential equations (FDEs) which are infinite dimensional, unlike ordinary

differential equations (ODEs) which are finite dimensional (Richard 2003). Much of the research in this area concerns determining the existence, uniqueness, and convergence of solutions to these DDEs (Olbrot 1984; Conte and Perdon 1995; Kolmanovskii 1999). There are also specific ways to properly numerically evaluate DDEs (Virk 1985) which differ from the typical methods of ODE evaluation (such as the Runge-Kutte methods). Unfortunately, due to the stochastic nature of our approaches to modelling the time-delayed coherent feedback systems, much of the conclusions from this field are difficult to apply to the systems in this thesis.

In quantum optics research, coherent optical feedback has been studied with a variety of different approaches. Indeed, in the linear regime, the response of the system can be solved analytically (Dorner and Zoller 2002; Carmele et al. 2013; N emet, Carmele, et al. 2019), however the rich physics of nonlinear optics is missing. Non-linearity in the few-quanta regime has been treated by employing fictitious cascading systems (Grimsmo 2015; S. J. Whalen et al. 2017) or matrix product states (Pichler and Zoller 2016; Guimond et al. 2017; Droenner et al. 2019). These approaches are limited by severe computational limitations as photon numbers increase (in the case of matrix product states) or as the simulation length increases (in the case of cascading systems), and they can be complicated to understand and implement. Therefore, this topic would benefit from new approaches to modelling coherent feedback which are computationally efficient and offer clear physical insight into the underlying dynamics. Indeed a time-discretized waveguide approach was very recently presented by S. J. Whalen 2019 with some basic results which avoids many of these pitfalls, and is used later in this thesis.

An efficient quantum optics model for non-Markovian dynamics also has uses outside of coherent optical feedback. Often, quantum optic systems coupled via a waveguide are modelled with the assumption that there is no delay time between systems, i.e. that the photon leaves one system and instantly arrives at the next. This works well for short distances and media with linear dispersion, however as these systems grow in complexity, this approximation breaks down. With an efficient computational model, these time delays could be modeled alongside the system dynamics

and test the validity of these approximations.

1.3 Layout of the Thesis

In this thesis, we develop two models for time-delayed coherent optical feedback in open cavity-QED systems using quantum trajectory theory. The first model for the feedback uses its frequency mode representation (FMR) and extends the typical quantum trajectory theory to allow for the resulting non-Markovian dynamics of the cavity-QED system. The second model incorporates the feedback loop as part of the system with a time discretization of the waveguide creating a large Markovian system which is modelled with a more typical quantum trajectory method. These models are tested to ensure their agreement with current results for coherent feedback (in regimes where this is valid) and further results are shown explicitly. The typical “one photon in the loop” approximation is made to start with and limited multiquanta results in this regime are shown (which are beyond linear excitation, i.e., beyond the usual weak-excitation approximation). We then go beyond this approximation and extend the model to allow for two photons in the loop where further multiquanta results can be seen.

An overview of the relevant topics has been discussed in this introductory chapter. In Chapter 2, two approaches to modelling open quantum optic systems are presented: evolving density matrices using master equations and evolving individual realizations of the system using quantum trajectory theory. The time-discretized waveguide (TDW) model is also developed for use in going beyond the one photon in the loop approximation for coherent feedback. We discuss the main computational methods used throughout this thesis as well. In Chapter 3, we present a published manuscript which studies the application of quantum trajectory to coherent feedback in the one-photon-in-the-loop approximation, using the FMR model of the feedback loop. Chapter 4 then extends the FMR model to two photons in the loop and shows the computational issues which make this approach infeasible. The TDW model is then used to allow the system to have two photons in the loop and results are shown

highlighting the difference between the one and two photon regimes. In Chapter 5, the system of interest is expanded to consist of two TLS's coupled via a waveguide with a feedback loop. We present well studied entangled states for this system and investigate the effects of phase and feedback on the dynamics of these states. Lastly, in Chapter 6 we present our conclusions and give recommendations for future work.

Chapter 2

Theory and Methods

In this chapter, we present three methods of modelling the behaviour of open quantum optic systems. First, we derive the quantum master equation from the evolution of the density matrix of the system and discuss its inability to model a system with coherent feedback. We then present quantum trajectory (QT) theory as an alternative method evolving the system and show its equivalence to the master equation solution. We use QT theory in Chapter 3 to model coherent feedback in the few quanta regime, however to move beyond such a regime a modified version of QT theory is needed. This time-discretized waveguide (TDW) model is presented to cover the mathematics of its implementation before it is used in Chapter 4. The computational methods and software used to implement these models are also discussed.

2.1 Evolving Open Quantum Systems with Master Equations

An open quantum system is any quantum system that interacts with another, generally much larger, quantum system called the reservoir (Rivas and Huelga 2012). The approach taken in deriving the evolution of open quantum systems is a combination of the approaches by Miller 2008 and Carmichael 2002.

The Hilbert space associated with the system is denoted by \mathcal{H}_S with orthonormal basis $\mathcal{B}_S = \{|\phi_k\rangle_S | k = 1, 2, \dots, \dim(\mathcal{H}_S)\}$, while the Hilbert space associated with the reservoir is denoted by \mathcal{H}_R with orthonormal basis $\mathcal{B}_R = \{|\phi_l\rangle_R | l = 1, 2, \dots, \dim(\mathcal{H}_R)\}$. Then the combined system Hilbert space is given by $\mathcal{H} = \mathcal{H}_S \otimes \mathcal{H}_R$ with orthonormal

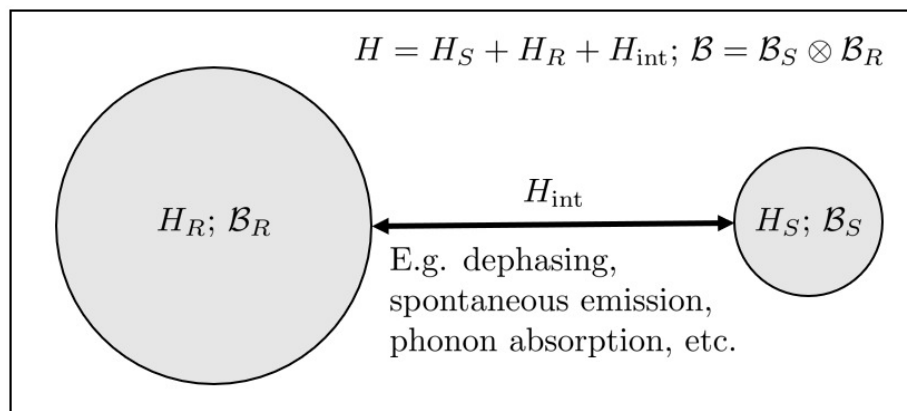


Figure 2.1: A general model for the open quantum system consisting of the system, the reservoir, and the interaction between them.

basis $\mathcal{B} = \mathcal{B}_S \otimes \mathcal{B}_R = \{|\phi_k\rangle \otimes |\phi_l\rangle | k = 1, 2, \dots, \dim(\mathcal{H}), l = 1, 2, \dots, \dim(\mathcal{H}_R)\}$. The combined system Hilbert space is then a closed quantum system and therefore satisfies the Schrödinger equation,

$$i \frac{d}{dt} |\psi(t)\rangle = H |\psi(t)\rangle, \quad (2.1)$$

where $|\psi(t)\rangle$ is a pure state and H is the Hamiltonian of the combined system. Note that we have adopted natural units throughout the thesis, where we set $\hbar = 1$. In general the Hamiltonian is given by

$$H = H_S + H_R + H_{\text{int}}, \quad (2.2)$$

where H_S is the Hamiltonian of the system, H_R is the Hamiltonian of the reservoir, and H_{int} is the Hamiltonian representing the interaction between the system and reservoir. Figure 2.1 gives a general model of the combined system along with some typical examples for the interaction between system and reservoir.

Next the density matrix for the combined system is given by

$$\chi(t) = |\psi(t)\rangle \langle \psi(t)|. \quad (2.3)$$

Taking the time derivative of this density matrix gives

$$\frac{d}{dt}\chi(t) = i[\chi(t), H], \quad (2.4)$$

where Eq. 2.1 was used after expanding $\chi(t)$. The final equation is known as the Von Neumann equation and gives the evolution of the density matrix under the combined system Hamiltonian.

In order to derive the master equation, we define

$$\tilde{\chi}(t) \equiv e^{i(H_S+H_R)t}\chi(t)e^{-i(H_S+H_R)t}, \quad (2.5)$$

in order to transform into the interaction picture. By taking the time derivative of $\tilde{\chi}(t)$, we get

$$\frac{d}{dt}\tilde{\chi}(t) = i[\tilde{\chi}(t), \tilde{H}_{\text{int}}(t)], \quad (2.6)$$

where $\tilde{H}_{\text{int}}(t)$ is

$$\tilde{H}_{\text{int}}(t) \equiv e^{i(H_S+H_R)t}H_{\text{int}}e^{-i(H_S+H_R)t}. \quad (2.7)$$

Then by integrating Eq. 2.6, an explicit expression for $\tilde{\chi}(t)$ is found:

$$\begin{aligned} \tilde{\chi}(t) &= \tilde{\chi}(0) + i \int_0^t [\tilde{\chi}(t'), \tilde{H}_{\text{int}}(t')] dt' \\ &= \chi(0) + i \int_0^t [\tilde{\chi}(t'), \tilde{H}_{\text{int}}(t')] dt', \end{aligned} \quad (2.8)$$

since $\tilde{\chi}(0) = e^{-0}\chi(0)e^0 = \chi(0)$. By subbing this back into Eq. 2.6 for $\tilde{\chi}(t)$, we obtain

$$\frac{d}{dt}\tilde{\chi}(t) = i[\chi(0), \tilde{H}_{\text{int}}(t)] - \int_0^t [[\tilde{\chi}(t'), \tilde{H}_{\text{int}}(t')], \tilde{H}_{\text{int}}(t)] dt'. \quad (2.9)$$

This equation describes the evolution of the combined system, however, in general the majority of the evolution of the reservoir is uninteresting as it is not affected by the presence of the system. In order to isolate for the evolution of the system, the trace of the reservoir dimensions is taken over the combined system density matrix,

giving

$$\rho(t) = \text{Tr}_R[\chi(t)], \quad (2.10)$$

where $\rho(t)$ is the system (or reduced system) density matrix. Furthermore, we make the assumption that the interaction between the system and reservoir begins at $t = 0$, and thus

$$\rho(0) = \text{Tr}_R[\chi(0)] = R'_0\chi(0), \quad (2.11)$$

where R'_0 is a constant. This simplification can be made because the off-diagonal elements of $\chi(0)$ are 0 since no interaction has taken place. This can be rewritten as $\chi(0) = R_0\rho(0)$ with $R_0 = (R'_0)^{-1}$.

By defining

$$\tilde{\rho}(t) \equiv e^{iH_S t} \rho(t) e^{-iH_S t} = \text{Tr}_R[\tilde{\chi}(t)], \quad (2.12)$$

and tracing over the reservoir in Eq. 2.9 as well as substituting in Eqs. 2.10 and 2.11 into Eq. 2.9, we obtain

$$\frac{d}{dt}\tilde{\rho}(t) = - \int_0^t \text{Tr}_R\{[[\tilde{\chi}(t'), \tilde{H}_{\text{int}}(t')], \tilde{H}_{\text{int}}(t)]\} dt', \quad (2.13)$$

which is the exact master equation in the interaction picture.

From here we make two approximations in order to make Eq. 2.13 tractable in most cases: the Born approximation and the Markov approximation. First, for the Born approximation, we assume that the reservoir is a very large system that is largely unaffected by its interaction with the system of interest because the coupling is weak. Therefore the combined system density matrix only varies from its initial condition to first order in H_{int} . Thus we can write

$$\tilde{\chi}(t) = \tilde{\rho}(t)R_0 + O(H_{\text{int}}), \quad (2.14)$$

which can then be substituted into the master equation to give

$$\frac{d}{dt}\tilde{\rho}(t) = - \int_0^t \text{Tr}_R\{[[\tilde{\rho}(t')R_0 + O(H_{\text{int}}), \tilde{H}_{\text{int}}(t')], \tilde{H}_{\text{int}}(t)]\} dt'. \quad (2.15)$$

However, notice that the term $O(H_{\text{int}})$ will only create terms which are second order or larger in H_{int} when the equation is expanded. Since we have assumed that the coupling is weak, these second order terms are negligible and we can remove $O(H_{\text{int}})$ from our equation to obtain

$$\frac{d}{dt}\tilde{\rho}(t) = - \int_0^t \text{Tr}_R\{[[\tilde{\rho}(t')R_0, \tilde{H}_{\text{int}}(t')], \tilde{H}_{\text{int}}(t)]\}dt'. \quad (2.16)$$

In order for a system to be Markovian, the future evolution of that system only depends on the present state of the system. Since our equation currently has the integral run over all $\rho(t'), t' \in [0, t]$, then in order to find the evolution of $\tilde{\rho}$ at any time, t , we must know the state of the system in the past, specifically the state of the system from $t' = 0$ to $t' = t$. Therefore, we make the Markov approximation which is simply that the system is Markovian, i.e. it does not depend on past versions of itself. The Markov approximation is good in the limit that there is no back action from the reservoir on the system. For any sufficiently large reservoir, this is very good, as long as the reservoir is not engineered to have back action on the system, which is the case with feedback. This allows us to replace $\tilde{\rho}(t')$ with $\tilde{\rho}(t)$ giving the master equation in the interaction picture under the combined Born-Markov approximation:

$$\frac{d}{dt}\tilde{\rho}(t) = - \int_0^t \text{Tr}_R\{[[\tilde{\rho}(t)R_0, \tilde{H}_{\text{int}}(t')], \tilde{H}_{\text{int}}(t)]\}dt'. \quad (2.17)$$

From this point it is common practice to work with the form of \tilde{H}_{int} directly in Eq. 2.17 and transform it into the more common form of the master equation,

$$\frac{d}{dt}\rho(t) = i[\rho(t), H_S] + \mathcal{L}_{\text{relax}}(\rho(t)), \quad (2.18)$$

where $\mathcal{L}_{\text{relax}}$ is the relaxation superoperator of the system. However, since we will not be using the master equation after this point (except to show the equivalence of evolving under Eq. 2.18 and QT Theory), we end the derivation here since it is only necessary to see how the Markov approximation is introduced during the derivation. In order to evolve a system with feedback (specifically, coherent feedback), both the

present state of the system and the state of the feedback must be known. The most common practice for dealing with the feedback is to relate it to the past state of the system when the feedback left, thus making the evolution of the system itself non-Markovian. Therefore the master equation of the system cannot be used to evolve the system. Of course, by expanding the system to include the source of the feedback (most commonly a waveguide loop) the overall system can be made Markovian again, but then a much more complicated (and possibly intractable) system must be evolved. Even going to higher orders of approximations, such as 2nd, 4th or 6th order Born, the results quickly break down with the introduction of feedback (S. Whalen 2015). Therefore, an alternative approach which can accept non-Markovian dynamics is required, in this case QT theory.

2.2 Quantum Trajectory Theory

The QT technique was first described by Dalibard et al. 1992 (who termed it the stochastic wavefunction approach), Tian and Carmichael 1992, and Dum et al. 1992 concurrently, and was fully developed in Carmichael's *Quantum Optics* textbook (Carmichael 2008). It has been used to model a variety of quantum optic phenomena including dissipation (Plenio and Knight 1998), stationary inversion via off-resonant pumping (Hughes and Carmichael 2011), and reversing a quantum jump (Mineev et al. 2019) in addition to coherent feedback (S. J. Whalen 2019; Crowder et al. 2020).

In the QT approach, single realizations of the system are simulated and then averaged in order to find the response of the ensemble average. This is a conceptual strength of the technique because not only is the average response calculated, but the individual trajectories can be analyzed as well. These trajectories can give you insight into the underlying dynamics that contribute to the average behaviour to better understand the physics behind the results. The trajectories are produced by directly evolving the ket vector, and so the computation time scales with the size of the Hilbert space, N . This is in contrast to the ME approach which evolves the density matrix and thus, scales with N^2 . Therefore, for large Hilbert spaces, the QT

technique can be more computationally efficient even with Markovian dynamics.

In order to use the conventional QT approach, as developed below, the relaxation superoperator must be in the well known Lindblad form,

$$\mathcal{L}_{\text{relax}}(\rho(t)) = -\frac{1}{2} \sum_m (C_m^\dagger C_m \rho + \rho C_m^\dagger C_m) + \sum_m C_m \rho C_m^\dagger, \quad (2.19)$$

where each C_i is a dissipation operator that acts on the open system under investigation, e.g., spontaneous emission from a two-level atom, and m runs over as many operators as needed to model the system. In the QT approach, these dissipation operators are termed quantum jump operators as they are responsible for the stochastic nature of each trajectory. In the systems modelled in this thesis, the jump operators that are included are the relaxation channels for the system without thermal effects. However, other types of jump operators are often used such as incoherent pumping, dephasing, phonon absorption, and thermal excitation (Mølmer et al. 1993).

The idea behind the QT technique is that a pure initial state is evolved under Schrödinger's equation using an "effective" non-Hermitian Hamiltonian, H_{eff} , until a quantum jump occurs. This evolution continues until the desired time is reached, for a single evolution trajectory. In order to find the ensemble average as given by the density matrix, many trajectories can be obtained and then averaged to get the expected behaviour of the system.

In order to evolve the system, the initial state of the system, $|\psi(0)\rangle$, is evolved forward in time steps of length δt . At each step the decision as to whether a quantum jump occurs, i.e., one of the C_i operators is applied to the system, is made stochastically. To make this decision, the probability of each individual quantum jump occurring during the time step is computed and compared against a random number, ϵ (uniformly distributed between 0 and 1). The probability for quantum jump C_i , denoted by δp_i , at time t is

$$\delta p_i = \delta t \langle \psi(t) | C_i^\dagger C_i | \psi(t) \rangle, \quad (2.20)$$

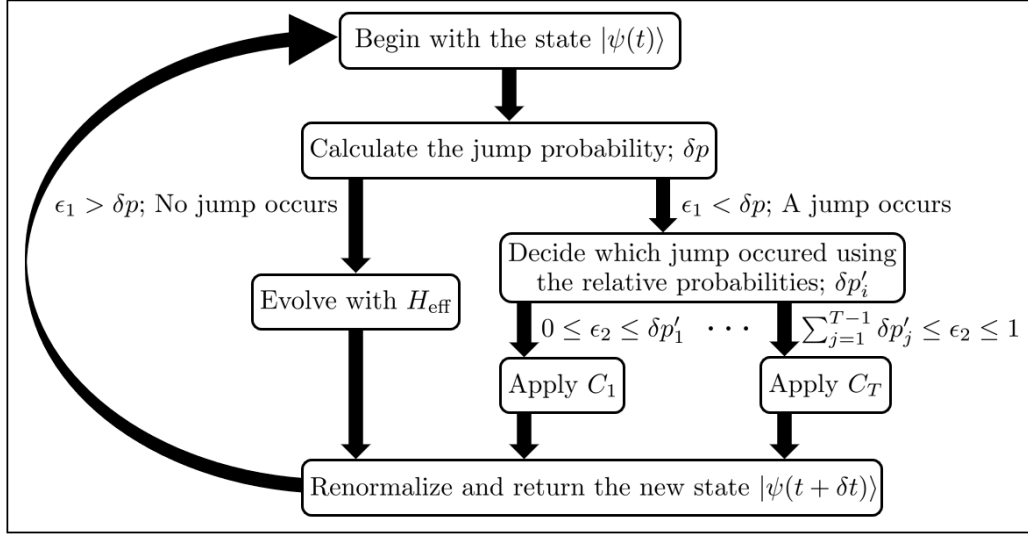


Figure 2.2: Schematic of a single time step during a QT evolution.

and then the probability that a quantum jump occurs during this time step, denoted by δp , is the sum of all of the individual quantum jump probabilities: $\delta p = \sum_m \delta p_m$. Note that this introduces a restriction on δt to ensure that the simulation is physical. In order for an accurate simulation, the assumption must be made that in any individual time step the chance of two quantum jumps occurring is negligible and the chance of any one quantum jump occurring is small. These are satisfied when $\delta p \ll 1$, and since the size of the time step scales with δp linearly, δt must be adjusted so that this condition is always valid.

If $\epsilon < \delta p$, then a quantum jump occurs and the trajectory continues in (i) , and if $\epsilon > \delta p$, then the trajectory continues in (ii) . This is shown schematically in Fig. 2.2, and described as follows:

(i) If the decision is made that a quantum jump does happen, then a further decision must be made as to which quantum jump occurs (if there are more than 1). The relative probabilities of each quantum jump occurring, relative that is, to the other quantum jumps, are used to bisect the interval $[0, 1]$. The relative probability for quantum jump C_i is given by

$$\delta p'_i = \frac{\delta p_i}{\delta p}. \quad (2.21)$$

Note that by defining the relative probabilities in this way, two relevant features appear. First that $0 \leq \delta p'_i \leq 1$ for each $\delta p'_i$ and also that $\sum_m \delta p'_m = 1$. Then a new random number, ϵ_2 , is compared against the cumulative relative probability of each quantum jump occurring. If there are T total possible quantum jumps, then this means that if

$$\begin{aligned}
0 \leq \epsilon_2 \leq \delta p'_1 &\Rightarrow \text{Operator } C_1 \text{ occurs,} \\
\delta p'_1 < \epsilon_2 \leq \delta p'_1 + \delta p'_2 &\Rightarrow \text{Operator } C_2 \text{ occurs,} \\
&\vdots \\
\sum_{j=1}^{i-1} \delta p'_j < \epsilon_2 \leq \sum_{j=1}^i \delta p'_j &\Rightarrow \text{Operator } C_i \text{ occurs,} \\
&\vdots \\
\sum_{j=1}^{T-1} \delta p'_j < \epsilon_2 \leq \sum_{j=1}^T \delta p'_j = 1 &\Rightarrow \text{Operator } C_T \text{ occurs.}
\end{aligned} \tag{2.22}$$

Once the decision has been made, the responsible quantum jump operator is applied to the state of the system at time t . For example, if operator C_i was responsible, then the new state of the system would be

$$|\tilde{\psi}(t + \delta t)\rangle = C_i |\psi(t)\rangle. \tag{2.23}$$

However, this is not necessarily normalized and so the function must be normalized before moving to the next time step. Thus the state that is handed to the next time step is

$$|\psi(t + \delta t)\rangle = \frac{|\tilde{\psi}(t + \delta t)\rangle}{\sqrt{\langle \tilde{\psi}(t + \delta t) | \tilde{\psi}(t + \delta t) \rangle}}. \tag{2.24}$$

(ii) If the decision is made that no quantum jump occurs, then the evolution of the system is given by the Schrödinger equation with a modified effective Hamiltonian,

$$H_{\text{eff}} = H_S - \frac{i}{2} \sum_m C_m^\dagger C_m, \tag{2.25}$$

where H_S is the system Hamiltonian. Then the evolution of the system for one time

step is

$$|\tilde{\psi}(t + \delta t)\rangle = e^{-iH_{\text{eff}}\delta t} |\psi(t)\rangle, \quad (2.26)$$

which again is not normalized, and so the state of the system is renormalized as in Eq. 2.24 and the process begins again for a new δt time step.

Once the desired end-time is reached, then the quantum trajectory has finished and the state of the system for this trajectory at each time is known. With this knowledge, any desired observable can be calculated at each time step and these can be averaged across all of the trajectories to find the ensemble average of the observable (if one wishes). Most importantly throughout this technique, no assumptions about the past time of the system has been made. Thus, we are free to include time delays in the evolution and this technique can be used to simulate coherent feedback systems.

2.2.1 Example System Dynamics Solved Using QT Theory

In order to highlight the stochastic nature of QT Theory as well as highlight the strengths of the approach, two examples are developed below. First, the simple example of decay from an excited cavity to an open reservoir is shown to discuss the convergence to the master equation solution. Next, a more sophisticated system from Hughes and Carmichael 2011 is presented that highlights the insights that can be gained by examining individual trajectories.

Perhaps the cleanest example of modelling a system using QT theory, the dynamics of cavity decay to an open reservoir is shown Fig. 2.3(a). The Hamiltonian for this system is $H_S = \omega c^\dagger c$, where c^\dagger and c are the cavity raising and lowering operators and ω is the cavity energy level transition frequency. This is augmented by one quantum jump operator, $C_1 = \sqrt{\gamma}c$, which represents cavity decay to the open reservoir at a rate of γ . Figure 2.3(a) shows the evolution of this system for three different numbers of total trajectories along with the analytical solution. The single trajectory readily shows the stochastic nature of this approach. The cavity begins in its excited state and sits there until a jump occurs and the population steps down one level. In an experimental setting each one of these steps would be associated with a photon

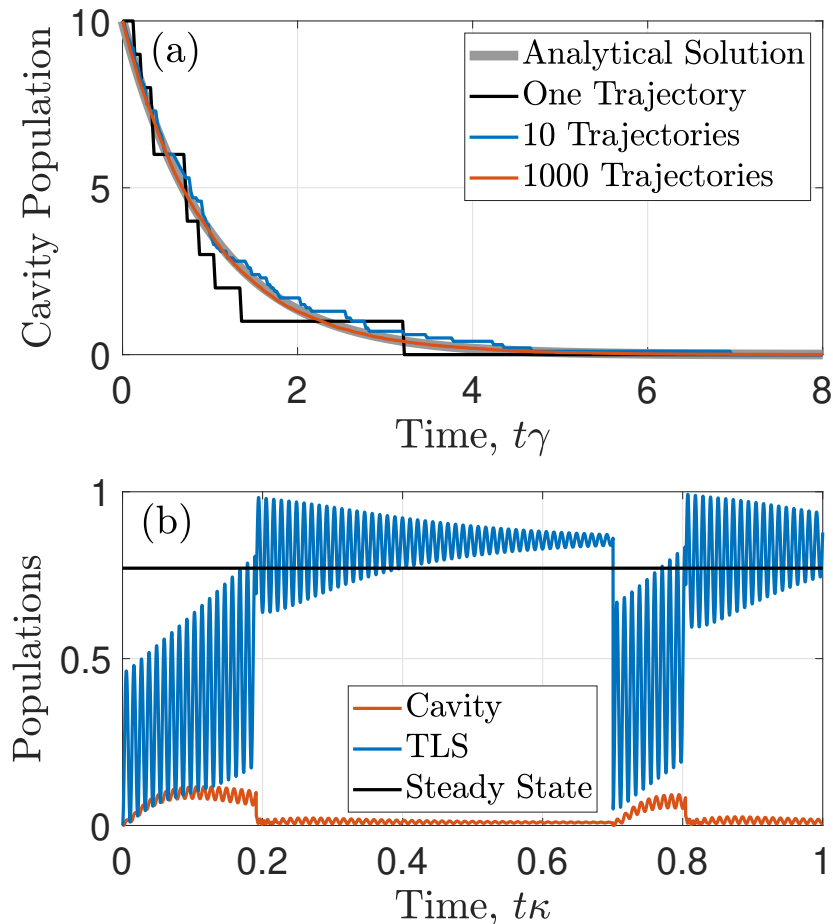


Figure 2.3: In (a), the decay of an excited cavity to an open reservoir is shown for three different values of total trajectories, along with the analytical solution. In (b), a sample QT is shown, recovering the cavity-QED results of Hughes and Carmichael 2011. The black line is the steady state TLS population showing population inversion.

detector recording one count. Most quantum jump operators can be thought of as having some experimental observable that detects when a jump occurs. As the number of trajectories that are averaged increases, the behaviour approaches that of the analytical solution.

Figure 2.3(b) shows the dynamics of a more sophisticated system investigated previously by Hughes and Carmichael 2011. This paper explored a TLS coupled with a quantized cavity and pumped off resonance in order to produce stationary inversion of the system. The quantum jumps associated with this model were,

$C_1 = \sqrt{2\kappa c}$, representing cavity decay (where the half-width cavity decay rate, κ , is used here rather than the full width decay rate used in the feedback model of later sections), $C_2 = \sqrt{\gamma}\sigma^-$, representing spontaneous emission from the TLS, and $C_3 = \sqrt{\gamma_p/4}(\sigma^+\sigma^- - \sigma^-\sigma^+)$, representing “pure dephasing” events in the TLS. In the setup investigated in the paper, C_1 dominated the two other jump events.

When this system is investigated using the ME approach, the steady state population of the TLS is solved which simply returns a value between 0 and 1 where anything > 0.5 represents population inversion. However, no information on what is causing this inversion is obtained. When a single QT is analysed, the explanation for the TLS population inversion becomes apparent. Whenever a cavity decay occurs, the cavity population falls and the TLS population greatly increases. Thus, by having the cavity decay dominate the other output channels, the TLS sits closer to its excited state and better population inversion is obtained. This example is shown to highlight how single QTs are useful on their own and give unique insight into system dynamics, unavailable from solutions obtained using the master equation.

2.2.2 Equivalence of QT Theory to the Master Equation

Before moving forward and using QT theory to model coherent feedback, we should verify that using this technique will return the same solution as using the typical master equation approach. To do that we will show that evolving the average of the QTs is the same as evolving the density matrix under the ME.

Let the outer product of a QT be $\sigma(t) = |\psi(t)\rangle \langle\psi(t)|$, and so $\overline{\sigma(t)}$ is the average of all QTs with the initial condition $|\psi(0)\rangle$. Then after a single time step under the QT formalism the new average is

$$\sigma(t + \delta t) = (1 - \delta p) \frac{|\psi'(t + \delta t)\rangle \langle\psi'(t + \delta t)|}{\langle\psi'(t + \delta t)|\psi'(t + \delta t)\rangle} + \sum_m \delta p_m \frac{C_m |\psi(t)\rangle \langle\psi(t)| C_m^\dagger}{\langle\psi(t)|C_m^\dagger C_m|\psi(t)\rangle}, \quad (2.27)$$

where the first term represents the trajectories which evolve without a jump and the sum represents the trajectories which undergo a quantum jump. Notice each term is weighted by the probability of each event happening (i.e. the probability for no jump

is $(1 - \delta p)$ so the first term is weighted by this).

Subsequently, taking the average and using Eqs. 2.20, 2.25, and 2.26 this can be rewritten as

$$\begin{aligned} \overline{\sigma(t + \delta t)} &= \overline{\sigma(t)} + i\delta t[\overline{\sigma(t)}, H_S] - \frac{\delta t}{2} \sum_m (C_m^\dagger C_m \overline{\sigma(t)} + \overline{\sigma(t)} C_m^\dagger C_m) + \delta t \sum_m C_m \overline{\sigma(t)} C_m^\dagger \\ &= \overline{\sigma(t)} + i\delta t[\overline{\sigma(t)}, H_S] + \delta t \mathcal{L}_{\text{relax}}(\overline{\sigma(t)}). \end{aligned} \quad (2.28)$$

This tells us that the average of the QTs evolves as

$$\frac{d}{dt} \overline{\sigma(t)} = i[\overline{\sigma(t)}, H_S] + \mathcal{L}_{\text{relax}}(\overline{\sigma(t)}), \quad (2.29)$$

which is identical to the evolution of $\rho(t)$ in the master equation, Eq. 2.18. Therefore as long as the initial state of the system can be written as $\rho(0) = |\psi(0)\rangle \langle\psi(0)|$, i.e. as a pure state, then using either QTs or the master equation will result in the same solution for averaged quantities. It is possible to use QT theory for an initial mixed state. In this case, the initial state of the trajectory needs to be chosen at random between the pure states that are present in the mixed state according to the statistics of the mixture.

2.2.3 Generalized Conditioning of the Quantum Trajectories

It is important to note that the renormalization at the end of each time step is not just a mathematical necessity, but is rooted in physical meaning. By renormalizing the state after each time step whether jumping or not, we are essentially resetting our knowledge of the state of the system. Therefore, we begin the next time step as if the state is an initial condition at the start of a new trajectory. However, this is not the only way to “condition” trajectories on whether or not a jump occurs. In this section we will discuss two other methods of conditioning trajectories; a second approach for Lindblad operators which is more computationally efficient and a more general approach which allows for non-Lindblad decay channels.

It is important to note that before renormalization, the norm of the state after not jumping carries the information of the probability to jump. Explicitly, before renormalization we have

$$\langle \psi'(t + \delta t) | \psi'(t + \delta t) \rangle = \langle \psi(t) | \left(1 + iH_{\text{eff}}^\dagger \delta t \right) \left(1 - iH_{\text{eff}} \delta t \right) | \psi(t) \rangle, \quad (2.30)$$

which to first order in δt , and noting that H_S is Hermitian, simplifies to

$$\langle \psi'(t + \delta t) | \psi'(t + \delta t) \rangle = \langle \psi(t) | \psi(t) \rangle - \delta t \langle \psi(t) | \sum_m C_m^\dagger C_m | \psi(t) \rangle = 1 - \delta p. \quad (2.31)$$

The change in the norm of the state from the non-Hermitian part of H_{eff} is the probability to jump from that time step.

This can be used to our numerical advantage by not renormalizing after each time step and allowing the norm of the state to carry the information on the jump probability. By only renormalizing after a quantum jump, after N time steps without a jump, the norm of the state is given by

$$\langle \psi'(t_0 + N\delta t) | \psi'(t_0 + N\delta t) \rangle = 1 - \sum_{j=1}^N \delta p(t_0 + j\delta t), \quad (2.32)$$

where t_0 is the time of the last quantum jump (and thus the last time that the state was normalized). Therefore, rather than pick a new random number each time step to test if a jump occurs, a single random number can be chosen and then a quantum jump occurs once the decreasing norm is smaller than the random number. This saves renormalizing each time step (although any calculated observables must be calculated using a renormalized state) which leads to a slight decrease in computation time.

The real advantage to this approach is realized for systems which have a very low rate of jump events. Since the system is deterministic up until the first jump occurs, when the initial random number is chosen for a trajectory, the dynamics are known until the norm decreases past the quantum number. This can save significant computation time as the dynamics do not need to be simulated until after the first

jump. For systems where jumps occur infrequently, this could be the majority, or even the entire, trajectory. When open-source quantum optics software use QTs, this is the numerical method most commonly used, for example QuTiP (Johansson et al. 2013) in Python and QO Toolbox (Tan 1999) in Matlab both use this approach and so they are restricted to Markovian jump operators.

It is also possible to adjust the conditioning technique to allow for non-Lindblad decay channels. Let J be some non-Lindblad decay channel from a system, S , to a reservoir, R ; we will condition a trajectory of this system at time t on last having jumped at time t_0 . Then the unconditioned system state, $\tilde{\chi}(t)$, is

$$\tilde{\chi}(t) = e^{(-i[H_S, \cdot] - J^\dagger \cdot J)(t-t_0)} \chi(t_0), \quad (2.33)$$

where H_S is the system Hamiltonian and $\chi(t_0) = |\psi(t_0)\rangle \langle \psi(t_0)|$. Then with this system state in hand we can condition it in the same way as a Lindblad decay channel,

$$\rho(t) = \frac{\text{tr}_R[\tilde{\chi}(t)]}{\text{tr}_{S \otimes R}[\tilde{\chi}(t)]}, \quad (2.34)$$

and so any desired observables can be calculated from this conditioned state. The full derivation of 2.33 is given in Appendix A of Carmichael 1987 and further details on the motivation for this approach from a conditional probability perspective are covered in Ch. 3.3.5 (when this approach is applied to conditioning the feedback system state). It is important to note that this process is general and so a Lindblad process could also be conditioned in this way. However, it is numerically very slow to compute $\tilde{\chi}(t)$ due to integrals over the time interval $[t_0, t]$ appearing.

2.3 Time-Discretized Waveguide Model

As discussed previously, another method of turning a non-Markovian problem into a Markovian problem is to expand the system to include the source of the past time dependence directly. In the systems analyzed in this thesis (TLS's, cavity), the systems are coupled to a waveguide which introduces time-delayed feedback to

the system. Therefore, if we include the evolution of the waveguide modes in our model, the system is again Markovian. To do this we follow an approach taken by S. J. Whalen 2019; discretizing the waveguide in the time domain. This model has applications beyond modelling feedback due to the variety of systems which utilise waveguides. For example, quantum circuits (Koren 1994) and many-body systems such as long range spin chains (Lodahl, Mahmoodian, Stobbe, et al. 2017) both benefit from new methods of modelling the waveguides present in these systems. In this section, the mathematics of this approach is covered and it will be applied to coherent feedback in Ch. 4.

We model a waveguide on an interval $[-L, 0]$ which would typically be described by the annihilation operators, b_k , for a waveguide mode in the frequency domain. In order to model the waveguide in the time domain, these operators are transformed into the time domain operators, B_n , using the discrete Fourier transform. The explicit relationship between the operators is

$$\begin{aligned} B_n &= \frac{1}{\sqrt{N}} \sum_{k=0}^{N-1} b_k e^{i\omega_k n \Delta t}, \\ b_k &= \frac{1}{\sqrt{N}} \sum_{n=0}^{N-1} B_n e^{-i\omega_k n \Delta t}, \end{aligned} \quad (2.35)$$

where $\Delta t = L/N$ is the time domain sampling and the waveguide is assumed to have linear dispersion so that $\omega_k = 2\pi k/L$. This is normally a very good approximation. The time domain operators can be thought of as representing all relevant frequencies of the field in a small box of the waveguide. Then the operator B_n represents the field between $-n\Delta t$ and $-(n+1)\Delta t$.

The Hamiltonian of the waveguide is

$$H_W = \sum_{k=0}^{N-1} \omega_k b_k^\dagger b_k, \quad (2.36)$$

and so the evolution of the waveguide is described by the operator $U_W(t) = e^{-iH_W t}$.

Then over a single time step of size Δt , the time domain operators evolve as

$$U_W^\dagger(\Delta t)B_nU_W(\Delta t) = \frac{1}{\sqrt{N}} \sum_{k=0}^{N-1} b_k e^{i\omega_k(n-1)\Delta t} = B_{n-1}, \quad (2.37)$$

where we have used the identity $U_W^\dagger(\Delta t)b_kU_W(\Delta t) = b_k e^{-i\omega_k\Delta t}$. Therefore, when modelling the evolution of the waveguide, the field can simply be passed along from one “box” of the waveguide to the next each time step. It is important to note that this effect only occurs with linear dispersion. If the dispersion is non-linear, the different frequencies in each box of the waveguide will travel different lengths and they will not all end up perfectly in the next box of the waveguide.

Now it is simple to pass along the field from one box to the next, but in order to properly model the start and end of the waveguide we turn back to QT theory. The first step in setting this system up for modelling with QTs is to explicitly fix the state of the waveguide to be

$$|\psi_W\rangle = |l_{N-1}, \dots, l_0\rangle = |l_{N-1}\rangle \dots |l_0\rangle, \quad (2.38)$$

where $|l_n\rangle$ is the number state for the field from $-n\Delta t$ to $-(n+1)\Delta t$. Then the evolution of a waveguide using periodic boundary conditions is given by

$$U_W(\Delta t) |l_{N-1}, \dots, l_0\rangle = |l_0, l_{N-1}, \dots, l_1\rangle. \quad (2.39)$$

It is quickly apparent that the size of this basis quickly becomes too large to allow for numerical simulation of the system and so two approximations are made to avoid this. First, $l_n \in \{0, 1\}$ so that there is only up to one excitation allowed in each box of the waveguide, which is a good approximation as long as N is sufficiently large (equivalently, Δt is sufficiently small, since $\Delta t = L/N$). Even with this in hand there can still be up to N excitations in the waveguide, and thus a basis size of 2^N , which remains unfeasible to simulate. Therefore, we set $\sum_{n=0}^{N-1} l_n = M$, so there is a maximum of M excitations in the waveguide. Thus the size of the basis is

$\sum_{n=0}^M \binom{N-1}{n}$, and M can be chosen to keep the basis size numerically accessible.

With these conditions on the waveguide in hand, the QT formalism can be used to remove the periodic boundary conditions by introducing a quantum jump out of the waveguide from the last box of the waveguide. The state can be separated into two components

$$|\psi_W(t)\rangle = |\psi_0(t)\rangle |0 = l_0\rangle + |\psi_1(t)\rangle |1 = l_0\rangle, \quad (2.40)$$

where the first term is the component of the system with no excitation in the final box and the second term is the component with an excitation. Then the “jump” out of the final box of the waveguide mimics an excitation continuing down the waveguide with probability $\langle \psi_1(t) | \psi_1(t) \rangle$, and jump operator B_0 . With this setup, whether or not a jump occurs, the system is projected into a state where $l_0 = 0$. Then applying $U_W(\Delta t)$ leads to a single time step taking the form

$$|\psi_W(t)\rangle = |l_{N-1}, \dots, l_0\rangle \Rightarrow |\psi_W(t + \Delta t)\rangle = |0, l_{N-1}, \dots, l_1\rangle. \quad (2.41)$$

Clearly, this waveguide model will only be interesting for N time steps, after which the waveguide will be empty. Therefore it is also useful to allow for an incoming field down the waveguide. By defining the probability function for a photon to enter the waveguide as $P(t)$ (derived from the time representation of the pulse), the box coming into the waveguide can be stochastically chosen to contain an excitation or not based on this probability. This occurs much the same way a quantum jump is decided upon. Before introducing the new box into the waveguide, a random number, $\epsilon \in (0, 1)$, is compared to the probability and the box can come in either containing ($\epsilon < P(t)$) or not containing an excitation ($\epsilon > P(t)$).

With this model in hand, many systems of interest which couple to the waveguide can be introduced through the QT formalism by coupling to the waveguide box at the location of the system. For example, if the annihilation and creation operation operators for the system are given by a and a^\dagger respectively, and the system couples

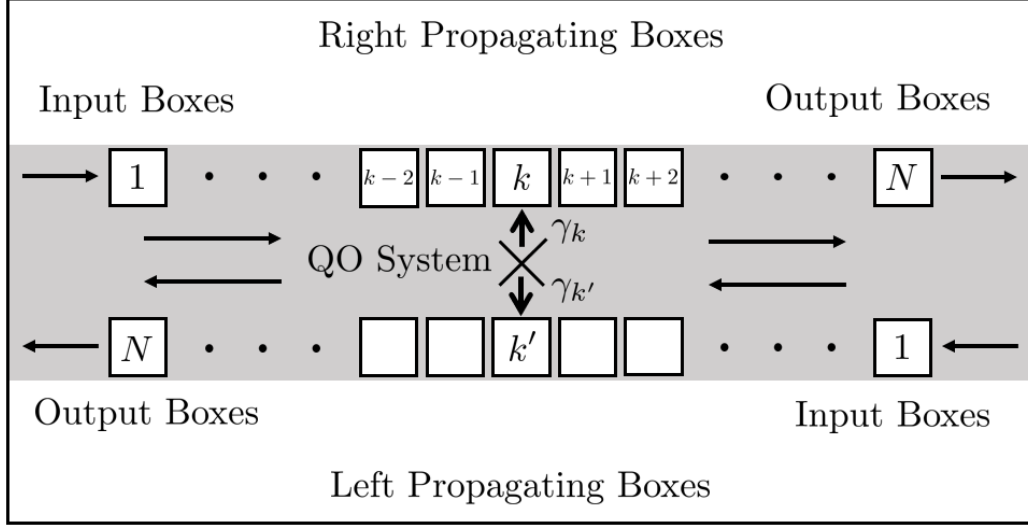


Figure 2.4: Schematic of the TDW model for an open waveguide with an integrated QO system. There is a set of boxes modelling the photons travelling to the right and a set of boxes modelling photons travelling to the left. The system couples to the right propagating field at position k and to the left propagating field as k' , with coupling rates γ_k and $\gamma_{k'}$ respectively. Note that the output boxes are measured to stochastically decide if there is a photon leaving the system, which is treated as a quantum jump.

to the k 'th waveguide box, then the interaction Hamiltonian is

$$H_I = \frac{1}{\sqrt{\Delta t}} \left(\gamma_k a^\dagger B_k + \gamma_{k'}^* B_{k'}^\dagger a \right), \quad (2.42)$$

where the factor $\frac{1}{\sqrt{\Delta t}}$ is introduced to maintain the correct box flux out of the waveguide. This model is schematically shown in Fig. 2.4 for a general QO system coupled to an open waveguide.

The total Hamiltonian for the system is

$$H = H_W + H_I + H_S, \quad (2.43)$$

where H_S is the system Hamiltonian. Then the evolution of the combined waveguide and system over one time step is governed by the operator

$$U(\Delta t) = U_W(\Delta t)U_{SI}(\Delta t), \quad (2.44)$$

where $U_{SI}(\Delta t) = e^{-i(H_S+H_I)\Delta t}$. Thus, to complete a time step with a system coupled to the waveguide, the first step is to evolve the system alone and its interaction with the k^{th} box and then move the boxes forward introducing any input excitations and checking for any jump down the waveguide from the N^{th} box.

2.4 Computational Methods

In this thesis, both `Matlab` and `Python` were used for numerical simulations. The work in Ch. 3 and the beginning of Ch. 4 was done in `Matlab` while the TDW model of Ch. 4 was implemented in `Python`. `Matlab` was originally used because of its efficient matrix operations, which are the majority of mathematical operations done in the trajectories. However, the implementation of the TDW model creates very large matrices which begin to run into memory issues. Thus, the model was implemented in `Python` to make use of previously existing packages which focus on efficient memory allocation.

Due to the non-Markovian nature of the problem, the typical quantum optics numerical packages (`QOToolbox` for `Matlab` (Tan 1999) and `QuTiP` for `Python` (Johansson et al. 2013)) could not be used since they are not set up for time-delay Hamiltonians in their QT methods. `QuTiP` does have the ability to simulate time-delayed coherent feedback using the cascading systems formalism (Grimsmo 2015), but this quickly becomes computationally inefficient for long run times or large systems. The QT formalism was directly implemented for our quantum jumps of interest and the evolution between jumps was done using either a fourth-order Runge-Kutta (RK4) method or a fifth-order Runge-Kutta (RK5) method when additional precision was required (Runge 1895; Kutta 1901; Butcher 2008).

The Runge-Kutta methods have been extended to solve delay differential equations for a function $\dot{x}(t) = f(x(t), x(t - \tau), u(t), t)$ (Virk 1985) where τ is the delay time, much like the between jump evolution dealt with in this thesis. Unfortunately, when progressing one time step, say from t to $t + dt$, these techniques require evaluations between $x(t - \tau)$ and $x(t - \tau + dt)$, which are unavailable during a QT. Therefore, we

adjust our method as follows, any evaluations in between just use either $x(t - \tau)$ and $x(t - \tau + dt)$ directly. For example, in RK4, two evaluations are made at $x(t - \tau + dt/2)$ and these are replaced with an evaluation at $x(t - \tau)$ and $x(t - \tau + dt)$.

For both models, the Runge-Kutta method was implemented as direct matrix multiplication of the ket vector with the propagator for efficiency. For the TDW model, due to the size of the Hilbert space, the Hamiltonian matrix was very large, making full multiplication in the RK4/RK5 subroutine very slow. Therefore, sparse matrix techniques were employed to speed up this calculation as much as possible and limit excessive memory use.

Finally, in both languages, parallelization was employed to speed up the computation time of the QTs. Since each trajectory is completely independent, it is a simple implementation to parallelize the codes, and the final result is the average over all trajectories. The Parallel Computing Toolbox was used in `Matlab` while the `mpi4py` package was used in `Python`.

A comparison of the computational performance of the two models is presented in Ch. 4.3 for a variety of parameter sets to highlight the strengths and weaknesses of each model.

Chapter 3

Quantum trajectory theory of few photon cavity-QED systems with a time-delayed coherent feedback

This work is published as G. Crowder, H. Carmichael, and S. Hughes, “Quantum trajectory theory of few-photon cavity-QED systems with a time-delayed coherent feedback”, [Phys. Rev. A **101**, 023807 \(2020\)](#). It presents our quantum-trajectory-based approach to modelling time-delayed coherent feedback in a typical cavity-QED model. The formalism used to model the non-Markovian dynamics is derived and the new population conditioning that must be done is explained. Previous results in the weak-excitation regime are recovered and the effect of feedback on the photon lifetime is investigated. Some initial nonlinear effects are also explored through the cavity photoluminescence, under the approximation of one photon in the feedback loop. All the calculations and writing were done by myself, using notes by Howard Carmichael as a starting point for the technique. Feedback and edits were provided by Stephen Hughes and Howard Carmichael and all of the authors revised the work following comments from the review process.

Abstract

We describe an efficient approach to modelling cavity quantum electrodynamics (QED) with a time-delayed coherent feedback using quantum trajectory simulations. An analytical set of equations is derived to exploit the advantages

of trajectories in the presence of the non-Markovian dynamics, where adjustments to the standard stochastic dynamics are discussed. In the weak excitation regime, we first verify that our approach recovers known results obtained with other simulation methods and demonstrate how a coherent feedback loop can increase the photon lifetime in typical cavity-QED systems. We then explore the nonlinear few-photon regime of cavity-QED, under the restriction of at most one photon at a time in the feedback loop. In particular, we show how feedback affects the cavity photoluminescence (populations versus laser detuning), and describe how one must account for conditioning in the presence of feedback, specifically the system observables must be conditioned on no photon detections at the feedback output channel occurring.

3.1 Introduction

Cavity quantum electrodynamics (cavity-QED), where two-level systems [TLSs (quantum bits or qubits)] are strongly coupled to optical cavities, has been studied in many works, both theoretically (Jaynes and Cummings 1963; Hughes and Carmichael 2011; Carmele et al. 2013) and experimentally (Ulrich et al. 2011; Albert et al. 2011; Nomura et al. 2010), with emerging experiments also using qubits embedded in integrated semiconductor microcavities (Lodahl, Mahmoodian, and Stobbe 2015) or implemented in super-conducting circuits (circuit-QED) (Xiu et al. 2017). These elementary quantum systems often couple to integrated waveguides to give greater “on-chip” control, emitting single photons into a waveguide mode (Hoang et al. 2016), even in only one direction – “chiral waveguides” (Coles et al. 2016; Young et al. 2015). Cavity-QED systems can also aid quantum information objectives in other ways, e.g., by generating squeezed light (Wiseman and G. J. Milburn 2002). Due to their often short photon lifetimes, however, they can lack the long-term stability required by applications.

Quantum feedback has been proposed as a method to increase stability (and coherent lifetime) in cavity-QED, by coupling the system to an optical feedback loop that coherently returns photons after a time delay (Lloyd 2000). Other suggested

applications of coherent feedback include stabilization in optomechanics (L. N. Naumann et al. 2016), enhancement of photon entanglement (Hein, Carmele, et al. 2016) and squeezing (Kraft et al. 2016; Német and Parkins 2016), enhanced photon bunching/antibunching and improved photon distribution in quantum emitters (Lu et al. 2017; Droenner et al. 2019).

The most commonly used approach to solve for the evolution of cavity-QED systems employs open-system quantum master equations (Gardiner and Zoller 2004), which readily include dissipation by tracing over the reservoir (Carmichael 2002). Time-delayed coherent feedback, however, contradicts one of the fundamental assumptions of the approach, namely the assumption of a Markovian dynamic. Under the Markov approximation, the system evolution must depend on the present system state only (local time) and not draw on information from the past. Time-delayed feedback explicitly violates this requirement and so a new approach is called for.

Due to complexities arising from the continuum of modes in the feedback reservoir and the non-Markovian dynamic, the majority of studies have been limited to the linear regime; although nonlinearity at the few-quanta level has been treated by employing fictitious cascading systems (Grimsmo 2015; S. J. Whalen et al. 2017) or matrix product states (N. L. Naumann et al. 2017; Pichler and Zoller 2016; Droenner et al. 2019; Guimond et al. 2017). These treatments focus on particular model systems, however, and they can meet with severe computational limitations as photon numbers increase. There is thus reason to develop alternative approaches to the modeling of time-delayed coherent feedback in quantum optics, especially ones that offer more physical insight into the underlying dynamics.

In this work, we introduce an intuitive approach that exploits the physical insight and numerical efficiency provided by quantum trajectory (QT) simulations. It is naturally suited to the coherent feedback problem, allowing us to incorporate the non-Markovian effects while preserving the usual benefits of a QT evolution – in particular, the linear scaling with the overall size of the Hilbert space, which brings distinct advantages in the multiphoton regime.

A QT evolves the (not necessarily normalized) ket vector, $|\tilde{\psi}(t)\rangle$, of a cavity-QED system (Dalibard et al. 1992; Mølmer et al. 1993; Tian and Carmichael 1992) according to the nonunitary Schrödinger equation

$$\frac{d}{dt} |\tilde{\psi}(t)\rangle = -iH_{\text{eff}} |\tilde{\psi}(t)\rangle, \quad (3.1)$$

where H_{eff} is the effective non-Hermitian Hamiltonian and we adopt natural units with $\hbar = 1$. This evolution is augmented by quantum jumps, at random times, which account for the dissipation operators, $\{C_i\}$, in the master equation; thus, at each time step, the integrated probability (cumulative distribution to time t) for a jump to occur and no jump to have occurred since the last jump at time t_0 , is given by

$$P(t) = \int_{t_0}^t w(t') dt', \quad (3.2)$$

where $w(t') = \sum_j \langle \tilde{\psi}(t') | C_j^\dagger C_j | \tilde{\psi}(t') \rangle$ is the waiting-time distribution; which C_j terminates the no-jump interval is determined randomly, with probabilities in proportion to the rates summed in $w(t)$ (see Sec. 17.3.2 of Carmichael 2008). A schematic representation of the evolution for one time step is shown in Fig. 3.1. The average over many QTs can be shown to recover the evolution of the density operator of the open system (Mølmer et al. 1993) (if desired), and single trajectories provide unique insight into the underlying stochastic dynamics. Furthermore, since each trajectory is independent of the others, numerical computations can easily be parallelized.

The rest of our paper is organized as follows. In Sec. 3.2, we present the main model of interest and show how the feedback loop is added to the QT formalism and treated in the Hamiltonian; a discussion of the “good” and “bad” cavity regimes is also presented. In Sec. 3.3, we implement the proposed approach and highlight the key analytical steps that are taken to make the evolution under H_{eff} tractable for this system; we also show how to evaluate the probability of a quantum jump occurring and how to execute a quantum jump. To enable the computation of system observable expectations (e.g., the mean cavity photon number), we also discuss the

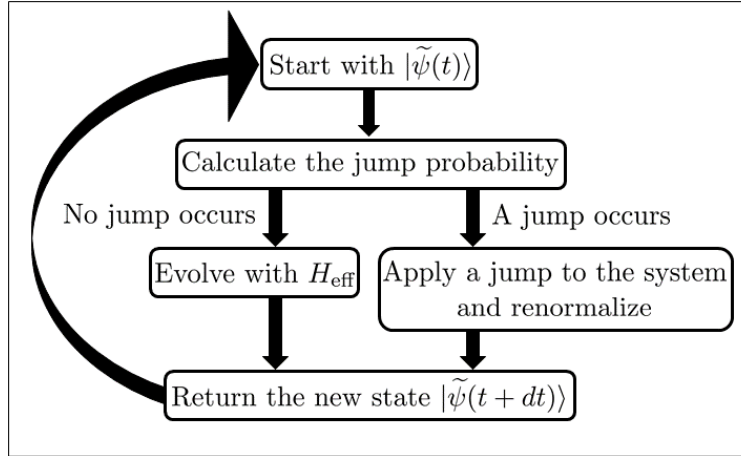


Figure 3.1: Schematic representation of one time step in the quantum trajectory evolution.

need for conditioning in the presence of feedback, and present a numerical solution to this problem. We then discuss the numerical algorithm built to sample QTs in Sec. 3.4. Lastly, in Sec. 3.5, we run through a variety of results from simulations made in different parameter regimes: first, previous results are replicated to confirm the accuracy of the treatment, and coherent feedback is shown to increase photon lifetimes; second, multiphoton effects (beyond weak excitation) are then discussed and examples of possible improvements arising from coherent feedback are explored. Our conclusions are presented in Sec. 3.6. We also derive the feedback coupling term in Appendix 3.8.1 and some details from Sec. 3.3 are moved to Appendices 3.8.2 and 3.8.3. An optimized QT technique for a simplified version of the model is presented in Appendix 3.8.4.

3.2 Model and Hamiltonian

The cavity-QED feedback model under investigation comprises a cavity coupled to a TLS as depicted in Fig. 3.2. The TLS has raising and lowering operators σ^+ and σ^- , and the creation and annihilation operators for the cavity mode are c^\dagger and c . The system is driven by a continuous-wave (cw) laser of Rabi frequency Ω and coupled to three output channels: C_0 representing cavity decay to an open reservoir (no feedback), C_1 representing spontaneous decay from the TLS, and $\mathcal{E}_+(L/2)$ representing

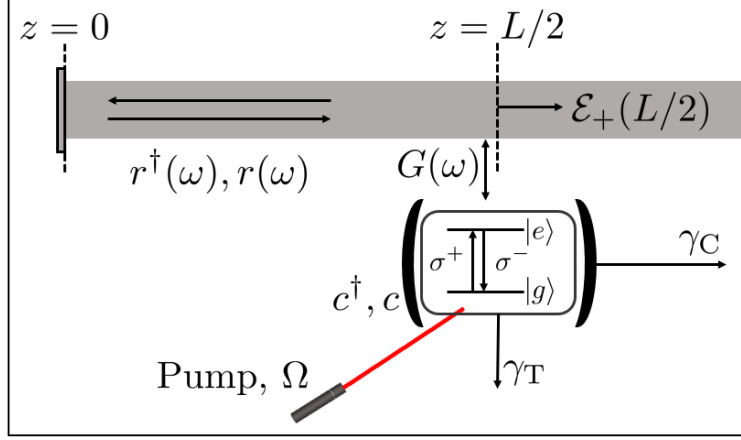


Figure 3.2: Schematic of the cavity-TLS coupled to a waveguide at $L/2$. The system has output channels C_0 (decay rate γ_C), C_1 (decay rate γ_T), and $\mathcal{E}_+(L/2)$ (the field propagating to the right out of the waveguide); has a feedback loop (round-trip length L) with a perfect mirror at $z = 0$; and is driven by a cw laser of strength Ω . The cavity creation and annihilation operators are c^\dagger and c ; the TLS raising and lowering operators are σ^+ and σ^- ; and the feedback loop creation and annihilation operators are $r^\dagger(\omega)$ and $r(\omega)$. The ground and excited states for the TLS are denoted by $|g\rangle$ and $|e\rangle$.

the field propagating to the right at $z = L/2$ in the waveguide (the field leaving the feedback loop, superposed with the emission from the cavity into the waveguide traveling to the right). Of particular interest is the coupling to the feedback reservoir, which takes photons emitted from the cavity to the left in the waveguide and feeds them back *coherently*, as shown in Fig. 3.2, photons entering the feedback loop are reflected by a mirror – e.g., a microcavity, which could introduce additional loss (Hughes 2007) – and returned to the cavity after a time delay $\tau = L/c(\omega)$, with L the round-trip length and $c(\omega)$ the speed of photons, of frequency ω , in the feedback loop. The feedback loop is modeled as a continuum of photon modes, with creation and annihilation operators $r^\dagger(\omega)$ and $r(\omega)$. In practice, such schemes can be realized in solid state circuits, e.g., using quantum dots in photonic waveguide crystal structures (Zadeh et al. 2016; Lodahl, Mahmoodian, and Stobbe 2015; Hughes 2007).

The system is investigated in both the good and bad cavity regimes. In the former case, photons have a non-negligible lifetime in the cavity and nonvanishing photon populations accrue; this is usually achieved with $g > \gamma_C, \gamma_L$, and γ_T , where g is the

cavity-TLS coupling rate; γ_C and γ_T are the decay rates of the cavity and TLS to the open reservoir, respectively; and γ_L is the decay rate into the waveguide. In the bad cavity case, the photon population in the cavity should quickly decay to zero; different choices of parameters achieve this but there is no clear bad cavity response: setting $\gamma_C, \gamma_T = 0$ and $\gamma_L \gg g$, the loop can be engineered such that little population is lost from the overall system (cavity-TLS plus feedback reservoir) and the feedback loop maintains a photon population in the TLS; on the other hand, setting $\gamma_L = 0$ and $\gamma_C, \gamma_T \gg g$, the cavity quickly decays and no photon population is present. Both parameter choices yield a bad cavity, but the dynamic is completely different and so care must be taken in this regime.

Our model is captured by the Hamiltonian

$$\begin{aligned}
 H = & \delta_{aL}\sigma^+\sigma^- + \delta_{cL}c^\dagger c + \int_{-\infty}^{\infty} [\omega' r^\dagger(\omega') r(\omega')] d\omega' \\
 & + g(\sigma^+ c + c^\dagger \sigma^-) + \Omega(\sigma^+ + \sigma^-) \\
 & + \int_{-\infty}^{\infty} \{G(\omega') [c^\dagger r(\omega') + r^\dagger(\omega') c]\} d\omega',
 \end{aligned} \tag{3.3}$$

where $\delta_{aL} = \omega_a - \omega_L$ and $\delta_{cL} = \omega_c - \omega_L$ are the detunings of the TLS and cavity, respectively, from the frequency, ω_L , of the laser drive, and $G(\omega) = \sqrt{\gamma_L/2\pi} \sin[(\omega\tau + \phi)/2]$ (Carmele et al. 2013; Német, Carmele, et al. 2019) is the frequency dependent coupling between the cavity and the feedback reservoir, where ϕ is the overall phase change around the feedback loop. The form of $\mathcal{E}_+(L/2)$ is shown in Appendix 3.8.1, where it is used to derive $G(\omega)$. The Hamiltonian is written in an interaction picture designed to remove the oscillation at the frequency of the drive, and we have made a rotating wave approximation.

3.3 Quantum Trajectory Theory

In QT theory (Dalibard et al. 1992; Mølmer et al. 1993; Tian and Carmichael 1992), when no quantum jump occurs, the system evolves coherently according to (3.1), where the non-Hermitian Hamiltonian, $H_{\text{eff}} = H - \frac{i}{2}(C_0^\dagger C_0 + C_1^\dagger C_1)$, is the system

Hamiltonian augmented by the Lindblad jump operators that represent cavity decay to the open reservoir and spontaneous emission. If a quantum jump occurs, then one of the jump operators, C_0 , C_1 , or $\mathcal{E}_+(L/2)$, is applied to the system and the state is renormalized.

The challenge in applying this method to our model arises in the algebraic form of the system state, which must encompass both the cavity-TLS and the feedback loop:

$$|\psi(t)\rangle = \sum_{n=0}^N \left\{ [\alpha_n(t) |g\rangle + \beta_n(t) |e\rangle] |\{0\}\rangle + \int_{-\infty}^{\infty} [R_{g,n}(\omega', t) |g\rangle + R_{e,n}(\omega', t) |e\rangle] |1, \omega'\rangle d\omega' \right\} |n\rangle_C, \quad (3.4)$$

where we restrict the expansion to just one photon in the feedback loop, though many photons may occupy the cavity (denoted by the index n in the state $|n\rangle_C$); α and β represent the amplitudes of the ground and excited state, respectively, of the TLS when there is no photon in the feedback loop, while R_g and R_e represent those amplitudes with one photon in the feedback loop; the frequency of the photon in the feedback loop is indicated by ω' , and the notation $\{0\}$ indicates no photon in every mode of the loop, i.e., the vacuum of the feedback loop. The restriction to at most one photon in the feedback loop at any time assumes either $\gamma_L \tau \ll 1$ or $\Omega \ll 1$; thus, it neglects multiphoton interference effects, which will be incorporated in future work. This is expected to be a reasonable approximation for small feedback loops and low loss.

Since there is a continuum of reservoir modes, $R_{g,n}(\omega, t)$ or $R_{e,n}(\omega, t)$ cannot be evolved individually, or at least it would be numerically cumbersome to do so. For a more efficient approach, we first find an expression for these amplitudes in terms of $\alpha_n(t)$ and $\beta_n(t)$, with the number of photons in the cavity truncated at $n_{\max} = N$.

Substituting the expansion of (3.4) into (3.1), and employing the above expression for H_{eff} with $C_0 = \sqrt{\gamma_C} c$ and $C_1 = \sqrt{\gamma_T} \sigma^-$, we arrive at a set of $4(N + 1)$ coupled

differential equations:

$$\begin{aligned}
\frac{d\alpha_n}{dt} &= -A_n\alpha_n - ig\sqrt{n}\beta_{n-1} \\
&\quad - i\Omega\beta_n - i\int_{-\infty}^{\infty} G(\omega')\sqrt{n}R_{g,n-1}(\omega')d\omega', \\
\frac{d\beta_n}{dt} &= -B_n\beta_n - ig\sqrt{n+1}\alpha_{n+1} \\
&\quad - i\Omega\alpha_n - i\int_{-\infty}^{\infty} G(\omega')\sqrt{n}R_{e,n-1}(\omega')d\omega', \\
\frac{dR_{g,n}(\omega)}{dt} &= -(A_n + i\omega)R_{g,n}(\omega) - ig\sqrt{n}R_{e,n-1}(\omega) \\
&\quad - i\Omega R_{e,n}(\omega) - iG(\omega)\sqrt{n+1}\alpha_{n+1}, \\
\frac{dR_{e,n}(\omega)}{dt} &= -(B_n + i\omega)R_{e,n}(\omega) - ig\sqrt{n+1}R_{g,n+1}(\omega) \\
&\quad - i\Omega R_{g,n}(\omega) - iG(\omega)\sqrt{n+1}\beta_{n+1},
\end{aligned} \tag{3.5}$$

where $A_n = n\gamma_C/2 + in\delta_{cL}$ (note $A_0 = 0$) and $B_n = (\gamma_T + n\gamma_C)/2 + i(\delta_{aL} + n\delta_{cL})$; amplitudes indexed by n with $n \notin [0, N]$ are zero, e.g., $R_{g,N+1}(\omega, t) = 0$ at all times.

Keeping our goal in mind, i.e., to obtain a set of easy to evolve equations for $\alpha_n(t)$ and $\beta_n(t)$, our task now is to obtain suitable expressions for $R_{g,n-1}(\omega, t)$ and $R_{e,n-1}(\omega, t)$ for substitution on the right-hand sides of the first two state amplitude equations, (3.5); with the integrals over $d\omega'$ evaluated, we aim for a closed set of coupled differential equations. We show here how to proceed in the $N = 1$ case, with the general N case following the same approach but with more algebraic complexity. This allows for up to two quanta in the cavity-TLS (the cavity and TLS both excited) and goes beyond the one-quantum treatments commonly encountered in the literature (e.g., see Carmele et al. 2013). We note that the next three subsections track the evolution from the initial time ($t = 0$) up to the time of the first jump, so the lower limit of integration is zero in (3.2).

3.3.1 Decoupling $R_{\mu,n}$ in the $N = 1$ Case

With the maximum number of photon states in the cavity set to $N = 1$, the coupled differential equations for $R_{\mu,n}(\omega, t)$ reduce to

$$\begin{aligned}
\frac{dR_{g,0}(\omega)}{dt} &= -i\omega R_{g,0}(\omega) - i\Omega R_{e,0}(\omega) - iG(\omega)\alpha_1, \\
\frac{dR_{e,0}(\omega)}{dt} &= -(B_0 + i\omega)R_{e,0}(\omega) - i\Omega R_{g,0}(\omega) \\
&\quad - igR_{g,1}(\omega) - iG(\omega)\beta_1, \\
\frac{dR_{g,1}(\omega)}{dt} &= -(A_1 + i\omega)R_{g,1}(\omega) - i\Omega R_{e,1}(\omega) \\
&\quad - igR_{e,0}(\omega), \\
\frac{dR_{e,1}(\omega)}{dt} &= -(B_1 + i\omega)R_{e,1}(\omega) - i\Omega R_{g,1}(\omega).
\end{aligned} \tag{3.6}$$

If we then define two vectors,

$$\mathbf{R}(\omega, t) \equiv \begin{pmatrix} R_{g,0}(\omega, t) \\ R_{e,0}(\omega, t) \\ R_{g,1}(\omega, t) \\ R_{e,1}(\omega, t) \end{pmatrix}, \quad \boldsymbol{\alpha}\boldsymbol{\beta}(t) \equiv \begin{pmatrix} \alpha_1(t) \\ \beta_1(t) \\ 0 \\ 0 \end{pmatrix}, \tag{3.7}$$

and the matrix

$$\mathbf{A} \equiv \begin{bmatrix} -i\omega & -i\Omega & 0 & 0 \\ -i\Omega & -(B_0 + i\omega) & -ig & 0 \\ 0 & -ig & -(A_1 + i\omega) & -i\Omega \\ 0 & 0 & -i\Omega & -(B_1 + i\omega) \end{bmatrix}, \tag{3.8}$$

this system may be written in the simple form

$$\frac{d}{dt}\mathbf{R}(\omega, t) = \mathbf{A}\mathbf{R}(\omega, t) - iG(\omega)\boldsymbol{\alpha}\boldsymbol{\beta}(t), \tag{3.9}$$

with solution

$$\mathbf{R}(\omega, t) = -iG(\omega) \int_0^t \mathbf{E} e^{-\boldsymbol{\lambda}(t'-t)} \mathbf{E}^{-1} \boldsymbol{\alpha} \beta(t') dt', \quad (3.10)$$

where \mathbf{E} is a matrix formed from the eigenvectors of \mathbf{A} and $\boldsymbol{\lambda}$ is a diagonal matrix of eigenvalues. Clearly, the eigenvalues take the form $\lambda_j = -i\omega + c_j$, $c_j \in \mathbb{C}$. Thus, we may write

$$\mathbf{R}(\omega, t) = -iG(\omega) \int_0^t e^{i\omega(t'-t)} \mathbf{E} \cdot \mathbf{n}(t, t') dt', \quad (3.11)$$

where \mathbf{E} and $\mathbf{n}(t, t')$ are frequency independent. Further details are provided in Appendix 3.8.2, where the explicit expression for $\mathbf{n}(t, t')$ appears as (3.53).

3.3.2 Solving the Dynamical Evolution Equations in the $N = 1$ Case

Often one is interested in just a few quanta, especially for low loss and good cavity systems; in this case we may restrict the Hilbert space to $N = 1$. This recovers all of the physics in the weak excitation regime – up to one quantum in the cavity-TLS plus feedback loop – and, in addition, some multiphoton effects, as we demonstrate in Sec. 3.5.3. The coupled differential equations for the α and β amplitudes are now

$$\begin{aligned} \frac{d\alpha_0}{dt} &= -i\Omega\beta_0, \\ \frac{d\beta_0}{dt} &= -B_0\beta_0 - i\Omega\alpha_0 - ig\alpha_1, \\ \frac{d\alpha_1}{dt} &= -A_1\alpha_1 - i\Omega\beta_1 - ig\beta_0 - i \int_{-\infty}^{\infty} G(\omega') R_{g,0}(\omega') d\omega', \\ \frac{d\beta_1}{dt} &= -B_1\beta_1 - i\Omega\alpha_1 - i \int_{-\infty}^{\infty} G(\omega') R_{e,0}(\omega') d\omega', \end{aligned} \quad (3.12)$$

where the coupling to the feedback loop is made through the quantities (3.11):

$$\begin{aligned} R_{g,0}(\omega, t) &= -iG(\omega) \int_0^t e^{i\omega(t'-t)} \mathbf{E}_{g,0} \cdot \mathbf{n}(t, t') dt', \\ R_{e,0}(\omega, t) &= -iG(\omega) \int_0^t e^{i\omega(t'-t)} \mathbf{E}_{e,0} \cdot \mathbf{n}(t, t') dt', \end{aligned} \quad (3.13)$$

where $\mathbf{E}_{g,0}$ and $\mathbf{E}_{e,0}$ are the first and second rows of \mathbf{E} , respectively. As is shown in Appendix 3.8.3, the required double integrals simplify to give

$$\begin{aligned}
 -i \int_{-\infty}^{\infty} G(\omega') R_{g,0}(\omega', t) d\omega' = & \quad (3.14) \\
 \frac{\gamma_L}{4} [-\mathbf{E}_{g,0} \cdot \mathbf{n}(t, t) + e^{i\phi} \theta(t - \tau) \mathbf{E}_{g,0} \cdot \mathbf{n}(t, t - \tau)], &
 \end{aligned}$$

and

$$\begin{aligned}
 -i \int_{-\infty}^{\infty} G(\omega') R_{e,0}(\omega', t) d\omega' = & \quad (3.15) \\
 \frac{\gamma_L}{4} [-\mathbf{E}_{e,0} \cdot \mathbf{n}(t, t) + e^{i\phi} \theta(t - \tau) \mathbf{E}_{e,0} \cdot \mathbf{n}(t, t - \tau)], &
 \end{aligned}$$

where $\theta(t - \tau)$ is the Heaviside step function, which is introduced to clarify that the feedback does not affect the system until $t \geq \tau$.

The set of equations for α and β amplitudes is now closed and can be used to evolve the state of the entire system, (3.4) with $N = 1$, between quantum jumps. It is worth noting that $\mathbf{R}(\omega, t)$ can be determined at any time (t) and frequency (ω) as it only depends on the history of $\alpha(t)$ and $\beta(t)$, which is known. Thus, expectations relating to the feedback loop can be calculated, such as the photon population in the loop.

3.3.3 Calculating the Probability for a Quantum Jump

Now that the evolution between jumps has been solved, the integrated probability of a quantum jump occurring after an interval t with no jump must be determined. To do this we need to calculate the waiting-time distribution, $w(t)$, which is given by a sum of expectation values with respect to the *un-normalized* state:

$$w(t) = \left\langle \tilde{\psi}(t) \left| \mathcal{E}_+^\dagger(L/2) \mathcal{E}_+(L/2) + \sum_{i=0}^1 C_i^\dagger C_i \right| \tilde{\psi}(t) \right\rangle, \quad (3.16)$$

where $C_0 = \sqrt{\gamma_C}c$, $C_1 = \sqrt{\gamma_T}\sigma^-$, and $\mathcal{E}_+(L/2) = \frac{-i}{\sqrt{2\pi}} \int_{-\infty}^{\infty} e^{i\omega\tau/2} r(\omega) d\omega$. Note that the form of $\mathcal{E}_+(L/2)$ comes from the spatial representation of the field $\mathcal{E}(z)$ as outlined in Appendix 3.8.1. We then are interested in the field propagating to the right at $z = L/2$ [i.e. $\mathcal{E}_+(L/2)$] as this is where the output from the feedback loop occurs. Only the evaluation of the $C_0^\dagger C_0$ expectation is shown as all three are evaluated in a similar way. We have

$$\langle \tilde{\psi}(t) | C_0^\dagger C_0 | \tilde{\psi}(t) \rangle = \gamma_C \left[|\alpha_1(t)|^2 + |\beta_1(t)|^2 + \int_{-\infty}^{\infty} |R_{g,1}(\omega', t)|^2 + |R_{e,1}(\omega', t)|^2 d\omega' \right], \quad (3.17)$$

where, from (3.11):

$$\begin{aligned} R_{g,1}(\omega, t) &= -iG(\omega) \int_0^t e^{i\omega(t-t')} \mathbf{E}_{g,1} \cdot \mathbf{n}(t, t') dt', \\ R_{e,1}(\omega, t) &= -iG(\omega) \int_0^t e^{i\omega(t-t')} \mathbf{E}_{e,1} \cdot \mathbf{n}(t, t') dt', \end{aligned} \quad (3.18)$$

where $\mathbf{E}_{g,1}$ and $\mathbf{E}_{e,1}$ are the third and fourth rows of \mathbf{E} , respectively. Thus, we need the integral

$$I_{\mu,1} = \int_{-\infty}^{\infty} R_{\mu,1}^*(\omega', t) R_{\mu,1}(\omega', t) d\omega', \quad (3.19)$$

where $\mu = g$ or e , which expands as

$$I_{\mu,1} = \int_0^t \int_0^t [\mathbf{E}_{\mu,1} \cdot \mathbf{n}(t, t'')]^* [\mathbf{E}_{\mu,1} \cdot \mathbf{n}(t, t')] \int_{-\infty}^{\infty} G^2(\omega') e^{-i\omega'(t''-t)} e^{i\omega'(t'-t)} d\omega' dt' dt''. \quad (3.20)$$

Substituting the exponential form of $G(\omega')$, we subsequently carry out the integration over frequency to arrive at

$$\begin{aligned} I_{\mu,1} &= \frac{\gamma_L}{4} \int_0^t \int_0^t dt' dt'' [\mathbf{E}_{\mu,1} \cdot \mathbf{n}(t, t'')]^* [\mathbf{E}_{\mu,1} \cdot \mathbf{n}(t, t')] \\ &\quad \times [2\delta(t'' - t') - e^{i\phi} \delta(t'' - \tau - t') - e^{-i\phi} \delta(t'' + \tau - t')]. \end{aligned} \quad (3.21)$$

Finally, the integral with respect to t' is carried out to yield a sum of three terms:

$$\begin{aligned}
 I_{\mu,1} = & \frac{\gamma_L}{4} \left[\int_0^t 2|\mathbf{E}_{\mu,1} \cdot \mathbf{n}(t, t'')|^2 dt'' \right. \\
 & - e^{i\phi} \int_\tau^t (\mathbf{E}_{\mu,1} \cdot \mathbf{n}(t, t''))^* (\mathbf{E}_{\mu,1} \cdot \mathbf{n}(t, t'' - \tau)) dt'' \\
 & \left. - e^{-i\phi} \int_0^{t-\tau} (\mathbf{E}_{\mu,1} \cdot \mathbf{n}(t, t''))^* (\mathbf{E}_{\mu,1} \cdot \mathbf{n}(t, t'' + \tau)) dt'' \right]. \tag{3.22}
 \end{aligned}$$

It is readily shown that the second and third terms are complex conjugates of one another so there are just two integrals to compute in a numerical implementation. From (3.17) and the similar result for the expectation of $C_1^\dagger C_1$, we now have:

$$\begin{aligned}
 \langle \tilde{\psi}(t) | C_0^\dagger C_0 | \tilde{\psi}(t) \rangle &= \gamma_C [|\alpha_1(t)|^2 + |\beta_1(t)|^2 + I_{g,1} + I_{e,1}], \tag{3.23} \\
 \langle \tilde{\psi}(t) | C_1^\dagger C_1 | \tilde{\psi}(t) \rangle &= \gamma_T [|\beta_0(t)|^2 + |\beta_1(t)|^2 + I_{e,0} + I_{e,1}].
 \end{aligned}$$

Although derived in a similar way, the expectation of $\mathcal{E}_+^\dagger(L/2)\mathcal{E}_+(L/2)$ does not require integrals over the past time and is

$$\begin{aligned}
 \langle \tilde{\psi}(t) | \mathcal{E}_+^\dagger(L/2)\mathcal{E}_+(L/2) | \tilde{\psi}(t) \rangle &= \frac{\gamma_L}{4} \times \\
 & \sum_{\mu=\{g,e\}} \sum_{n=0}^1 |\mathbf{E}_{\mu,n} \cdot \mathbf{n}(t, t) - e^{i\phi}\theta(t-\tau)\mathbf{E}_{\mu,n} \cdot \mathbf{n}(t, t-\tau)|^2. \tag{3.24}
 \end{aligned}$$

3.3.4 Applying the Quantum Jump Operator

Once a jump is determined to occur and the type of jump chosen using the relative probabilities, one of the jump operators is applied to the system state. For the purposes of illustration, let us assume that a cavity jump occurred and $C_0 = \sqrt{\gamma_C}c$ operates on the system state. The new un-normalized ket vector, at time t_0 , following

the time step in which the jump occurred, is

$$\begin{aligned}
 |\tilde{\psi}(t_0)\rangle = & \sqrt{\gamma_C} \left\{ [\alpha_1(\bar{t}_0) |g\rangle + \beta_1(\bar{t}_0) |e\rangle] |\{0\}\rangle \right. \\
 & \left. + \int_{-\infty}^{\infty} [R_{g,1}(\omega', \bar{t}_0) |g\rangle + R_{e,1}(\omega', \bar{t}_0) |e\rangle] |1, \omega'\rangle d\omega' \right\} |0\rangle_C.
 \end{aligned} \tag{3.25}$$

where $\bar{t}_0 \equiv t_0 - \delta t$; thus the new nonzero amplitudes are

$$\begin{aligned}
 \alpha_0(t_0) &= \sqrt{\gamma_C} \alpha_1(\bar{t}_0), \\
 \beta_0(t_0) &= \sqrt{\gamma_C} \beta_1(\bar{t}_0), \\
 R_{g,0}(\omega, t_0) &= \sqrt{\gamma_C} R_{g,1}(\omega, \bar{t}_0), \\
 R_{e,0}(\omega, t_0) &= \sqrt{\gamma_C} R_{e,1}(\omega, \bar{t}_0),
 \end{aligned} \tag{3.26}$$

while, furthermore, for $t > t_0$, the amplitudes $R_{\mu,n}(\omega, t)$ are given by:

$$\begin{aligned}
 iG^{-1}(\omega)R_{g,0}(\omega, t) &= \int_{t_0}^t e^{i\omega(t'-t)} \mathbf{E}_{g,0} \cdot \mathbf{n}(t, t') dt' \\
 &+ \sqrt{\gamma_C} \left[\int_0^{\bar{t}_0} e^{i\omega(t'-t)} \mathbf{E}_{g,1} \cdot \mathbf{n}(\bar{t}_0, t') dt' \right], \\
 iG^{-1}(\omega)R_{e,0}(\omega, t) &= \int_{t_0}^t e^{i\omega(t'-t)} \mathbf{E}_{e,0} \cdot \mathbf{n}(t, t') dt' \\
 &+ \sqrt{\gamma_C} \left[\int_0^{\bar{t}_0} e^{i\omega(t'-t)} \mathbf{E}_{e,1} \cdot \mathbf{n}(\bar{t}_0, t') dt' \right], \\
 iG^{-1}(\omega)R_{g,1}(\omega, t) &= \int_{t_0}^t e^{i\omega(t'-t)} \mathbf{E}_{g,1} \cdot \mathbf{n}(t, t') dt', \\
 iG^{-1}(\omega)R_{e,1}(\omega, t) &= \int_{t_0}^t e^{i\omega(t'-t)} \mathbf{E}_{e,1} \cdot \mathbf{n}(t, t') dt'.
 \end{aligned} \tag{3.27}$$

Thus, both $R_{g,1}$ and $R_{e,1}$ are reset after the jump, while $R_{g,0}$ and $R_{e,0}$ carry the memory of $R_{g,1}$ and $R_{e,1}$ immediately prior to the jump through their initial values at time t_0 .

This suggests a convenient strategy for implementing $-i \int_{-\infty}^{\infty} G(\omega') R_{\mu,0}(\omega', t) d\omega'$ in the evolution of α and β following a jump. For the time interval of length τ

following a jump, the terms $\mathbf{E}_{g,0} \cdot \mathbf{n}(t, t - \tau)$ and $\mathbf{E}_{e,0} \cdot \mathbf{n}(t, t - \tau)$ are replaced by $\mathbf{E}_{g,1} \cdot \mathbf{n}(t, t - \tau)$ and $\mathbf{E}_{e,1} \cdot \mathbf{n}(t, t - \tau)$, respectively. This occurs because after the jump the value of $R_{g,0}$ and $R_{e,0}$ evaluated at a time τ in the past lands in the integrals from zero to \bar{t}_0 in (3.27). Care must also be taken when computing the $I_{g,0}$ and $I_{e,0}$ integrals to ensure that the nonzero overlap of the time integrals is considered when numerically evaluating these quantities.

When a quantum jump down the waveguide is determined to occur – i.e., when we apply $\mathcal{E}_+(L/2)$ to the system – a reset of the memory occurs; that is, the history up to that point can be thrown away. Specifically, this means that the integrals over all past time restart and we only need to calculate them starting from the jump time, t_0 . We define $|\tilde{\psi}_{\text{reset}}(t_0)\rangle = \mathcal{E}_+(L/2) |\tilde{\psi}(\bar{t}_0)\rangle$ to be the unnormalized state of the system after such a jump, where the label “reset” is used to denote the memory reset that accompanies this jump. This state is

$$|\tilde{\psi}_{\text{reset}}(t_0)\rangle = \frac{-i\sqrt{\gamma_L}}{2} \sum_{\mu=\{g,e\}} \sum_{n=0}^1 \{ \mathbf{E}_{\mu,n} \cdot \mathbf{n}(\bar{t}_0, \bar{t}_0) - e^{i\phi}\theta(\bar{t}_0 - \tau) [\mathbf{E}_{\mu,n} \cdot \mathbf{n}(\bar{t}_0, \bar{t}_0 - \tau)] \} |\mu\rangle |n\rangle_C |\{0\}\rangle. \quad (3.28)$$

3.3.5 Conditioning in the Presence of Feedback

Due to the non-Markovian nature of the output channel $\mathcal{E}_+(L/2)$, the populations of the system must be conditioned on no jump occurring in a different way to typical Markovian output channels such as C_0 . Rather than introducing a non-unitary part to the system Hamiltonian (since photon loss from the feedback loop is not of Lindblad form), the conditioning is implemented explicitly by hand. We argue from the standard theory of photon counting, specifically, from the conditional probability for a count in the interval $[t, t + \delta t)$, *given* no count in the interval since the last count, $[t_0, t)$. This probability is the ratio of two unconditional probabilities:

$$P(C_{[t,t+\delta t)} | \text{NC}_{[t_0,t)}) = \frac{P(C_{[t,t+\delta t)} \wedge \text{NC}_{[t_0,t)})}{P(\text{NC}_{[t_0,t)})}, \quad (3.29)$$

with

$$\begin{aligned} P(C_{[t,t+\delta t)} \wedge \text{NC}_{[t_0,t)}) & \\ &= \text{tr}_{\text{S} \otimes \text{W}} \left\{ \left[\mathcal{E}_+^\dagger(L/2) \mathcal{E}_+(L/2) + \sum_{i=0}^1 C_i^\dagger C_i \right] \tilde{\chi}(t) \right\} \delta t \end{aligned} \quad (3.30)$$

the probability for a count in $[t, t + \delta t)$ and no count in $[t_0, t)$, and

$$P(\text{NC}_{[t_0,t)}) = \text{tr}_{\text{S} \otimes \text{W}}[\tilde{\chi}(t)] \quad (3.31)$$

the probability for no count in $[t_0, t)$, where the trace is taken over the system S and waveguide W, and

$$\tilde{\chi}(t) = e^{[\mathcal{L} - \mathcal{E}_+(L/2) \cdot \mathcal{E}_+^\dagger(L/2)](t-t_0)} \chi(t_0), \quad (3.32)$$

with $\mathcal{L} = -i[H_{\text{eff}}, \cdot]$ and $\chi(t_0) = |\psi(t_0)\rangle \langle \psi(t_0)|$; for the explicit expressions see Appendix A of Carmichael 1987. We may now extract the normalized state $\tilde{\chi}(t)/\text{tr}_{\text{S} \otimes \text{W}}[\tilde{\chi}(t)]$ from (3.29)-(3.31), and hence the system state conditioned on no count in the interval $[t_0, t)$

$$\rho(t) = \frac{\text{tr}_{\text{W}}[\tilde{\chi}(t)]}{\text{tr}_{\text{S} \otimes \text{W}}[\tilde{\chi}(t)]}, \quad (3.33)$$

where, under the approximation of only one photon in the feedback loop at any time, a first-order Dyson expansion yields

$$\tilde{\chi}(t) = |\tilde{\psi}(t)\rangle \langle \tilde{\psi}(t)| - \int_{t_0}^t e^{\mathcal{L}(t-t')} |\tilde{\psi}_{\text{reset}}(t')\rangle \langle \tilde{\psi}_{\text{reset}}(t')| dt'. \quad (3.34)$$

Note that $\rho(t)$ is normalized, so desired observable expectations can be calculated from this quantity.

This process is computationally demanding and can quickly cause the trajectories to take significant amounts of time to run. The interaction with the feedback loop is therefore dropped from \mathcal{L} , which is a good approximation under the assumption of

at most one photon in the loop – i.e. $\mathcal{L} \longrightarrow \mathcal{L}_0 = -i[H_{\text{eff}}^0, \cdot]$, where

$$\begin{aligned} H_{\text{eff}}^0 &= \delta_{aL}\sigma^+\sigma^- + \delta_{cL}c^\dagger c + g(\sigma^+c + c^\dagger\sigma^-) \\ &+ \Omega(\sigma^+ + \sigma^-) - \frac{i}{2} [\gamma_C a^\dagger a + \gamma_T \sigma^+ \sigma^-]. \end{aligned} \quad (3.35)$$

After making this approximation, when $\gamma_C = \gamma_T = 0$ the denominator of (3.33) reduces to the probability that no photon has travelled to the right down the waveguide (left the system) since the last jump, i.e., to $1 - P_{\mathcal{E}_+(L/2)}(t)$, where $P_{\mathcal{E}_+(L/2)}(t)$ is the integrated probability of jump $\mathcal{E}_+(L/2)$.

3.4 Numerical Implementation

We implemented this algorithm in MATLAB employing the Parallel Computing Toolbox (though it could readily be implemented in other computational languages such as PYTHON). The matrices \mathbf{E} and $\boldsymbol{\lambda}$ are first computed from the provided system parameters, and then passed to a parallelized for-loop which runs the QT simulations; since each QT is independent of the others, this calculation is readily parallelized, which leads to a significant saving in computation time. Once the desired ensemble of expectations has been obtained, it is passed back to the main program to be averaged. The approach would work in a similar way with no parallelization, on a single processor, although the computation time would more quickly become prohibitive with increasing complexity of the system.

The QT simulation evolves the provided initial state through enough time steps of sufficient resolution to reach the desired end time. At the start of each time step, the waiting-time distribution, $w(t')$, for a jump to occur is evaluated and the integrated probability, $P(t) = \int_{t_0}^t w(t')dt'$ where t_0 is the time of the last jump, is compared against a uniformly distributed random number ϵ : if $\epsilon < P(t)$, a jump is implemented, with the jump operator selected on the basis of a second uniformly distributed random number and the relative jump probabilities from the most recent time step; otherwise the system state is advanced one time step by a modified fourth-order Runge-Kutta

algorithm (Butcher 2008) (RK4) applied to the equations of motion from Sec. 3.3.2 – note that RK4 makes two evaluations of $\mathbf{n}(t, t - \tau + \delta t/2)$, which is unavailable, and we therefore substitute $\mathbf{n}(t, t - \tau)$ for the first evaluation and $\mathbf{n}(t, t - \tau + \delta t)$ for the second. Since we are using the integrated probability for a jump at time t' and no jump prior to t' (waiting-time distribution), the state is only renormalized after a jump occurs. After the trajectory has completed, the conditioning is done on the system and any desired expectations – e.g., the population in the TLS, or photon population in the cavity or feedback loop – can be calculated.

The integrals $I_{\mu,n}$, for $\mu = \{g, e\}$ and $n = 0, 1$, must be evaluated once each time step. As they extend over the entire past, they make the largest demand on computation time, which scales quadratically, as a result, with the number of time steps. Since the algorithm scales linearly with the number of QTs, it is more efficient to average many QTs with coarse time resolution than fewer with fine time resolution. An optimized numerical technique for QTs when our system is simplified is presented in Appendix 3.8.4.

3.5 Results

Throughout the results section, we will refer to the TLS population and the cavity population, defined explicitly through the quantities $n_a = \langle \psi(t) | \sigma^+ \sigma^- | \psi(t) \rangle$ and $n_c = \langle \psi(t) | c^\dagger c | \psi(t) \rangle$, respectively.

3.5.1 Replication of Previous Results and Quantum Trajectory Insights

To first demonstrate the accuracy of this approach, the numerical model was tested under regimes where the response of the system is already known, or studied elsewhere using different approaches (not QT). Figure 3.3(a) shows the model as an isolated cavity-TLS system (i.e., $\gamma_L = \gamma_T = \gamma_C = \Omega = 0$) and everything is on resonance, while Fig. 3.3(b) adds in the waveguide without feedback (i.e., the long loop limit when $\tau \rightarrow \infty$) and with $\gamma_L = g$. Note that Fig. 3.3(b) is created by averaging 1000 trajectories, while Fig. 3.3(a) is created with a single trajectory. This is because

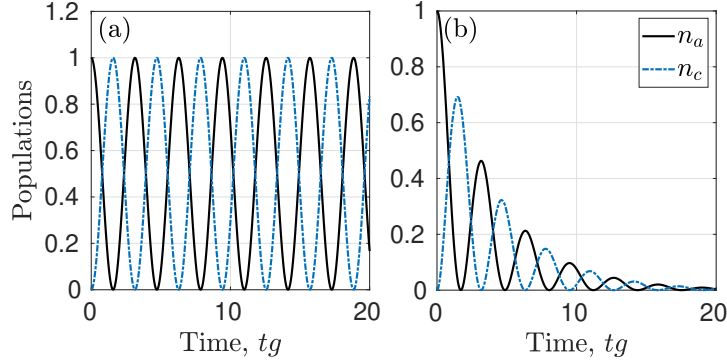


Figure 3.3: Evolution of the cavity-TLS using the derived QT approach with no feedback loop or drive. The TLS is initially in its excited state so that $\beta_0(t=0) = 1$. In (a), there is no output and vacuum Rabi oscillations occur, while in (b) there is a non-zero output rate ($\gamma_L = g$) and decaying Rabi oscillations are produced.

without a stochastic decay channel all trajectories will be identical, and so Fig. 3.3(a) can be created with one trajectory. Since Fig. 3.3(b) does include a decay channel, an average must be taken in order to recover the ensemble behaviour of the system. These results indeed replicate this relatively simple aspect of cavity-TLS systems (Ashhab et al. 2006).

Furthermore, the cavity was removed from the model and the TLS coupled directly to the waveguide in order to recover previously studied results (Dorner and Zoller 2002; Tufarelli et al. 2013; S. J. Whalen 2019; Droenner et al. 2019). As shown in Fig. 3.4(a), by tuning the phase of the feedback loop the system can be made to exhibit enhanced spontaneous emission, when $\phi = \pi$, or trap the excitation, when $\phi = 0$, as long as there are no other losses, $\gamma_T = \gamma_C = 0$. Before $t = \tau = g^{-1}$, the time delay introduced by the feedback, the dynamics are identical in all three cases shown as the TLS simply decays. However, as soon as the feedback is first introduced, the dynamics completely change due to interference between the departing and returning fields emitted by the TLS. The same phenomenon can be seen when the cavity is replaced as part of the system, shown in Fig. 3.4(b), however rather than stabilizing either the TLS or cavity population, the Rabi oscillations are stabilized.

For both of the trapping regimes presented in Fig. 3.4 there are two types of trajectories that are being averaged together as shown in Figs. 3.5(a) and 3.5(b).

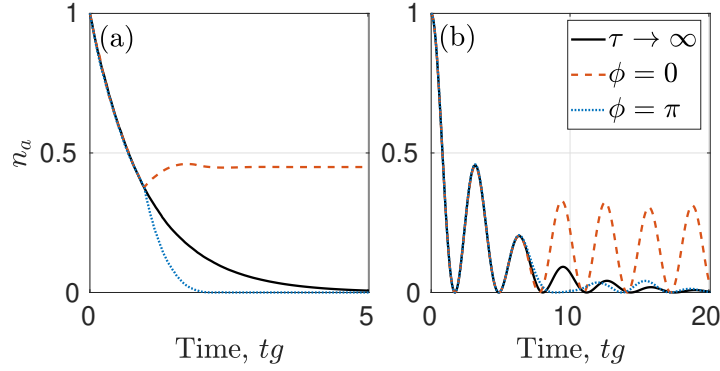


Figure 3.4: Population dynamics showing the effect of feedback with different ϕ , when (a) the system consists of a TLS and (b) the system is a cavity-TLS setup discussed in Sec. 3.2. Everything is on resonance and there is no drive or Lindblad decay channels; in (a) $\tau = g^{-1}$ and $\gamma_L = 2g$ while in (b) $\tau = 2\pi g^{-1}$ and $\gamma_L = g$. Each set of results is an average of 2000 QTs.

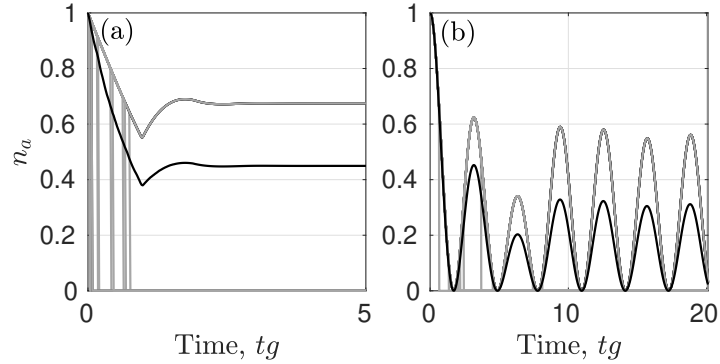


Figure 3.5: Sample trajectories for the trapping regimes, $\phi = 0$, of Figs. 3.4(a) and 3.4(b). The averaged TLS population is given in black while the individual trajectories are in grey. Note that if the system does not emit a photon to the right (shown by a jump of n_a to 0) before the feedback returns then the excitation becomes trapped in the system.

The individual trajectories for each case are overlaid in grey in the figures; either the system decays and the jump $\mathcal{E}_+(L/2)$ would occur or the jump does not occur and we are left with a trapped excitation. Note that the jump only occurs before the feedback has returned from its first round trip, after this time the excitation is trapped if the jump has not occurred. The final average, shown in black, is the average of the trajectories sitting in the ground state and the trajectories with a trapped excitation.

Lastly, the recent results by N emet *et al.* (N emet, Carmele, et al. 2019) are also

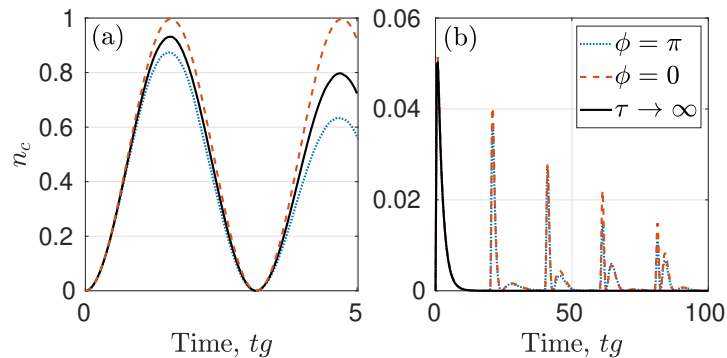


Figure 3.6: Population dynamics of (a) a short delay time ($\tau = 0.1g^{-1}$) and (b) a long delay time ($\tau = 20g^{-1}$). Both sets of results are the average of 2000 QTs with everything on resonance and no drive or Lindblad decay channels. The decay rate into the waveguide is (a) $\gamma_L = 0.2g$ and (b) $\gamma_L = 5\pi g$.

recovered by this approach as shown in Fig. 3.6. In this setup, the effects of a very short or very long feedback loop were investigated. When the delay time is very small compared to the lifetime of the system, the phase change, ϕ , from the loop has an immediate and significant effect on the system as shown in Fig. 3.6(a). Figure 3.6(b) shows the dynamics for a delay time which is longer than the lifetime of the system. In this case the feedback acts to reintroduce the excitation to the system, in a short pulse, rather than to stabilize or enhance the decay. The phase also becomes much less important and has little effect on the system. This is because the cavity-TLS is essentially in the ground state when the feedback returns; there is no emission for the returning pulse to interfere with.

By replicating these previously studied results – each addressing its own solution space – in our QT formalism, we validate the method for the study of feedback effects in cavity-QED systems, at least within the scope of the stated approximations. We have also added extra insight into these regimes by showing example QT graphs and stochastic dynamics.

3.5.2 Investigation of the Effect of the Feedback Loop on Excitation Trapping

In the previous section, enhanced spontaneous emission was shown to occur when $\phi = \pi$ and stabilized populations were shown when $\phi = 0$. Which behaviour occurs is not only dependent on the phase, but also the length of the loop, as shown in Fig. 3.7. The peaks in each curve represent the phase at which stabilized populations occur at the chosen loop length. Conversely the troughs of the curve represent regions where enhanced spontaneous emission can be found. Note that the height of the peaks of each curve is dependent on the length of the loop as well. Since the system is an initially excited TLS allowed to decay with no drive, the longer loop lengths essentially “store” population so the stabilized values are lower. Furthermore, the longer feedback time creates more time for the system to decay to the right (and thus out of the system) before the feedback returns.

The location of the peaks in Fig. 3.7 is dependent on the phase required to return the reflected field out of phase with the field emitted by the system in order to suppress net emission down the waveguide to the right – the field $\mathcal{E}_+(L/2)$ in Fig. 3.2. When $g\tau = \pi$ or 2π , this only occurs at one phase, $\phi = \pi$ or 0 respectively, and leads to stabilized Rabi oscillations as shown in Figs. 3.8(a) and 3.8(b). However, when $g\tau = \pi/2$, this stabilization happens at two different phases, $\phi = \pi/2$ and $3\pi/2$. This is because when $\tau = \pi/2$ there is both a real and imaginary component to $\alpha_1(t)$ and so the two phases act to match – and stabilize – their respective component. However, since only one component can be matched for each ϕ , the coherence of the Rabi oscillations is lost and a steady state population – trapped superposition of the TLS and cavity – is reached as shown in Figs. 3.8(c) and 3.8(d). The general condition to achieve excitation trapping, derived in Appendix 3.8.4, is given by $\pm g\tau - \phi = 2\pi k$ for $k \in \mathbb{Z}$. Note that when there is only one unique solution for ϕ , as is the case when $g\tau = \pi n$ or $g\tau = 2\pi n$ for $n \in \mathbb{Z}$, then stabilized Rabi oscillations occur. If there is more than one unique solution, then the coherent oscillation is lost and a steady state population is reached. Also, when ϕ is moved off of the perfect condition for

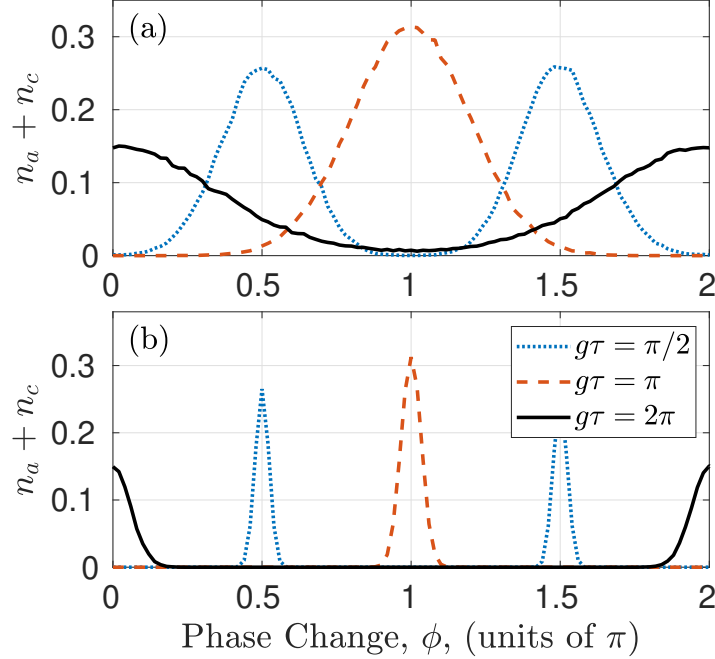


Figure 3.7: Mean populations of the cavity and TLS at finite t , as a function of phase, for (a) $t = 30g^{-1}$ and (b) $t = 1000g^{-1}$, averaged over 10000 QTs. These QTs were calculated using the optimized technique outlined in Appendix 3.8.4. By varying the phase change, ϕ , of the feedback loop, the optimized phase to improve the lifetime of the system excitation can be found which is different for each loop length. Three example loop lengths are plotted in the figures, defined by the values of $g\tau$ in the legend. The output to the waveguide for each loop length is $\gamma_L = 2g$ with everything on resonance, no drive, and no other Lindblad outputs.

a trapped excitation, the system excitation will decay away at a rate dependent on how close the parameters are to perfect trapping. In Fig. 3.7(a), the system evolution is truncated at $t = 30g^{-1}$ while in Fig. 3.7(b) it is truncated after a longer time, at $t = 1000g^{-1}$, and the width of the peaks decreases while the heights remain the same. If $t \rightarrow \infty$, we would be left with a series of delta functions rather than peaks of finite width when we truncate at finite t .

Figure 3.9 shows this relationship when we fix the phase and allow the delay time to vary. The system oscillates between periods of stabilized Rabi oscillations and enhanced spontaneous emission as the loop length increases. The height of each peak is also decreasing as the delay time grows due to more population being held in the

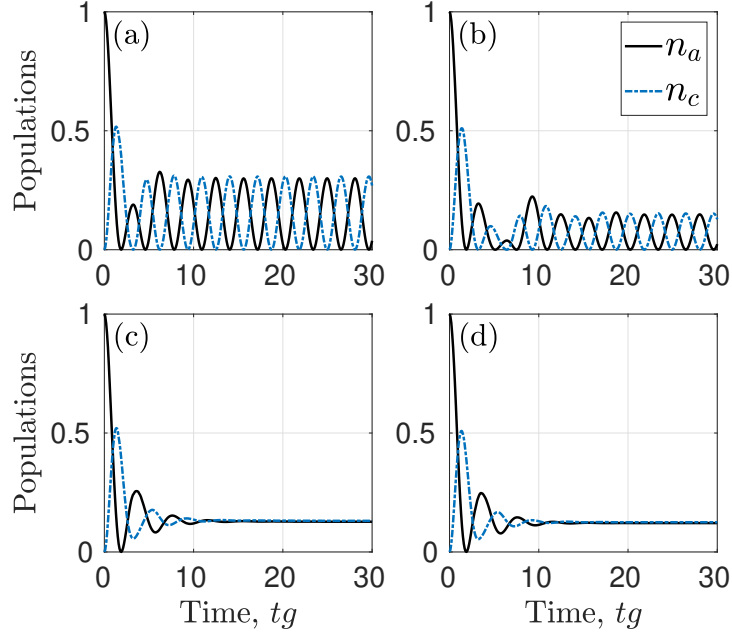


Figure 3.8: Populations dynamics showing the excitation trapping for different delay times and the required respective phases: (a) $\tau = \pi g^{-1}, \phi = \pi$, (b) $\tau = 2\pi g^{-1}, \phi = 0$, (c) $\tau = (\pi/2)g^{-1}, \phi = \pi/2$, and (d) $\tau = (\pi/2)g^{-1}, \phi = 3\pi/2$. Each example is an average of 1000 QTs with $\gamma_L = 2g$, everything is on resonance, and there is no drive or other Lindblad output channels.

loop rather than in the system and increased time for the system to decay before the feedback returns. As discussed with Fig. 3.6, when the loop length is increasing the effect of the phase on the system becomes less pronounced. This is seen here through the broadening of each peak as coherence is lost due to the longer round-trip time.

3.5.3 Nonlinear Cavity-QED Effects

So far, all of these results have been simulated by setting an initial condition of an excited TLS in vacuum. Since the pump has been turned off, $\Omega = 0$, effectively the system has only had one quanta in it (maximum). Thus the system is essentially linear, and the solution can usually always be solved trivially using frequency-space techniques (e.g., see Hughes 2007) or using an analysis of the delay differential equations (e.g., see Kabuss et al. 2015). By turning on the pump beyond a weak excitation, the higher order states of the system can be populated. For example, the $|e\rangle |1\rangle_C |\{0\}\rangle$

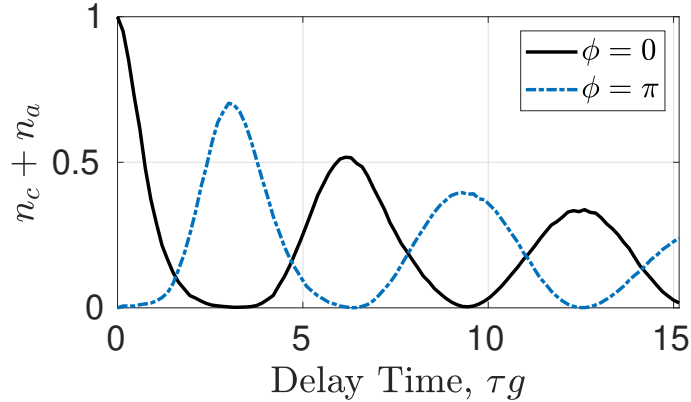


Figure 3.9: Average populations at time $t = 20g^{-1}$ for different delay times, τ . As the delay time is longer, less population is held in the cavity-TLS as it spends more time in the loop. The output to the waveguide for each loop length is $\gamma_L = 0.5g$ with everything on resonance, no drive, and no other Lindblad outputs. Each point is the population in the cavity-TLS (at $t = 20g^{-1}$) averaged over 10000 QTs generated using the technique outlined in Appendix 3.8.4.

state (i.e., an excited TLS and one photon in the cavity with no photon in the loop) or the $|e\rangle|0\rangle_C|1, \omega\rangle$ state (i.e., an excited TLS and one photon in the feedback with the cavity in the vacuum state) will be populated. Therefore, by turning on the pump we can begin to look at multiquanta effects in this system, which cannot be modelled semiclassically, or using the usual weak-excitation approximations.

The system is driven at moderate field strength, $\Omega = 0.1g$, in order to remain within the one photon in the loop approximation while also beginning to see non-linear effects in the system. Figure 3.10 shows the cavity photoluminescence spectrum (proportional to the cavity population) of the system with and without feedback when the cavity and TLS have a detuning of g . Without feedback, there are only two peaks present, the stronger peak on the left coming from the resonance of the TLS and the weaker peak on the right coming from the cavity resonance. When the feedback is added to the system there is significant enhancement of the two peaks, especially of the cavity resonance due to the feedback returning and stabilizing the cavity population rather than it decaying away.

There are also new peaks that arise from the inclusion of feedback-induced dressed

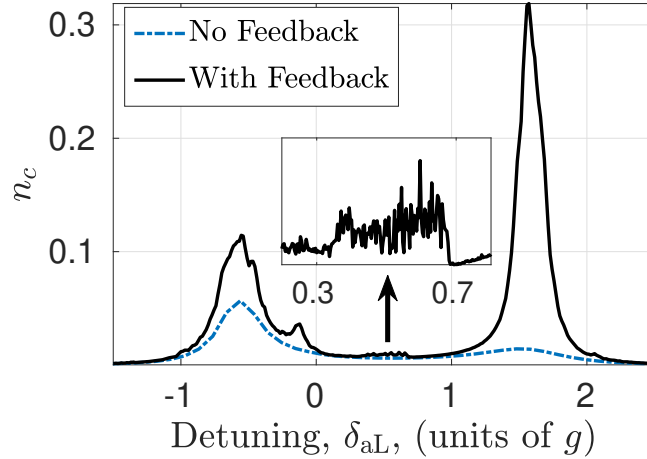


Figure 3.10: By scanning the detuning from the laser, of strength $\Omega = 0.1g$, the cavity photoluminescence spectrum (proportional to the cavity population) is found by plotting the steady-state population of the cavity as a function of detuning. The decay channels have rates $\gamma_L = 2g$, $\gamma_C = 0.05g$, and $\gamma_T = 0.01g$. The delay time is $\tau = g^{-1}$ and there is no phase introduced by the loop, $\phi = 0$. The detuning between the cavity and TLS is g , so that $\delta_{aL} = \delta_{cL} + g$. Each point is the average of 1500 QTs. The peak introduced by the feedback state is highlighted in the inset at higher detuning resolution.

states, which cause additional resonances near $\delta_{aL} \sim -0.5g$. These additional peaks are not seen without feedback and are due to the nonlinear behaviour introduced and enhanced by the feedback loop. With a stronger pump these non-linear effects will be easier to identify; however, in order to use a stronger pump, higher orders of quanta will need to be allowed in the feedback loop which will be addressed in future work. There are also peaks introduced by the feedback state, $|g\rangle|0\rangle_C|1, \omega\rangle$, shown in the inset of Fig. 3.10. These peaks occur because of round-trip resonances in the feedback loop (Yao and Hughes 2009), which appear at $\pm 1/\tau = \pm ng$ (with $n \in \mathbb{Z}$), and we see some signatures of such a retardation peak near $\delta_{aL} \sim 0.5g$.

It is also important to recognize the importance of correctly conditioning the populations in the presence of the feedback loop. Figure 3.11 compares the technique of conditioning outlined in Sec. 3.3.5 with the typical renormalization used in Markovian QT theory. In Fig. 3.11(a) the damping of the Rabi oscillations without conditioning is much faster than when the populations are properly conditioned.

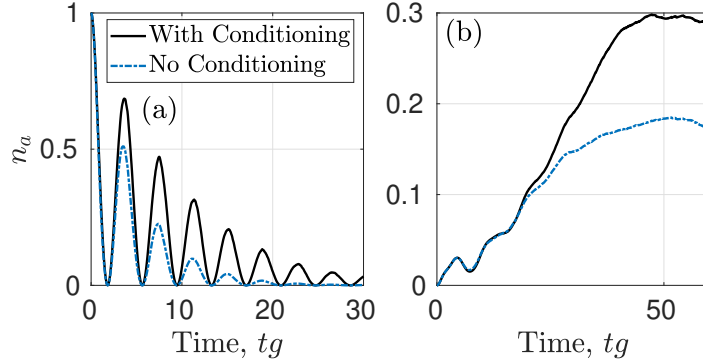


Figure 3.11: A comparison of the system dynamics with and without conditioning. (a) Decaying Rabi oscillations when $\gamma_L = 2g$, with no other Lindblad output channels or drive and everything on resonance. The delay time is $\tau = g^{-1}$ without a phase change, $\phi = 0$. (b) The system driven by a weak pump, $\Omega = 0.1g$, with decay rates of $\gamma_L = 2g$, $\gamma_C = 0.05g$, $\gamma_L = 0.01g$, and a detuning of $\delta_{aL} = \delta_{cL} + g$. The delay time is $\tau = \pi g^{-1}$ and has an overall phase change of $\phi = \pi$. Both figures are an average of 1000 QTs.

Indeed, without conditioning it seems as if there is negligible population left in the system at $t = 30g^{-1}$, but when calculated properly there are still significant Rabi oscillations occurring with the system. When a drive is introduced to the system as in Fig. 3.11(b), if conditioning is not done properly then not only the incorrect dynamics but also the incorrect steady state population will be found. This is important in order to calculate the correct spectra for the system.

3.6 Conclusions

We have presented a QT formalism for simulating the evolution of cavity-QED systems with coherent optical feedback. The equations of motion required to evolve such a system under QT theory are developed and the key quantities required in the numerical simulation are derived. Previous results are recovered using these equations of motion to confirm the accuracy of our derived approach, with QT insights into the stochastic dynamics. Results in the single quanta regime and nonlinear regime are then presented to show the potential of coherent optical feedback to stabilize nonlinear cavity-QED systems and increase their coherent lifetimes. Possible areas of future work for developing this approach with coherent feedback, include extending

our model to allow for more than one photon in the loop and computing nonlinear spectra produced from the system.

3.7 Acknowledgements

This work was supported by the Natural Sciences and Engineering Research Council of Canada, the Canadian Foundation for Innovation and Queen's University. H.J.C. acknowledges the support of the New Zealand Tertiary Education Committee through the Dodd-Walls Centre for Photonic and Quantum Technologies.

3.8 Appendices

3.8.1 Appendix A: Deriving the Feedback Coupling Term

As denoted in Fig. 3.2 we set the location of the mirror to be $z = 0$, and so the free field in the waveguide at a point z is given by

$$\mathcal{E}(z) = \mathcal{E}_-(z) + \mathcal{E}_+(z), \quad (3.36)$$

where $\mathcal{E}_-(z)$ and $\mathcal{E}_+(z)$ are the left and right propagating waves, respectively. The form of these fields is given by

$$\mathcal{E}_\pm(z) = \mp \frac{i}{\sqrt{2\pi}} \int_{-\infty}^{\infty} e^{\pm i\omega z/c} r(\omega) d\omega. \quad (3.37)$$

Then since the cavity couples to the waveguide at $z = L/2$, we are interested in

$$\mathcal{E}_\pm(L/2) = \mp \frac{i}{\sqrt{2\pi}} \int_{-\infty}^{\infty} e^{\pm i\omega\tau/2} r(\omega) d\omega, \quad (3.38)$$

where we introduce $\tau = L/c$. The interaction between the cavity and this field at $z = L/2$ is thus given by

$$H_{\text{int}} = \sqrt{\gamma L} \left(c^\dagger \frac{\mathcal{E}_-(L/2) + \mathcal{E}_+(L/2)}{2} + \text{H.c.} \right), \quad (3.39)$$

where H.c. is the Hermitian conjugate. Now plugging in the form of $\mathcal{E}_\pm(L/2)$ from (3.38) and converting the sum of exponentials into the sine function we have

$$H_{\text{int}} = \sqrt{\frac{\gamma_L}{2\pi}} \int_{-\infty}^{\infty} \{ \sin(\omega\tau/2) [c^\dagger r(\omega) + \text{H.c.}] \} d\omega. \quad (3.40)$$

Lastly we need to move into the interaction picture and so we write $\omega = \omega' + \omega_L$ and let $r(\omega' + \omega_L) \rightarrow r(\omega')$, to get

$$H_{\text{int}} = \sqrt{\frac{\gamma_L}{2\pi}} \int_{-\infty}^{\infty} \{ \sin[(\omega'\tau + \phi)/2] [c^\dagger r(\omega') + \text{H.c.}] \} d\omega', \quad (3.41)$$

where $\phi = \omega_L\tau/2$, and the frequency dependent coupling constant is $G(\omega') = \sqrt{\gamma_L/2\pi} \sin[(\omega'\tau + \phi)/2]$.

3.8.2 Appendix B: Deriving (3.11)

We begin deriving (3.11) from the differential equation presented in (3.9). It is clear from the structure of \mathbf{A} that it is diagonalizable and more importantly that \mathbf{A} has four eigenvalues. These eigenvalues are labelled as $\lambda_1, \lambda_2, \lambda_3$, and λ_4 and their corresponding eigenvectors as $\mathbf{\Lambda}_1, \mathbf{\Lambda}_2, \mathbf{\Lambda}_3$, and $\mathbf{\Lambda}_4$. Then

$$\mathbf{A}\mathbf{\Lambda}_k = \lambda_k\mathbf{\Lambda}_k = \mathbf{\Lambda}_k\lambda_k, \quad k = 1, 2, 3, 4. \quad (3.42)$$

Now define a new matrix \mathbf{E} where each column is an eigenvector of \mathbf{A} ,

$$\mathbf{E} = [\mathbf{\Lambda}_1, \mathbf{\Lambda}_2, \mathbf{\Lambda}_3, \mathbf{\Lambda}_4], \quad (3.43)$$

so then

$$\mathbf{A}\mathbf{E} = \mathbf{E} \begin{bmatrix} \lambda_1 & 0 & 0 & 0 \\ 0 & \lambda_2 & 0 & 0 \\ 0 & 0 & \lambda_3 & 0 \\ 0 & 0 & 0 & \lambda_4 \end{bmatrix} = \mathbf{E}\boldsymbol{\lambda}. \quad (3.44)$$

The decoupled variables are thus $\mathbf{u} = \mathbf{E}^{-1}\mathbf{R}$ so that $\mathbf{R} = \mathbf{E}\mathbf{u}$. Substituting this

into (3.9) gives

$$\frac{d}{dt}\mathbf{E}\mathbf{u} = \mathbf{A}\mathbf{E}\mathbf{u} - iG(\omega)\boldsymbol{\alpha}\boldsymbol{\beta}, \quad (3.45)$$

and since \mathbf{E} is time independent (because all entries of \mathbf{A} are time independent) both sides can be multiplied by \mathbf{E}^{-1} to get

$$\frac{d}{dt}\mathbf{u} = \mathbf{E}^{-1}\mathbf{A}\mathbf{E}\mathbf{u} - iG(\omega)\mathbf{E}^{-1}\boldsymbol{\alpha}\boldsymbol{\beta}. \quad (3.46)$$

Furthermore, by substituting (3.44), this simplifies to

$$\frac{d}{dt}\mathbf{u} = \boldsymbol{\lambda}\mathbf{u} - iG(\omega)\mathbf{E}^{-1}\boldsymbol{\alpha}\boldsymbol{\beta}. \quad (3.47)$$

Now since $\boldsymbol{\lambda}$ is a diagonal matrix this can be solved to give an expression for \mathbf{u} :

$$\mathbf{u} = -iG(\omega) \int_0^t e^{-\boldsymbol{\lambda}(t'-t)} \mathbf{E}^{-1}\boldsymbol{\alpha}\boldsymbol{\beta} dt'. \quad (3.48)$$

Lastly, we can multiply both sides by \mathbf{E} and substitute $\mathbf{R} = \mathbf{E}\mathbf{u}$ to get our final expression for \mathbf{R} :

$$\mathbf{R}(\omega, t) = -iG(\omega) \int_0^t \mathbf{E}e^{-\boldsymbol{\lambda}(t'-t)} \mathbf{E}^{-1}\boldsymbol{\alpha}\boldsymbol{\beta} dt'. \quad (3.49)$$

When the eigenvalues are computed they are all of the form $\lambda_j = -i\omega + c_j$ where $c_j \in \mathbb{C}$ is some constant dependent on the parameters in the Hamiltonian, i.e. Ω , g , δ_{aL} , etc. Furthermore, the eigenvectors are frequency independent so they can be written as

$$\boldsymbol{\Lambda}_j = \begin{bmatrix} a_{1,j} \\ a_{2,j} \\ a_{3,j} \\ a_{4,j} \end{bmatrix}, \quad a_{i,j} \in \mathbb{C}. \quad (3.50)$$

Then \mathbf{E} and \mathbf{E}^{-1} are just two matrices of complex numbers:

$$\mathbf{E} = [a_{i,j}]_{i,j}, \quad \mathbf{E}^{-1} = [b_{i,j}]_{i,j}, \quad i, j \in \{1, 2, 3, 4\}. \quad (3.51)$$

Then using this new representation for \mathbf{E}^{-1} , $\mathbf{E}^{-1}\boldsymbol{\alpha}\boldsymbol{\beta}(t')$ is

$$\mathbf{E}^{-1}\boldsymbol{\alpha}\boldsymbol{\beta}(t') = \begin{bmatrix} b_{1,1}\alpha_1(t') + b_{1,2}\beta_1(t') \\ b_{2,1}\alpha_1(t') + b_{2,2}\beta_1(t') \\ b_{3,1}\alpha_1(t') + b_{3,2}\beta_1(t') \\ b_{4,1}\alpha_1(t') + b_{4,2}\beta_1(t') \end{bmatrix}. \quad (3.52)$$

Also, because $\boldsymbol{\lambda}$ is a diagonal matrix, then $e^{-\boldsymbol{\lambda}(t'-t)}$ is a diagonal matrix as well and using the form of each λ_j a factor of $e^{i\omega(t'-t)}$ can be taken out of $e^{-\boldsymbol{\lambda}(t'-t)}\mathbf{E}^{-1}\boldsymbol{\alpha}\boldsymbol{\beta}(t') = e^{i\omega(t'-t)}\mathbf{n}(t, t')$ and the vector \mathbf{n} is

$$\mathbf{n}(t, t') = \begin{bmatrix} e^{-c_1(t'-t)}(b_{1,1}\alpha_1(t') + b_{1,2}\beta_1(t')) \\ e^{-c_2(t'-t)}(b_{2,1}\alpha_1(t') + b_{2,2}\beta_1(t')) \\ e^{-c_3(t'-t)}(b_{3,1}\alpha_1(t') + b_{3,2}\beta_1(t')) \\ e^{-c_4(t'-t)}(b_{4,1}\alpha_1(t') + b_{4,2}\beta_1(t')) \end{bmatrix}. \quad (3.53)$$

The important thing to note is that $\mathbf{n}(t, t')$ is only a function of t and t' but not ω . Using this expression in the solution for $\mathbf{R}(\omega, t)$ gives

$$\mathbf{R}(\omega, t) = -iG(\omega) \int_0^t e^{i\omega(t'-t)} \mathbf{E} \cdot \mathbf{n}(t, t') dt'. \quad (3.54)$$

3.8.3 Appendix C: Deriving (3.14) and (3.15)

In the equations of motion, the $R_{g,0}(\omega, t)$ and $R_{e,0}(\omega, t)$ terms come in as frequency integrals over all possible frequencies. The form of these two coefficients, shown in (3.11), already contains a time integral over all past time so we focus on simplifying this double integral for the differential equation of $\alpha_1(t)$, which we call I , as both double integrals simplify similarly. Explicitly I has the form

$$I = - \int_{-\infty}^{\infty} \int_0^t G(\omega')^2 e^{i\omega'(t'-t)} \mathbf{E}_{g,0} \cdot \mathbf{n}(t, t') dt' d\omega'. \quad (3.55)$$

Recalling that $G(\omega) = \sqrt{\gamma_L/2\pi} \sin[(\omega\tau + \phi)/2]$ and switching the order of integration this becomes

$$I = \frac{-\gamma_L}{2\pi} \int_0^t \mathbf{E}_{g,0} \cdot \mathbf{n}(t, t') \times \left[\int_{-\infty}^{\infty} \sin^2 \left(\frac{\omega\tau + \phi}{2} \right) e^{i\omega'(t'-t)} d\omega' \right] dt'. \quad (3.56)$$

Substituting

$$\sin[(\omega\tau + \phi)/2] = [1/2i(e^{i(\omega\tau + \phi)/2} - e^{-i(\omega\tau + \phi)/2})] \quad (3.57)$$

into the equation gives the following integral:

$$I = \frac{-\gamma_L}{2\pi} \int_0^t \mathbf{E}_{g,0} \cdot \mathbf{n}(t, t') \left[\int_{-\infty}^{\infty} \frac{1}{2} e^{-i\omega'(t-t')} - \frac{1}{4} \left(e^{-i\omega'(t-t'-\tau)} e^{i\phi} + e^{-i\omega'(t-t'+\tau)} e^{-i\phi} \right) d\omega' \right] dt'. \quad (3.58)$$

Noting that $\int_{-\infty}^{\infty} e^{-i\omega'X} d\omega' = 2\pi\delta(X)$ where $\delta(X)$ is the Dirac delta function, the integration of ω' can be carried out:

$$I = \frac{-\gamma_L}{2\pi} \int_0^t \mathbf{E}_{g,0} \cdot \mathbf{n}(t, t') \left[\pi\delta(t-t') - \frac{\pi}{2} (\delta(t-t'-\tau)e^{i\phi} + \delta(t-t'+\tau)e^{-i\phi}) \right] dt'. \quad (3.59)$$

Lastly, noting that $\int_0^t \delta(t''-t')f(t')dt' = f(t'')$ as long as $t'' \in (0, t)$ [or $\int_0^t \delta(t''-t')f(t')dt' = \frac{1}{2}f(t'')$ if $t'' \in \{0, t\}$] the integration of t' can be completed:

$$-i \int_{-\infty}^{\infty} G(\omega') R_{g,0}(\omega', t) d\omega' = \frac{\gamma_L}{4} \left\{ -[\mathbf{E}_{g,0} \cdot \mathbf{n}(t, t)] + e^{i\phi}\theta(t-\tau)(\mathbf{E}_{g,0} \cdot \mathbf{n}(t, t-\tau)) \right\}, \quad (3.60)$$

where $\theta(t-\tau)$ is the Heaviside step function.

3.8.4 Appendix D: Optimized Technique for Simulating Quantum Trajectories with No Drive

The general numerical technique outlined in Sec. 3.4 is unnecessarily complex when there is no drive and only one quanta present in the system, which is the case for Secs. 3.5.1 and 3.5.2. Since there is only one quanta, it is only possible for one jump to occur during a QT, and after such a jump the system is in the ground state. The only stochastic dynamics that are present in the QTs are when the quantum jumps are chosen to occur, which we can exploit to speed up the computation of our QTs.

By simulating (or solving) the delay differential equation associated with the system, (3.12) with (3.14) and (3.15) substituted in, and conditioning the result using Sec. 3.3.5, the QT without any jumps can be computed. Then each individual QT can be generated by choosing a uniformly distributed random number ϵ , and comparing it to the integrated probability $P(t)$ for a jump to occur. A jump is applied to the system when $\epsilon < P(t)$ and the system collapses to the ground state. Therefore, after the initial QT without jumps is computed, there is no other significant computation to be done for each subsequent trajectory. In the case of Figs. 3.7 and 3.9, each data point is simply the ratio of trajectories where $\epsilon > P(t_{\text{end}})$ to the total number of trajectories.

Subsequently, by solving the delay differential equation, there are other insights that can be found. In the case of the system parameters for Figs. 3.7 and 3.9, (3.12) reduces to

$$\begin{aligned} \frac{d\beta_0(t)}{dt} &= -ig\alpha_1(t), \\ \frac{d\alpha_1(t)}{dt} &= -ig\beta_0(t) - \frac{\gamma_L}{4}\alpha_1(t) + \frac{\gamma_L}{4}e^{i\phi}\alpha_1(t - \tau). \end{aligned} \quad (3.61)$$

By seeking solutions of the form $\alpha_1(t) = Ae^{i\Lambda t}$ and $\beta_0(t) = Be^{i\Lambda t}$, we arrive at the characteristic equation

$$-\left\{\Lambda - i\frac{\gamma_L}{4}[1 - e^{i(\phi - \Lambda\tau)}]\right\}\Lambda + g^2 = 0. \quad (3.62)$$

This equation has the solution $\Lambda = \pm g$ when

$$\pm g\tau - \phi = 2\pi k, k \in \mathbb{Z}, \quad (3.63)$$

which is precisely the condition we use to find the required phase to trap excitations in Sec. [3.5.2](#).

Chapter 4

Extending Beyond One Photon in the Feedback Loop

The results of Ch. 3 are limited by making the “one photon in the loop” approximation. The focus of this chapter is to derive and implement a slightly different method to obtain results beyond this approximation. First, the extension of the FMR model is derived but it quickly runs into intractable memory effects for efficient computation. Therefore, the time-discretized waveguide model as described in Ch. 2.3 is used instead. Initially, a basic model of a TLS coupled to a feedback loop is discussed in the one photon in the loop regime in order to obtain previous results for comparison. This is followed by extending the model to two photons in the loop and presenting results in this regime which highlight the improvements beyond the one photon in the loop approximation.

4.1 QT Theory with Two Photons in the Loop

In this section, the expansion to two photons in the loop is derived for the FMR model of feedback. However, the algebra becomes unnecessarily long when the previous cavity-TLS setup is used. Instead, a single TLS driven with the same cw-laser on resonance will be used and the only output channel will be out of the loop, i.e. $\mathcal{E}_+(L/2)$. This will maintain enough complexity to avoid over-simplifying the problem while also cutting down on unnecessary algebra. Furthermore, this derivation leads to

expressions with intractable computational problems. Thus, only the most significant results throughout the derivation will be shown in order to highlight the resulting problems, rather than present a complete derivation for all parts of this model as was done in Ch. 3.3.

The Hamiltonian for this system with feedback is

$$H = \Omega (\sigma^+ + \sigma^-) + \int_{-\infty}^{\infty} [\omega r^\dagger(\omega) r(\omega)] d\omega + \int_{-\infty}^{\infty} \{G(\omega) [\sigma^+ r(\omega) + r^\dagger(\omega) \sigma^-]\} d\omega, \quad (4.1)$$

where the same notation from Ch. 3 has been used but now the feedback loop is directly coupled with the TLS. Note the coupling to the loop keeps the same form, $G(\omega) = \sqrt{\gamma_L/2\pi} \sin[(\omega\tau + \phi)/2]$. The mathematics of expanding to two photons in the loop enters through the ket vector for the system which is now

$$\begin{aligned} |\psi(t)\rangle = & [\alpha(t) |g\rangle + \beta(t) |e\rangle] |\{0\}\rangle + \int_{-\infty}^{\infty} [R_g^{(1)}(\omega, t) |g\rangle + R_e^{(1)}(\omega, t) |e\rangle] |1, \omega\rangle d\omega \\ & + \int_{-\infty}^{\infty} \int_{\omega}^{\infty} [R_g^{(2)}(\omega, \omega', t) |g\rangle + R_e^{(2)}(\omega, \omega', t) |e\rangle] |1, \omega\rangle |1, \omega'\rangle d\omega' d\omega. \end{aligned} \quad (4.2)$$

The notation of Ch. 3 is expanded here so that $R_g^{(1)}$ and $R_e^{(1)}$ represents state amplitudes when there is one photon in the feedback loop while $R_g^{(2)}$ and $R_e^{(2)}$ represent state amplitudes when there is two photons in the feedback loop.

The double integral here allows for any pair of photon frequencies to be in the loop and the second integral starts at ω to avoid double counting of the states. Then, since there are no Lindblad output channels, $H = H_{\text{eff}}$, so (4.1) and (4.2) can be

substituted into (3.1) to get the coupled differential equations:

$$\begin{aligned}
i\frac{d\alpha}{dt} &= \Omega\beta, \\
i\frac{d\beta}{dt} &= \Omega\alpha + \int_{-\infty}^{\infty} G(\omega)R_g^{(1)}(\omega)d\omega, \\
i\frac{dR_g^{(1)}(\omega)}{dt} &= \omega R_g^{(1)}(\omega) + \Omega R_e^{(1)}(\omega) + G(\omega)\beta, \\
i\frac{dR_e^{(1)}(\omega)}{dt} &= \omega R_e^{(1)}(\omega) + \Omega R_g^{(1)}(\omega) + \int_{-\infty}^{\infty} G(\omega')R_g^{(2)}(\omega, \omega')d\omega', \\
i\frac{dR_g^{(2)}(\omega, \omega')}{dt} &= [\omega + \omega'] R_g^{(2)}(\omega, \omega') + \Omega R_e^{(2)}(\omega, \omega') + G(\omega)R_e^{(1)}(\omega'), \\
i\frac{dR_e^{(2)}(\omega, \omega')}{dt} &= [\omega + \omega'] R_e^{(2)}(\omega, \omega') + \Omega R_g^{(2)}(\omega, \omega'),
\end{aligned} \tag{4.3}$$

where the goal is to find a closed form set of coupled differential equations for $\alpha(t)$ and $\beta(t)$.

Notice that the differential equations for $R_g^{(2)}(\omega, \omega')$ and $R_e^{(2)}(\omega, \omega')$ are in the same form as the differential equations in (3.6) so the same type of approach can be taken. Following similar algebra, the solutions for the two photons in the loop coefficients are

$$\begin{aligned}
R_g^{(2)}(\omega, \omega', t) &= -iG(\omega) \int_0^t e^{i[\omega+\omega'](t'-t)} \cos[\Omega(t'-t)] R_e^{(1)}(\omega', t') dt', \\
R_e^{(2)}(\omega, \omega', t) &= G(\omega) \int_0^t e^{i[\omega+\omega'](t'-t)} \sin[\Omega(t'-t)] R_e^{(1)}(\omega', t') dt',
\end{aligned} \tag{4.4}$$

where \mathbf{E} and \mathbf{n} from the previous approach have been analytically evaluated due to the simpler algebra present in the system.

Then (4.4) can be substituted into the differential equation for $R_e^{(1)}(\omega, t)$ to get the coupled delay differential equations

$$\begin{aligned}
i\frac{dR_g^{(1)}(\omega, t)}{dt} &= \omega R_g^{(1)}(\omega, t) + \Omega R_e^{(1)}(\omega, t) + G(\omega)\beta(t), \\
i\frac{dR_e^{(1)}(\omega, t)}{dt} &= \left[\omega - i\frac{\gamma_L}{4} \right] R_e^{(1)}(\omega, t) + \Omega R_g^{(1)}(\omega, t) + i\frac{\gamma_L}{4} \cos(\Omega\tau) e^{-i[\omega\tau-\phi]} R_e^{(1)}(\omega, t-\tau).
\end{aligned} \tag{4.5}$$

This is the first indication of a problem in this approach. In order to get a closed form expression for $R_g^{(1)}(\omega, t)$, which is required for use in the differential equation of $\beta(t)$, these coupled delay differential equations need to be solved. Unfortunately there is no exact solution to this system in general, but the exact solution can be found for time intervals of length τ by repeated substitution of $R_e^{(1)}(\omega, t)$ into itself. Note from this point, the majority of the algebraic steps have been left out since it is mostly repeated application of techniques previously done in Ch. 3.

Before moving forward, a few new definitions are required in order to clean up the notation. Following the notation of Ch. 3,

$$\mathbf{A} \equiv \begin{bmatrix} -i\omega & -i\Omega \\ -i\Omega & -i\omega - \frac{\gamma_L}{4} \end{bmatrix}, \quad (4.6)$$

and thus \mathbf{E} is the matrix of eigenvalues of \mathbf{A} and $\boldsymbol{\lambda}$ is the diagonal matrix of the eigenvalues of \mathbf{A} . Then we next define

$$\mathbf{E}e^{-\boldsymbol{\lambda}(t'-t)}\mathbf{E}^{-1} = \mathbf{M}(t' - t)e^{i\omega(t'-t)}, \quad (4.7)$$

where \mathbf{M} is frequency independent. Therefore, the formal solution for $R_g^{(1)}(\omega, t)$ and $R_e^{(1)}(\omega, t)$ is

$$\begin{aligned} R_g^{(1)}(\omega, t) &= \int_0^t e^{i\omega(t'-t)} \mathbf{M}_g(t' - t) \begin{pmatrix} -iG(\omega)\beta(t') \\ \frac{\gamma_L}{4} \cos(\Omega\tau)e^{-i[\omega\tau-\phi]}R_e^{(1)}(\omega, t' - \tau) \end{pmatrix} dt', \\ R_e^{(1)}(\omega, t) &= \int_0^t e^{i\omega(t'-t)} \mathbf{M}_e(t' - t) \begin{pmatrix} -iG(\omega)\beta(t') \\ \frac{\gamma_L}{4} \cos(\Omega\tau)e^{-i[\omega\tau-\phi]}R_e^{(1)}(\omega, t' - \tau) \end{pmatrix} dt', \end{aligned} \quad (4.8)$$

where \mathbf{M}_g and \mathbf{M}_e is the top and bottom row of \mathbf{M} respectively. This form of $R_g^{(1)}(\omega, t)$ is not particularly useful for the current goal of finding a closed form expression for the differential equation of $\beta(t)$. Therefore, we perform an $(n - 1)$ 'th order Dyson expansion to find an explicit expression for $R_g^{(1)}(\omega, t)$ over the interval

$t \in [n\tau, (n+1)\tau]$ which is

$$R_g^{(1)}(\omega, t) = -iG(\omega) \sum_{j=0}^n \left[\frac{\gamma_L e^{i\phi} \cos(\Omega\tau)}{4} \right]^j \int_0^t \int_0^{t'-\tau} \cdots \int_0^{t^j-\tau} dt^{j+1} \cdots dt'' dt' \left[\right. \quad (4.9)$$

$$\left. M_g^{(2)}(t' - t) M_g^{(2)}(t'' - t' + \tau) \cdots M_g^{(2)}(t^j - t^{j-1} + \tau) M_g^{(1)}(t^{j+1} - t^j + \tau) e^{i\omega(t^{j+1}-t)} \beta(t^{j+1}) \right],$$

where $M_g^{(1)}$ and $M_g^{(2)}$ is the first and second entry of \mathbf{M}_g respectively.

This is the first explicit point where the challenges of moving to two photons in the loop become clear. When evaluating anything concerning $R_g^{(1)}(\omega, t)$ or $R_e^{(1)}(\omega, t)$, such as a jump probability or the TLS population, the result is a set of nested integrals each evaluating a function which is a large product of $M_{\{g,e\}}^{\{1,2\}}(x)$ terms. Not only is this large product a difficult bookkeeping task computationally, the nested integrals present an intractable numerical problem. For each multiple of τ that the current time passes, a new set of nested integrals is added onto the sum on top of increasing the length of all the previous integrals. This causes inherent terrible scaling issues for simulations with long end times. From the initial computational tests with this setup, trajectories with an end time of $\sim 5\tau$ ran on the order of minutes, an end time of $\sim 6\tau$ ran on the order of hours, and $\sim 7\tau$ ran on the order of days on a standard high performance workstation. Since QT theory requires averaging of a large number of trajectories, this is clearly a barrier to using this setup.

Interestingly, these nested integrals do not pose any problem to finding a closed form expression for the differential equation of $\beta(t)$. Indeed when (4.9) is substituted into (4.3), after algebraic simplification the differential equation is

$$\frac{d\beta(t)}{dt} = -i\Omega\alpha(t) + \frac{\gamma_L}{4} \left[-M_g^{(1)}(0)\beta(t) + e^{i\phi} M_g^{(1)}(\tau)\beta(t - \tau) \right] \quad (4.10)$$

$$+ \frac{e^{2i\phi} \gamma_L^2 \cos(\Omega\tau)}{32} M_g^{(2)}(0) M_g^{(1)}(0) \beta(t - \tau).$$

This form gives some insight into how feedback would enter into the evolution of this setup. The second and third terms represent the photon output to the feedback loop

and the returning single photon feedback. The fourth term represents the probability that two photons were emitted to the loop at $t - \tau$ and now the second photon is also returning to the loop. This term spoils the possibility of perfect feedback matching using ϕ as was seen in Fig. 3.4(a), this lack of perfect feedback is further shown in Ch. 4.2.2.

There are a few possible solutions to bypass the issues with this setup. First, the nested integrals get reset whenever there is a jump out of the feedback loop (since one of the goals of feedback is to increase coherence by recycling the photons). Therefore, this approach could be used for any parameter sets where there is a significant output from the loop to keep a high frequency of jumps. Unfortunately, most of the systems of interest aim to increase the stability of the system, which generally means less output out of the loop. A second solution would be to identify a frequency band of interest and numerically compute the R coefficients for some frequency comb over this bandwidth. This is possible to implement numerically, however it has not been studied how fine the comb would need to be or how large the bandwidth of interest is. Since this approach would likely lead to a large number of numerically evaluated coefficients, we opt for a third solution which requires significantly less coefficients. Rather than using the frequency modes to represent the loop, we decided to switch to the time domain representation of the feedback loop using the TDW model.

4.2 TDW Model with a Single TLS

In order to make progress towards a tractable computational model for two photons in the loop, the time discretized waveguide (TDW) model was considered. As previously described in Ch. 2.3, this model brings a portion of the environment, in this case the feedback loop, within the system evolution. This specific model was described by S. J. Whalen 2019, however other models of this sort have been used for a variety of problems such as analyzing the micromaser (Cresser 2006) and more fundamentally, to investigate the essential physics of Markovian, pure-state QTs (Brun 2002). Our system of interest is a single TLS coupled to the feedback loop to begin with, to easily

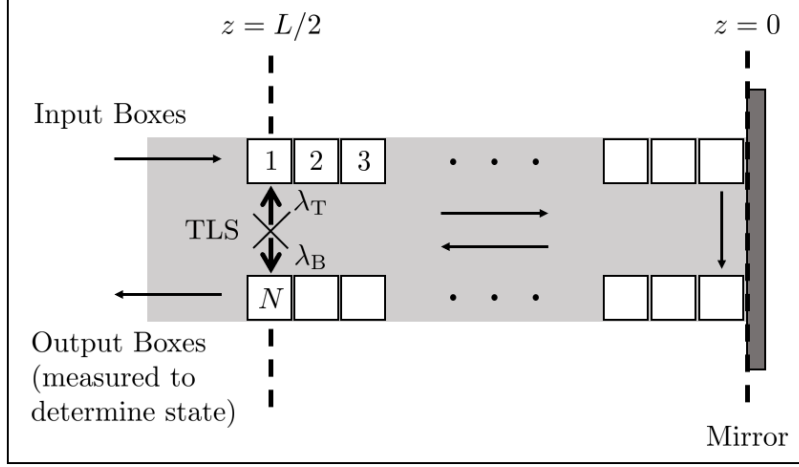


Figure 4.1: Schematic of the TLS embedded in the waveguide in the time discretized waveguide model.

illustrate the techniques in this new model. This new system is schematically shown in Fig. 4.1 in the TDW model.

Unlike the cavity-TLS setup previously studied, this conceptually simpler system allows for a photon blockade to be setup by the TLS. This will allow for interesting results in the reflection of incoming wavepackets, if they are resonantly coupled. For this system, it will be limited to a cw laser exciting the TLS and the detuning associated with that laser. Therefore the Hamiltonian (in the interaction picture) for the TLS and loop is

$$H = H_W + \delta_{aL} \sigma^+ \sigma^- + \Omega (\sigma^+ + \sigma^-) + (\lambda_T B_1^\dagger \sigma^- + H.a.) + (\lambda_B B_N^\dagger \sigma^- + H.a.), \quad (4.11)$$

where σ^- (σ^+) is the lowering (raising) operator of the TLS, B_k (B_k^\dagger) is the annihilation (creation) operator of the k 'th box, and λ_T (λ_B) is the coupling to the top (bottom) box from the TLS. The effective Rabi frequency of the laser-TLS interaction is Ω and the detuning of the laser from the TLS is $\delta_{aL} = \omega_a - \omega_L$. The coupling strength to the boxes is $\lambda_T = \sqrt{\gamma_T} \sqrt{N/\tau}$ and $\lambda_B = e^{-i\phi} \sqrt{\gamma_B} \sqrt{N/\tau}$ where γ_T (γ_B) is the decay rate to the top (bottom) box, N is the number of boxes (photon bins) in the discretization of the loop, τ is the round trip time, and ϕ is the round trip phase change.

4.2.1 Results in the One Photon in the Loop Limit

Before presenting results for the system with two photons in the loop, first the response in the one-photon-in-the-loop limit should be investigated since the system response differs greatly from the cavity-TLS system. The ket vector for the complete system in this limit is

$$|\psi(t)\rangle = [\alpha^{(0)}(t) |g\rangle + \beta^{(0)}(t) |e\rangle] |\{0\}\rangle + \sum_{j=1}^N [\alpha_j^{(1)}(t) |g\rangle + \beta_j^{(1)}(t) |e\rangle] |1_j\rangle, \quad (4.12)$$

where $|g\rangle$ ($|e\rangle$) is the ground (excited) state of the TLS, $|\{0\}\rangle$ represents no photons in any sections of the loop, and $|1_j\rangle$ represents one photon in the j 'th section on the loop.

Since there can be unique decay rates for coupling to the two different waveguide operators, we define $\gamma_L = \gamma_T + \gamma_B$ to be the total decay rate into the loop. This parameter is used as the reference point for the rest of the parameters throughout the results.

Moving through the same types of parameter sets used to investigate the cavity-TLS setup, we start without a drive and an initially excited TLS. As shown previously, ϕ can be used to tune the system to either trap population in the TLS or set up enhanced spontaneous emission. Figure 4.2(a) shows this with a loop length of $\tau = \gamma_L^{-1}$, where $\phi = \pi$ causes population trapping and $\phi = 0$ causes enhanced spontaneous emission. Unlike the cavity-TLS, when the loop length is varied, the behaviours at the two phases does not change. This is shown in Fig. 4.2(b), a phase change of $\phi = 0$ always causes enhanced spontaneous emission and $\phi = \pi$ always causes population trapping. Only the amount trapped decreases with increasing loop length since there is more population that can decay into the loop in the initial turn on time of the system.

The reason for this difference between the two systems comes from removing the oscillations between the cavity and TLS. The differential equations for the between

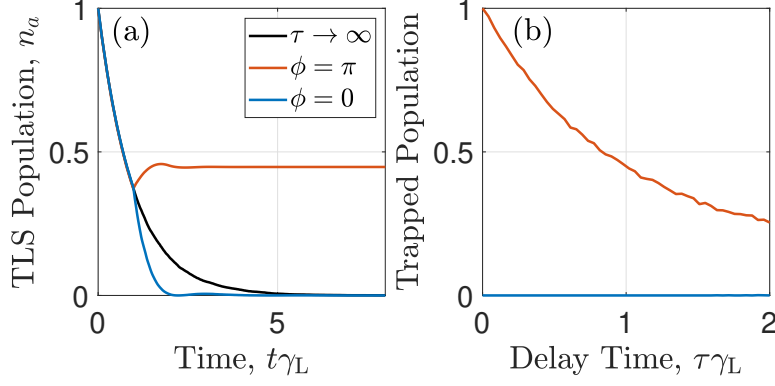


Figure 4.2: Spontaneous emission from the initially excited TLS with no drive. In (a) $\tau = \gamma_L^{-1}$ and population trapping or enhanced spontaneous emission can be found by tuning ϕ , each simulation is an average of 5000 QTs. In (b) the delay time is varied for the two choices of phase $\phi = \pi$ and $\phi = 0$, each point is an average of 1000 QTs.

jump evolution of the system are now

$$\begin{aligned} \frac{d}{dt}\alpha^{(0)} &= \frac{d}{dt}\beta_j^{(1)} = 0, \\ \frac{d}{dt}\beta^{(0)} &= -i \left[\lambda_T^* \alpha_1^{(1)} + \lambda_B^* \alpha_N^{(1)} \right], \\ \frac{d}{dt}\alpha_1^{(1)} &= -i\lambda_T\beta^{(0)}, \quad \frac{d}{dt}\alpha_N^{(1)} = -i\lambda_B\beta^{(0)}, \quad \frac{d}{dt}\alpha_j^{(1)} = 0, \quad j \notin \{1, N\}. \end{aligned} \quad (4.13)$$

Previously, the trapping condition was found by trying to tune the parameters such that $\frac{d}{dt}(\beta^{(0)}) = 0$ was possible. However, in this model the only possible system output channel is via a quantum jump from the N 'th box. Therefore, in order to block a jump from occurring, there needs to be no population in the N 'th box, so the trapping condition that needs to be satisfied is now $\alpha_N^{(1)}(t) = \beta_N^{(1)}(t) = 0$.

The differential equations are augmented by the application of H_W each time step which moves each box of the loop along. Therefore, since $\frac{d}{dt}\alpha_j^{(1)} = 0$ for $j \notin \{1, N\}$, then

$$\alpha_N^{(1)}(t) = \alpha_1^{(1)}(t - \tau) \sim -i\Delta t \lambda_T \beta^{(0)}(t - \tau), \quad (4.14)$$

where $\Delta t = \tau/N$. Note that Δt is used as the time resolution here for ease of notation, however a smaller time resolution $dt < \Delta t$ can be used. This gives a

more accurate evolution of the system between each box movement. For all systems, sufficient resolutions for the time step sizes are $\Delta t \ll 1/\gamma_L$ and δt small enough to resolve the system dynamics. The time steps used in the trajectories for Fig. 4.2 are $\Delta t = \delta t = 0.01\gamma_L^{-1}$ since emission from the TLS is the only dynamic. Then using the differential for $\frac{d}{dt}\alpha_N^{(1)}$ and that $\beta_j^{(1)} = 0$ at all time, the probability for a jump from box N is

$$\begin{aligned} |\alpha_N^{(1)}(t + \Delta t)|^2 &\sim \left| \alpha_N^{(1)}(t) - i\Delta t \lambda_B \beta^{(0)}(t) \right|^2, \\ &\sim (\Delta t)^2 \frac{\gamma N}{\tau} \left| \beta^{(0)}(t - \tau) + e^{-i\phi} \beta^{(0)}(t) \right|^2, \end{aligned} \quad (4.15)$$

where $\gamma_T = \gamma_B = \gamma$. Then population trapping is only possible if $\phi = \pi$ and $\beta^{(0)}(t) = \beta^{(0)}(t - \tau)$. Note that $\beta^{(0)}(t) = -\beta^{(0)}(t - \tau)$ will never occur with these parameter choices, thus $\phi = 0$ does not lead to population trapping.

Similarly, when a drive is introduced, the response follows the same pattern as shown in Fig. 4.3(a). When $\phi = \pi$, stabilized Rabi oscillations are found and when $\phi = 0$, we obtain enhanced loss of coherence compared to the no feedback case. The example in Fig. 4.3(a) has $\Omega\tau = 2\pi$, but if the drive strength is set at $\Omega = 8\pi$ then the delay time can be varied to find when stabilized Rabi oscillations are possible. Figure 4.3(b) shows that as τ is varied, peaks indicating stabilized Rabi oscillations occur whenever $\Omega\tau = n\pi$ for $n \in \mathbb{Z}$. The mathematics of this condition is derived below, but it stems from choosing a delay time and Rabi frequency which avoids setting up a photon blockade in the TLS when the feedback returns to the system. It is important to note that this choice of pump strength is significant and for the larger delay times is likely outside of the one photon in the loop limit. Nevertheless, this example is used to highlight the difference in matching conditions to the previous cavity-TLS setup.

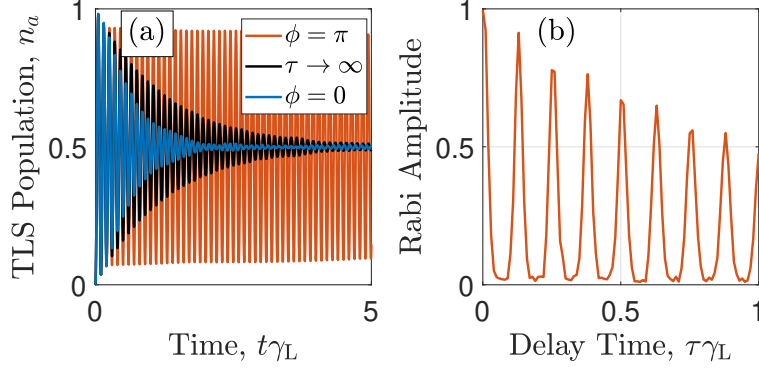


Figure 4.3: Rabi oscillations for the driven TLS with Rabi frequency $\Omega = 8\pi\gamma_L$. In (a) $\tau = 0.25\gamma_L^{-1}$ and stabilized Rabi oscillations or enhanced coherence decay can be found by tuning ϕ , each simulation is an average of 5000 QTs. In (b) the delay time is varied for $\phi = \pi$ and the amplitude of the stabilized Rabi oscillations at $t = 11\gamma_L^{-1}$ is recorded, each point is an average of 5000 QTs.

The differential equations for the between jump evolution when the drive is introduced are

$$\begin{aligned}
 \frac{d}{dt}\alpha^{(0)} &= -i\Omega\beta^{(0)}, \\
 \frac{d}{dt}\beta^{(0)} &= -i\Omega\alpha^{(0)} - i\left[\lambda_T^*\alpha_1^{(1)} + \lambda_B^*\alpha_N^{(1)}\right], \\
 \frac{d}{dt}\alpha_1^{(1)} &= -i\Omega\beta_1^{(1)} - i\lambda_T\beta^{(0)}, \quad \frac{d}{dt}\alpha_N^{(1)} = -i\Omega\beta_N^{(1)} - i\lambda_B\beta^{(0)}, \\
 \frac{d}{dt}\alpha_j^{(1)} &= -i\Omega\beta_j^{(1)}, \quad j \notin \{1, N\}, \\
 \frac{d}{dt}\beta_j^{(1)} &= -i\Omega\alpha_j^{(1)},
 \end{aligned} \tag{4.16}$$

where again we will focus on satisfying $\alpha_N^{(1)}(t) = \beta_N^{(1)}(t) = 0$ to obtain feedback-stabilized Rabi oscillations. Since there is no incoming pulse down the waveguide, $\beta_1^{(1)}$ is always 0 when it arrives and so $\alpha_1^{(1)}(t) \sim -i\Delta t\lambda_T\beta^{(0)}(t)$ as before. The evolution between box 1 and box N is a cosine function and so the value arriving at box N is

$$\alpha_N^{(1)}(t) = \alpha_1^{(1)}(t - \tau) \cos(\Omega\tau) \sim -i\Delta t\lambda_T\beta^{(0)}(t - \tau) \cos(\Omega\tau). \tag{4.17}$$

Thus, after the next time step, the population leaving the loop, which is checked for

a quantum jump, is

$$\begin{aligned} |\alpha_N^{(1)}(t + \Delta t)|^2 &\sim \left| \alpha_N^{(1)}(t) - i\Delta t \lambda_B \beta^{(0)}(t) - i\Delta t \Omega \beta_N^{(1)}(t) \right|^2, \\ &\sim \Delta t^2 \left| \sqrt{\frac{\gamma N}{\tau}} [\beta^{(0)}(t - \tau) \cos(\Omega\tau) + e^{-i\phi} \beta^{(0)}(t)] + \Omega \beta_N^{(1)}(t) \right|^2, \end{aligned} \quad (4.18)$$

where $\gamma_T = \gamma_B = \gamma$. Before moving forward to tune ϕ , the $\beta_N^{(1)}(t)$ contribution must be eliminated.

To find the form of $\beta_N^{(1)}(t)$, Eq. 4.17 can be directly substituted into the differential for $\beta_N^{(1)}(t)$ in Eq. 4.16. It is then a simple first-order ODE with initial condition $\beta_1^{(0)}(0) = 0$, giving

$$\beta_N^{(1)}(t) = -i\Delta t \lambda_T \beta^{(0)}(t - \tau) \sin(\Omega\tau). \quad (4.19)$$

Therefore, in order to eliminate the contribution of $\beta_N^{(1)}(t)$, the sine term must be 0 and thus the condition is $\Omega\tau = n\pi$ for $n \in \mathbb{Z}$. In essence, this is eliminating the possibility of the TLS being excited when the feedback returns to the system and so avoids a photon blockade. Taking this condition and applying it to Eq. 4.18 gives

$$|\alpha_N^{(1)}(t + \Delta t)|^2 \sim \Delta t^2 \frac{\gamma N}{\tau} |(\pm 1) \beta^{(0)}(t - \tau) + e^{-i\phi} \beta^{(0)}(t)|^2, \quad (4.20)$$

which at first glance seems to have both $\phi = \pi$ and $\phi = 0$ as solutions for stabilized Rabi oscillations. However, unlike the previous example where $\beta^{(0)}(t) = \beta^{(0)}(t - \tau)$, it now takes on a sinusoid form so that

$$\beta^{(0)}(t) = \sin(\Omega t), \quad \beta^{(0)}(t - \tau) = \sin(\Omega(t - \tau)) = (\pm 1) \sin(\Omega t), \quad (4.21)$$

where the previous condition on $\Omega\tau$ was used. With this in hand, the population leaving the loop is now

$$|\alpha_N^{(1)}(t + \Delta t)|^2 \sim \Delta t^2 \frac{\gamma N}{\tau} |(\pm 1)^2 \sin(\Omega\tau) + e^{-i\phi} \sin(\Omega\tau)|^2, \quad (4.22)$$

which will be 0 only when $\phi = \pi$, as was seen in the numerical results.

4.2.2 Results in the Two Photon in the Loop Limit

By expanding the system to allow for two photons in the loop (which we stress is a significantly hard problem in quantum optics), the limits of the one photon case can be checked, and other interesting effects can be probed that are typically very difficult to model in standard quantum optics formalisms. Not only can the breakdown of previous results be seen by expanding to two photons, but also the improvement of some results of the system. Since more photons are allowed in the system, higher pump strengths can be used to further highlight multi-quanta effects in the system.

When expanding the system to allow for two photons in the loop, the Hamiltonian and jump operators remain unchanged but the ket vector is now

$$\begin{aligned}
|\psi(t)\rangle &= [\alpha^{(0)}(t) |g\rangle + \beta^{(0)}(t) |e\rangle] |\{0\}\rangle + \sum_{j=1}^N [\alpha_j^{(1)}(t) |g\rangle + \beta_j^{(1)}(t) |e\rangle] |1_j\rangle \\
&+ \sum_{j=1}^{N-1} \sum_{k=j+1}^N [\alpha_{j,k}^{(2)}(t) |g\rangle + \beta_{j,k}^{(2)}(t) |e\rangle] |1_j\rangle |1_k\rangle.
\end{aligned} \quad (4.23)$$

The third term encompasses the two photons in the loop coefficients, with the limits on the sums chosen to avoid double counting. The state can then be written as

$$|\psi(t)\rangle = |\psi_0(t)\rangle |0_N\rangle + |\psi_1(t)\rangle |1_N\rangle, \quad (4.24)$$

where

$$\begin{aligned}
|\psi_0(t)\rangle &= [\alpha^{(0)}(t) |g\rangle + \beta^{(0)}(t) |e\rangle] |\{0\}\rangle + \sum_{j=1}^{N-1} [\alpha_j^{(1)}(t) |g\rangle + \beta_j^{(1)}(t) |e\rangle] |1_j\rangle \\
&+ \sum_{j=1}^{N-2} \sum_{k=j+1}^{N-1} [\alpha_{j,k}^{(2)}(t) |g\rangle + \beta_{j,k}^{(2)}(t) |e\rangle] |1_j\rangle |1_k\rangle,
\end{aligned} \quad (4.25)$$

and

$$|\psi_1(t)\rangle = [\alpha_N^{(1)}(t) |g\rangle + \beta_N^{(1)}(t) |e\rangle] + \sum_{j=1}^{N-1} [\alpha_{j,N}^{(2)}(t) |g\rangle + \beta_{j,N}^{(2)}(t) |e\rangle] |1_j\rangle. \quad (4.26)$$

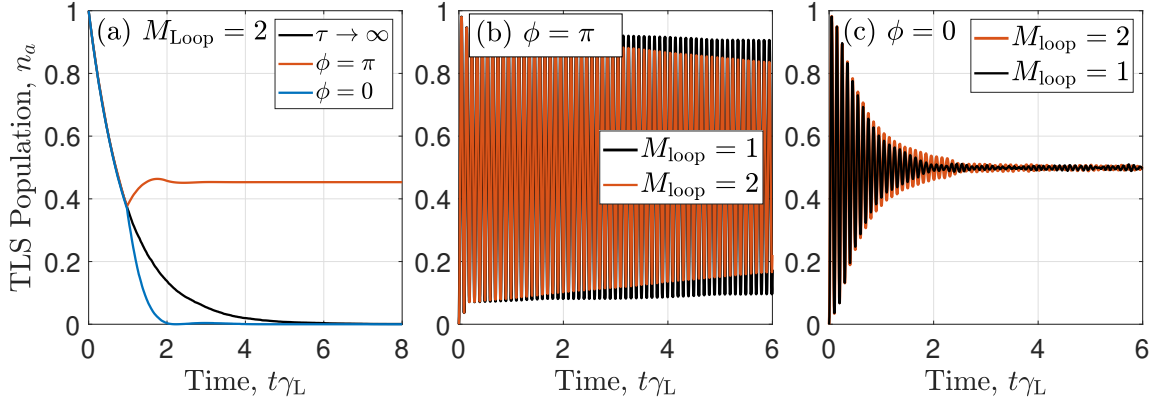


Figure 4.4: Population dynamics of the TLS for (a) an initially excited TLS with two photons allowed in the loop and the same parameters as Fig. 4.2(a). In (b) and (c) the TLS is driven with the same parameters as Fig. 4.3(a) and $M_{\text{Loop}} = 2$. The results from the one-photon-in-the-loop limit are also presented for comparison. Each simulation is an average of 5000 QTs.

Then the state can either be projected into $|\psi_0(t)\rangle$ or $|\psi_1(t)\rangle$ depending on whether a jump is determined to occur when the N 'th box leaves the system.

To compare the effect of increasing the maximum photon number in the loop to two ($M_{\text{Loop}} = 2$), the same parameter sets were rerun from Figs. 4.2 and 4.3. Figure 4.4(a) shows the behaviour of the initially excited TLS which is unchanged from the $M_{\text{Loop}} = 1$ case since there is formally only one quanta in the system. Once the drive is introduced to the system in Figs. 4.4(b) and 4.4(c) the results differ from the previous case. By increasing the maximum photon number in the loop, the ability to tune for perfect stabilization of Rabi oscillations can no longer occur and so a slow decay of the oscillations is seen as shown in Fig. 4.4(b). Similarly in Fig. 4.4(c), the enhanced decay of oscillations is slightly less enhanced when two photons are allowed in the loop.

These effects occur by tuning the phase of the returning field for either constructive (in the case of enhanced decay) or destructive (in the case of stabilization) interference. When two photons are allowed for in the loop, it is impossible to tune Ω for both photons present in the loop which do not necessarily have the same frequency. Mathematically, this comes in through the differential equations of the coefficients for

the two photons in the loop states;

$$\begin{aligned} \frac{d}{dt}\alpha_{1,k}^{(2)} &= -i\Omega\beta_{1,k}^{(2)} - i\lambda_T\beta_k^{(1)}, & \frac{d}{dt}\alpha_{j,N}^{(2)} &= -i\Omega\beta_{j,N}^{(2)} - i\lambda_B\beta_j^{(1)}, \\ \frac{d}{dt}\alpha_{j,k}^{(2)} &= -i\Omega\beta_{j,k}^{(2)}, & j \neq 1, k \neq N, \\ \frac{d}{dt}\beta_{j,k}^{(2)} &= -i\Omega\alpha_{j,k}^{(2)}. \end{aligned} \quad (4.27)$$

Again, in order to eliminate output from the system through the N 'th box, we need to satisfy $|\alpha_N^{(1)}(t)|^2 = |\beta_N^{(1)}(t)|^2 = 0$ as in the one photon in the loop case. However, in addition to this, the two photon in the loop coefficients for the N 'th box must also be empty, so we also need $\sum_{j=1}^{N-1} |\alpha_{j,N}^{(2)}(t)|^2 = \sum_{j=1}^{N-1} |\beta_{j,N}^{(2)}(t)|^2 = 0$.

Following the discussion in the previous section for the driven system in the one photon in the loop limit, the form of $\beta_{j,N}^{(2)}(t)$ is

$$\beta_{j,N}^{(2)}(t) = \beta_{1,N-j+1}^{(2)}(t - (j-1)\Delta t) \sin(\Omega(j-1)\Delta t). \quad (4.28)$$

This $(j-1)\Delta t$ term represents the $(j-1)$ time steps for the $(N-j+1)$ 'th box to arrive at the N 'th box. Then in order to have this coefficient be zero, the condition becomes $\Omega(j-1)\Delta t = n\pi$ for $n \in \mathbb{Z}$. Of course this condition cannot be met for all j , and so there will be non-zero population in the N 'th box leaving the loop. The conditions to remove the one photon in the loop approximation remains the same, and so the coherence of Rabi oscillations can be maintained for much longer since the two photon in the loop population is small. This is seen in Fig. 4.4(b) where the decay from perfectly stabilized Rabi oscillations is small.

By expanding to two photons in the loop, higher pump strengths can be used since we are not constrained to only one quanta in the loop. By using a stronger pump, higher order states can be populated and it is easier to see multi-quanta effects in the system. For example, the cavity-TLS setup from the paper showed weak multi-quanta effects in the cavity photoluminescence spectrum, recreated with the TDW model in Fig. 4.5(a) in the one photon in the loop limit. When this is expanded to allow for two photons, there is little change to the spectrum with the weak pump

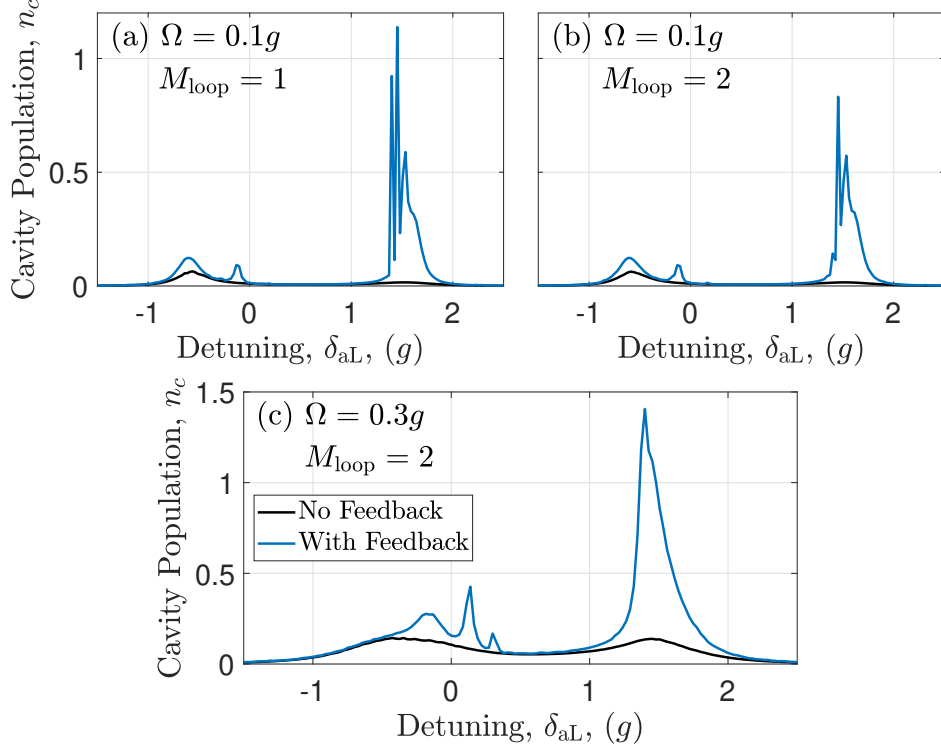


Figure 4.5: By scanning the detuning from the laser, of strength (a)/(b) $\Omega = 0.1g$ and (c) $\Omega = 0.3g$, the cavity photoluminescence spectrum (proportional to the cavity population) is found by plotting the steady state population of the cavity as a function of detuning. In (a) this is simulated in the one photon in the loop limit while in (b) and (c) this is in the two photon in the loop limit. The total output to the loop is $\gamma_L = g$ and the delay time is $\tau = g^{-1}$ and the phase is tuned for maximum population trapping, $\phi = \pi$. The detuning between the cavity and TLS is g , so that $\delta_{aL} = \delta_{cL} + g$. Each point is an average of 200 QTs once the steady state population has been reached in each trajectory.

($\Omega = 0.1g$) plotted in Fig. 4.5(b), meaning the original one photon approximation was good. Figure 4.5(c) shows the spectrum with a stronger pump strength of $\Omega = 0.3g$, the TLS and cavity resonances at $\delta_{aL} \sim -0.4g$ and $\delta_{aL} \sim 1.5g$ remain enhanced, and higher level resonances are now clearly seen on top of the TLS resonance. Two of these resonances are likely due to Rabi splitting of the TLS, these are the two peaks symmetric about $\delta_{aL} = 0g$. The final resonance, at $\delta_{aL} \sim 0.3$, we suspect is a slightly shifted retardation peak with the shift due to allowing for the second photon in the loop.

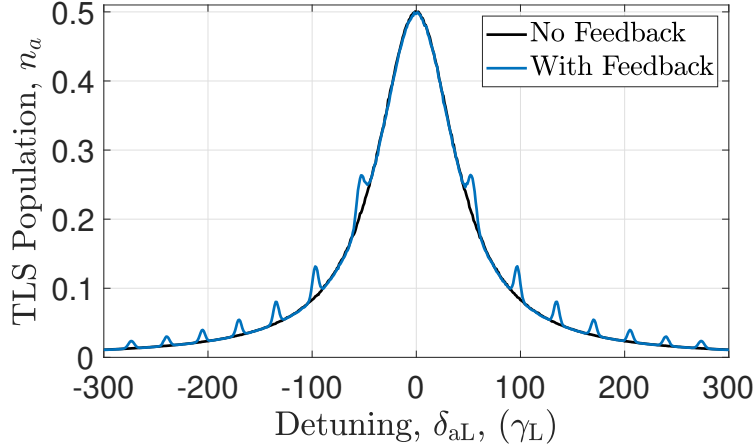


Figure 4.6: The single TLS coupled to a feedback loop setup is pumped with a cw laser at Rabi frequency, $\Omega = 10\pi\gamma_L$, and the detuning from the laser is scanned to obtain the TLS photoluminescence spectrum. Feedback is introduced with a delay time of $\tau = 0.2\gamma_L^{-1}$ and $\phi = 0$ in the limit of two photons in the loop. Each point in the spectrum is the average steady state TLS population for 500 QTs.

To emphasize the effect of feedback on a photoluminescence spectrum, the simpler setup with a single TLS coupled to the feedback loop from Fig. 4.1 is used. By removing the cavity, the many resonances introduced by the cavity levels are removed as well. The TLS is pumped at a Rabi frequency of $\Omega = 10\pi\gamma_L$ and the detuning from the laser is varied to obtain the TLS photoluminescence spectrum, shown in Fig. 4.6. Without feedback, the only resonance present in the system is from the TLS which is the large peak at $\delta_{aL} = 0\gamma_L$. When feedback is introduced, with $\tau = 0.2\gamma_L^{-1}$, $\phi = 0$, and in the limit of two photons in the loop, resonances from the feedback loop are seen. These resonances occur with a spacing of $\Delta\delta_{aL} = 2\pi/\tau$, however the resonances around the center of the spectrum are not seen because of the broadening from the high pump strength.

These peaks occur due to the feedback loop acting like a cavity and setting up Fabry-Perot resonances in the system. These are not due to a transition between dressed state energy levels present in the system, but rather from the standing waves set up between the TLS and mirror which have discrete allowed frequencies. This effect is completely non-perturbative and shows how QT theory can pick up this type

of effect naturally. A perturbative technique would only pick up a number of peaks equal to the degree of perturbation made in the approximation. QT theory naturally picks up all of the peaks without any adjustment, only limited by the time resolution of each trajectory and the number of trajectories that are run for averaging.

4.3 Computational Performance of the Models

Aside from the different analytical benefits to using the TDW model over the frequency mode representation (FMR) of feedback, there are also computational benefits in some regimes. The TDW model tends to perform better when long end times are required with a low frequency of jumps, while the FMR model can have better performance when the jump frequency is high or the decay rate into the loop is high. These simulations were all done on the same high performance workstation.

The first parameter set used to compare the two models is a driven TLS with enhanced decay of Rabi oscillations. The chosen Rabi frequency is $\Omega = 0.8\pi\gamma_L$ and the feedback loop introduces a delay time of $\tau = 0.2\gamma_L^{-1}$. This parameter set was chosen to have a high frequency of jumps out of the loop and requires a large number of boxes (equivalently a small Δt) in order to model the system properly, in this case $N = 100$ boxes was chosen. The run times for 100 QTs of this system is given in Table 4.1 for end times of $t_{\text{end}} = 0.2\gamma_L^{-1}$ (200 time steps) and $t_{\text{end}} = 1.0\gamma_L^{-1}$ (500 time steps). The TDW model with one photon in the loop runs much faster than the FMR model in all cases, whereas when two photons in the loop are present the FMR model is faster for the short end time and comparable in the longer end time.

The second parameter set that was used to compare the two models is the off-resonant driven cavity-TLS whose results are presented in Fig. 4.5. The drive was chosen to be $\Omega = 0.1g$ to stay in the one photon in the loop limit and so that a fairly low feedback resolution is needed. The system is modelled well with $N = 20$ boxes but the run times for $N = 50$ boxes is presented as well. The run times for 100 QTs of this system is given in Table 4.2 for an end time of $t_{\text{end}} = 10g^{-1}$ (1000 time steps). This is not nearly long enough to reach the steady state solution but is sufficient to

Model Type	Run Times (sec.)	
	$t_{\text{end}} = 0.2\gamma_{\text{L}}^{-1}$	$t_{\text{end}} = 1.0\gamma_{\text{L}}^{-1}$
FMR Model	14.9	142
TDW Model ($M_{\text{loop}} = 1$)	3.02	14.0
TDW Model ($M_{\text{loop}} = 2$)	34.8	168

Table 4.1: Comparison of run times between the FMR and TDW models for enhanced decay of Rabi oscillations.

illustrate the differences in run time for this system. Due to the large number of time steps needed to simulate this system and the low number of jumps out of the loop taking place, the FMR model struggles to maintain a competitive run time because of the long integrals over all past time that need to be calculated. Indeed, when the simulation is run closer to steady state (10000 time steps) a single QT using the FMR model takes 554 sec. to run, while a single QT using the TDW model with two photons in the loop and $N = 20$ boxes only takes 3.5 sec. to run, ~ 160 times faster.

Model Type	Run Times (sec.)	
	$N = 20$ Boxes	$N = 50$ Boxes
FMR Model	556	
TDW Model ($M_{\text{loop}} = 1$)	9.21	15.4
TDW Model ($M_{\text{loop}} = 2$)	29.9	234

Table 4.2: Comparison of run times between the FMR and TDW models for off resonant pumping of the cavity-TLS setup from Fig. 4.5 with $\Omega = 0.1g$.

Overall, the TDW model performs much better than the FMR model across most parameter sets. For this reason, and because it is much easier to expand the photon number in the loop, the TDW model seems to be the better method to model feedback in systems of interest. It is important to note for the TDW model that moving from one photon to two photons in the loop scales quadratically with memory. This is because the number of sets of loop coefficients changes from N , in the one photon in the loop case, to $(N^2 + N)/2$, in the two photons in the loop case. One can run into

memory issues, even on a standard high-performance workstation, when $N > 100$ is used, especially when parallelizing the code since the RAM is split between the nodes.

Chapter 5

Coupling Two TLS's via a Waveguide with Coherent Feedback

Using the TDW model developed in Ch. 4, we model a waveguide with two spatially separated TLS's both with and without feedback. This setup is closely linked to the results in Dicke 1954, which described so-called Dicke states for chains of oscillators. Our discussion will deal with two atom Dicke states, and the associated sub-radiance and super-radiance that occurs. This setup allows for quantum entanglement setups and longer chains have been used to study phase transitions and giant quantum oscillators (Garraway 2011).

First, the TDW model is applied to this system and the methods for simulating this system are discussed. Then, the system without feedback is investigated through the population dynamics in a variety of regimes including states which exhibit sub-radiance and super-radiance. Feedback is then introduced to the system and the same parameter regimes are simulated to investigate the feedback effects on the system. We find that the system is especially sensitive to both the phase changes for each TLS, but also the relative phase change between the two.

5.1 Embedding Two TLS's in the Feedback Loop Using the TDW Model

Another interesting system that can be investigated with this new feedback model is to embed two TLS's in the feedback loop at separate positions, which allows one

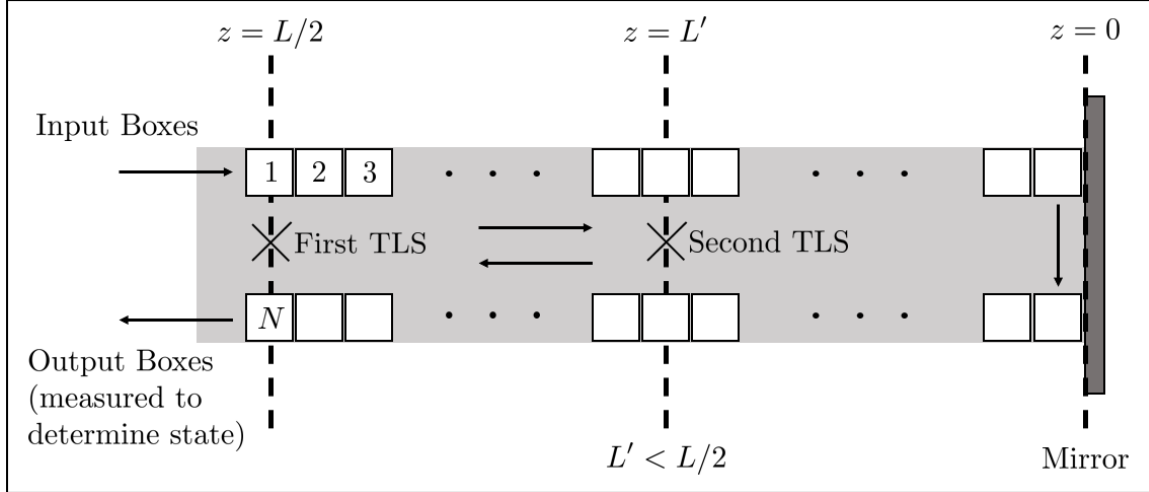


Figure 5.1: Schematic of the system when two TLS's are embedded in the waveguide.

to entangle quantum states over macroscopic distances. With retardation properly included, this is another example of a highly non-Markovian system, even though chains of TLS's are frequently treated in the Markovian limit (instantaneous coupling limit, and no system-level coupling to the waveguide photons). This model is also important to understand as a stepping stone for many-body quantum simulators with many TLS's on a chip, which are now being realized experimentally, for both circuit QED (Mirhosseini et al. 2019) and quantum dot QED (Türschmann et al. 2019). Figure 5.1 shows a schematic of this setup when N boxes span the distance around the loop starting from the first TLS. The boxes (time bins) travel from the left to the right on top and when they reach the mirror, they are moved to the bottom row and travel right to left. Each waveguide box has a maximum photon number of 1, which is a good approximation as long as the box flux is faster than the quickest decay process in the system. There are two (possibly driven) TLS's present in the waveguide at $L/2$ and at L' , indicated by the crosses. In theory, both of these could be driven at different frequencies, however, for now if both are pumped, then both pump fields are taken to have the same frequency.

When the system is truncated to two photons in the loop, the total state of the

two TLS's and waveguide is given by

$$\begin{aligned}
 |\psi(t)\rangle = & \left(\alpha^{(0)}(t) |g, g\rangle + \beta^{(0)}(t) |e, g\rangle + \eta^{(0)}(t) |g, e\rangle + \xi^{(0)}(t) |e, e\rangle \right) |\{0\}\rangle + \quad (5.1) \\
 & \sum_{j=1}^N \left(\alpha_j^{(1)}(t) |g, g\rangle + \beta_j^{(1)}(t) |e, g\rangle + \eta_j^{(1)}(t) |g, e\rangle + \xi_j^{(1)}(t) |e, e\rangle \right) |1_j\rangle + \\
 & \sum_{j=1}^{N-1} \sum_{k=j+1}^N \left(\alpha_{j,k}^{(2)}(t) |g, g\rangle + \beta_{j,k}^{(2)}(t) |e, g\rangle + \eta_{j,k}^{(2)}(t) |g, e\rangle + \xi_{j,k}^{(2)}(t) |e, e\rangle \right) |1_j, 1_k\rangle,
 \end{aligned}$$

with $|g\rangle$ ($|e\rangle$) denoting the ground (excited) state of a TLS, $|\{0\}\rangle$ denoting the vacuum state of all the boxes, $|1_j\rangle$ denoting one photon in the j 'th box, and $|1_j, 1_k\rangle$ denoting one photon in the j 'th box and one photon in the k 'th box (note that to avoid double counting $k > j$). Here we use α, β, η, ξ to be the time-dependent coefficients of the $|g, g\rangle, |e, g\rangle, |g, e\rangle, |e, e\rangle$ states, respectively, and the superscript (x) denotes there are a total of x quanta in the loop for that state.

Then the Hamiltonian for this entire system is given by

$$H = H_{\text{Sys},1} + H_{\text{Int},1} + H_{\text{Sys},2} + H_{\text{Int},2} + H_W, \quad (5.2)$$

where $H_{\text{Sys},j}$ is the system Hamiltonian of the j 'th TLS, $H_{\text{Int},j}$ is the interaction Hamiltonian between the boxes and the j 'th TLS, and H_W is the waveguide Hamiltonian which moves the boxes forward each time step. The system Hamiltonians will vary depending on what setups are investigated, but generally

$$H_{\text{Sys},j} = \delta_{\text{aL},j} \sigma_j^+ \sigma_j^- + \Omega_j (\sigma_j^+ + \sigma_j^-), \quad (5.3)$$

and the interaction Hamiltonians are given by

$$\begin{aligned}
 H_{\text{Int},1} &= \left(\lambda_{\text{T},1} B_1^\dagger \sigma_1^- + H.a. \right) + \left(\lambda_{\text{B},1} B_N^\dagger \sigma_1^- + H.a. \right), \quad (5.4) \\
 H_{\text{Int},2} &= \left(\lambda_{\text{T},2} B_x^\dagger \sigma_2^- + H.a. \right) + \left(\lambda_{\text{B},2} B_y^\dagger \sigma_2^- + H.a. \right),
 \end{aligned}$$

where σ_j^- (σ_j^+) is the lowering (raising) operator of the j 'th TLS, B_k (B_k^\dagger) is the

annihilation (creation) operator of the k 'th box, and $\lambda_{T,j}$ ($\lambda_{B,j}$) is the coupling to the top (bottom) box of the j 'th TLS. Note that x and y are dependent on the placement of the second TLS. The formulas for determining these in terms of L' are

$$\begin{aligned} x &= N \left(\frac{1}{2} - \frac{L'}{L} \right) = \frac{N}{2} \left(1 - \frac{\tau_2}{\tau_1} \right), \\ y &= N \left(\frac{1}{2} + \frac{L'}{L} \right) + 1 = \frac{N}{2} \left(1 + \frac{\tau_2}{\tau_1} \right) + 1, \end{aligned} \quad (5.5)$$

with the corresponding formulas in terms of the delay times (τ_1 being the full round trip time from box 1 to N , τ_2 being the round trip time from box x to y) also shown. The coupling between the TLS's and boxes (time bins) is given by

$$\begin{aligned} \lambda_{T,j} &= \sqrt{\gamma_{T,j}} \sqrt{\frac{N}{\tau_1}}, \\ \lambda_{B,j} &= e^{-i\phi_j} \sqrt{\gamma_{B,j}} \sqrt{\frac{N}{\tau_1}}, \end{aligned} \quad (5.6)$$

where $\gamma_{T,j}$ ($\gamma_{B,j}$) is the decay rates to the top (bottom) box of the j 'th TLS, ϕ_j is the round trip phase shift from the j 'th TLS, and N/τ_1 is the box flux. Following the derivations done previously, the two phase changes are given as $\phi_1 = \omega_L \tau_1 / 2$ and $\phi_2 = \omega_L \tau_2 / 2 = \phi_1 \tau_2 / \tau_1$. However, since ϕ_1 and ϕ_2 are only relevant as phase terms (i.e. modulus 2π phase terms) and ω_L is in the hundreds of Terahertz (10^{12} Hz) regime (for optical frequencies), this essentially makes ϕ_2 independent of ϕ_1 as long as $\tau_1 \neq \tau_2$.

The box passing scenario is essentially unchanged from the model with one TLS and two photons in the loop. Since the state can be written in the same way as before, i.e.

$$|\psi(t)\rangle = |\psi_0(t)\rangle |0\rangle_N + |\psi_1(t)\rangle |1\rangle_N, \quad (5.7)$$

then it can be projected onto either $|\psi_0(t)\rangle$ or $|\psi_1(t)\rangle$ depending on whether a photon from the N 'th box is observed when it leaves the system. Then the boxes are passed along by changing the j and k indices as before.

5.2 Results

In this results section, we change our notation slightly from previous sections. The population of the first TLS is referred to as $n_1 = \langle \psi(t) | \sigma_1^+ \sigma_1^- | \psi(t) \rangle$ and the population of the second TLS is referred to as $n_2 = \langle \psi(t) | \sigma_2^+ \sigma_2^- | \psi(t) \rangle$.

5.2.1 System Dynamics Without a Feedback Loop

We begin by analyzing the system dynamics without feedback present. In order to simulate this scenario, a second output channel is put in when boxes pass the second TLS. Even without a feedback loop, this is still a complex quantum system to model, and is usually solved in the linear excitation regime. The model works as follows: the boxes enter the system empty and moving to the right at the first TLS, they are measured leaving the system to the right of the second system TLS and emptied; they re-enter the system moving to the left at the second TLS, and then are measured leaving the system to the left of the first TLS. This system has many non-trivial results for quantum optics and has been studied in many papers for various phenomena such as sub- and super-radiance (Dinc and Brańczyk 2019; Sinha et al. 2020), transmission and reflection phenomena (Hughes 2007; Türschmann et al. 2019), and waveguide mediated strong coupling (Cheng et al. 2017). We will briefly show some of these phenomena taking into account the non-Markovian effects of travel time between the first and second TLS's, a difficult problem in quantum optics to simulate. For clarification, in this section, the “delay time,” τ , is measured as the time for a photon to travel from the first TLS to the second TLS and back as if it was reflected.

In order to show the basic behaviour of this system, we first follow the time dynamics of the system when one TLS is excited and the other is in the ground state. The system is undriven and we assume equal total decay rates of each TLS and that each TLS decays equally to the left and right. Since we will not look at any systems where the TLS's have different total decay rates, we use the total decay rate as the reference point for the rest of the parameters and denote it γ_L . The dynamics for a

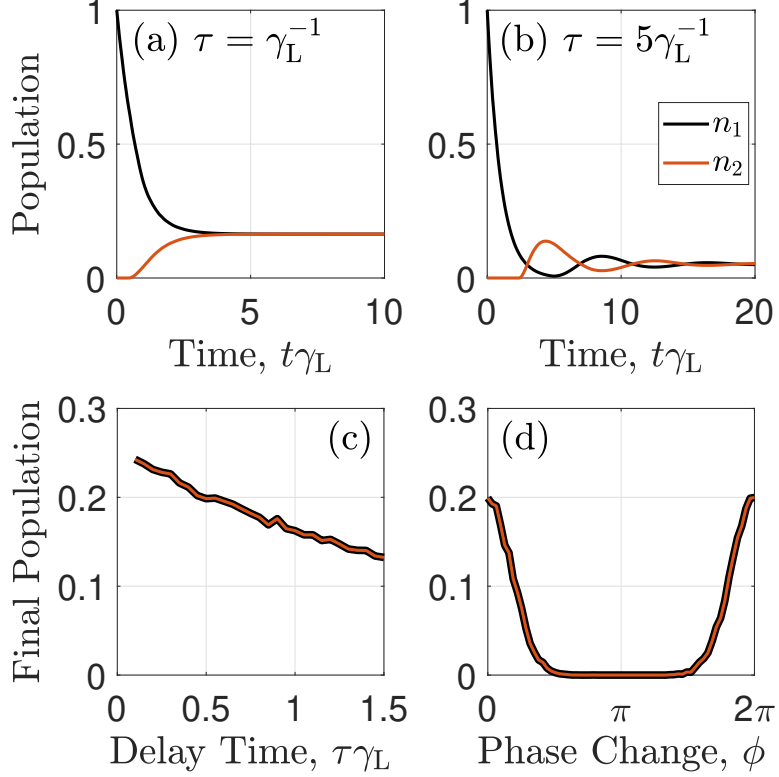


Figure 5.2: System dynamics of the undriven two-TLS setup without feedback with initial condition $\psi = |e, g\rangle$. For delay times (a) $\tau = \gamma_L^{-1}$ and (b) $\tau = 5\gamma_L^{-1}$, the population dynamics are shown with phase change $\phi = 0$. In (c), the final (trapped) population is shown as τ is increased when $\phi = 0$. In (d), the final population is shown as ϕ is varied and $\tau = \gamma_L^{-1}$. Both (a) and (b) are the average of 5000 QTs, each point in (c) is the average of 5000 QTs, and in (d) each point is the average of 2500 QTs.

short loop is shown in Fig. 5.2(a) and a longer loop is shown in Fig. 5.2(b). When the phase change around the loop is held at $\phi = 0$, as in these two examples, the system will always reach an equilibrium where population is trapped. Fig. 5.2(c) shows this as the delay time is increased and all that occurs is a decrease in trapped population rather than finding any untrapped states. Any of these examples where the system reaches a constant population is an indication of an entangled state between the two TLS's (Hughes 2005). In order to avoid population trapping for this setup, the phase change around the loop needs to be varied as shown in Fig. 5.2(d). As soon as the phase is moved off a multiple of 2π , the population is no longer perfectly trapped.

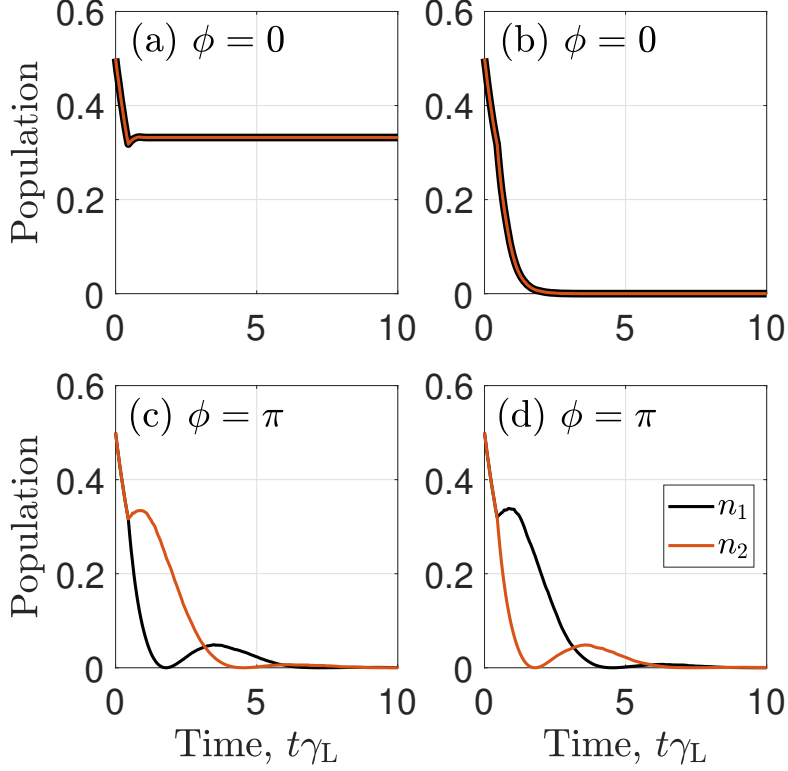


Figure 5.3: With the two-TLS setup we can show (a) sub-radiance or (b) super-radiance when $\phi = 0$ and $\tau = \gamma_L^{-1}$ by choice of the initial condition. However when the round trip phase change is $\phi = \pi$, neither (c) the sub-radiance initial conditions or (d) the super-radiance initial conditions lead to their respective decay phenomena. All four simulations are the average of 5000 QTs.

If these simulations were run for a longer end-time, the peaks would sharpen and become delta functions on the multiples of 2π .

By changing the initial conditions of the system, the system can exhibit sub- and super-radiant behaviour where the population is either completely trapped (sub-radiant) or exhibits enhanced emission (super-radiant). The sub-radiant state (an entangled state of the two TLS's) is shown in Fig. 5.3(a) where the initial condition is $|\psi\rangle = 1/\sqrt{2}|e, g\rangle - 1/\sqrt{2}|g, e\rangle$, and the super-radiant state is shown in Fig. 5.3(b) where the initial condition is $|\psi\rangle = 1/\sqrt{2}|e, g\rangle + 1/\sqrt{2}|g, e\rangle$.

The behaviour of this system is remarkably similar to that of a single TLS with feedback, since the system is weakly excited with one quanta. From Fig. 4.2(a), the

population is trapped when $\phi = \pi$ and enhanced emission occurs when $\phi = 0$. This is because the second TLS acts like a mirror and emits population back at the first TLS as if it had been reflected. The phase change of the reflection depends on the sign of the $|g, e\rangle$ state in the initial conditions. When nonlinearities are introduced to the system, either through a pump or initial conditions with higher quanta, the behaviour of the second TLS deviates from a bosonic mirror. Interestingly, these Dicke states only occur when the phase change for the two TLS setup is $\phi = 0$. As shown in Figs. 5.3(c) and (d), when $\phi = \pi$ the states no longer exhibit either sub-radiance or super-radiance due to the broken symmetry introduced by the phase change.

5.2.2 Introducing Feedback to the System

When feedback is introduced to this two-TLS setup, the dynamics significantly change due to the new control parameters that are introduced. Specifically, the phase change introduced for the second TLS, ϕ_2 , can be used to completely alter the results found without feedback. Figure 5.4 shows the setup when the initial condition is set to $|\psi\rangle = |e, g\rangle$ and feedback is included. When the two phases are matched as in Figs. 5.4(a) and 5.4(d), population is trapped in the system as an entangled state. In Fig. 5.4(a), the trapping occurs due to the inherent system equilibrium that is reached between the two TLS's as in Fig. 5.2(a). In Fig. 5.4(d), the trapping occurs through the excitation trapping from the feedback loop. When the field returns to the second TLS from the feedback loop, it sets off the excitation trapping while the second TLS is at a small population. Then, when the feedback arrives at the first TLS, it also sets up excitation trapping as if the second TLS was never there, since it is no longer outputting photons. When the phases are not equal, population trapping does not occur and the excitation will eventually leave the system as in Figs. 5.4(b) and 5.4(c).

Figure 5.5 shows how the population trapping changes when the delay time between the TLS's is increased for two choices of matching phases, showing population trapping at all delay times. When the phases are not matched, i.e. $\phi_1 \neq \phi_2$, then population trapping will not occur. This is because by introducing different phases, the

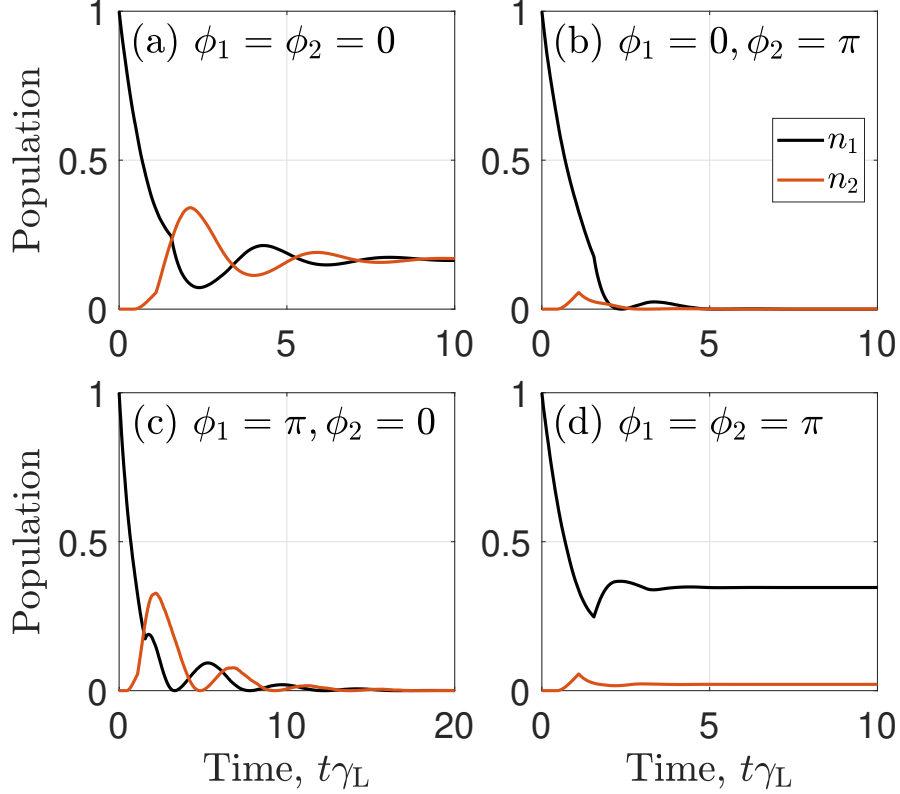


Figure 5.4: Population dynamics for the setup in 5.2(a) when feedback is introduced for a variety of choices for ϕ_1 and ϕ_2 when $\tau_1 = 1.5\gamma_L^{-1}$ and $\tau_2 = 0.5\gamma_L^{-1}$. Entangled states are found when the phases are matched such as in (a) and (d). Each simulation is the average of 5000 QTs.

fields no longer perfectly match up to interfere when leaving the system and perfect trapping cannot occur. By matching the phases, the populations in the two TLS's will eventually be stabilized and the overall system will have trapped population. This occurs at any choice for the phase, as long as they are matching. However, the only phase where the population of the two TLS's are not the same in the steady state is when $\phi_1 = \phi_2 = \pi$. With this choice, the population of the two TLS's is different as shown in Figs. 5.4(d) and 5.5(b). This is because of the perfect trapping occurring from the feedback loop at this phase for both systems. When this occurs, the field perfectly cancels on both sides of the second TLS before the populations are matched and so it stops outputting into the waveguide. This traps the first TLS in a

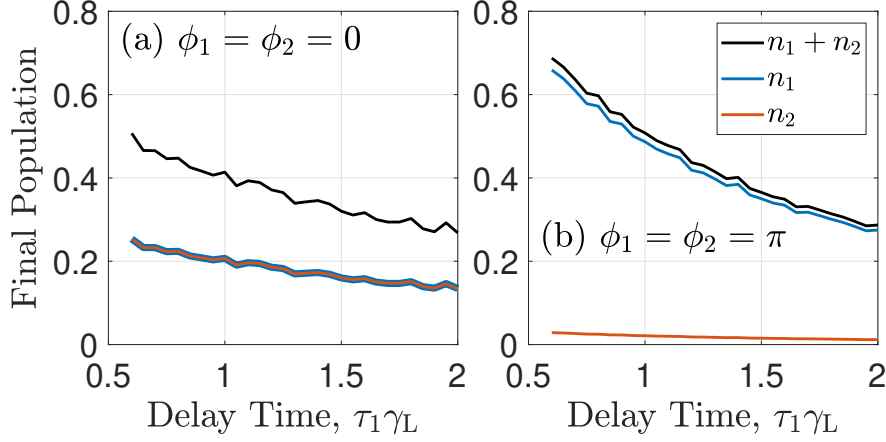


Figure 5.5: Variation of the final trapped population for the undriven two-TLS setup when $\tau_2 = 0.5\gamma_L^{-1}$ and τ_1 is varied. The initial condition for the system is $\psi = |e, g\rangle$ and the round trip phase changes are (a) $\phi_1 = \phi_2 = 0$ and (b) $\phi_1 = \phi_2 = \pi$. Each point in both figures is an average of 2000 QTs.

perfect matching condition as well which keeps the overall population trapped in the system. It is important to note that the theory predicts perfect trapping for these systems, whether through the feedback or through entangled states, but in reality there would always be long term decay. For example, out-of-plane radiative decay or pure dephasing processes would both contribute to the slow loss of population from the system (Shammah et al. 2017). These can easily be included in the general QT model, as discussed in Ch. 2.

We also want to look at the effect of feedback on the sub-radiant and super-radiant states shown in Fig. 5.3. In Fig. 5.6, the population dynamics of a sub-radiant state is shown for four choices of phases. Beginning with the initial condition $|\psi\rangle = 1/\sqrt{2}|e, g\rangle - 1/\sqrt{2}|g, e\rangle$, which without feedback would lead to sub-radiance, the system evolves and only reaches a sub-radiant state for three choices of phase. In Figs. 5.6(a), 5.6(b), and 5.6(d) the system eventually reaches some type of population trapping indicating a sub-radiant state. While Fig. 5.6(a) and 5.6(d) follow the trend from Fig. 5.4(a) and 5.4(d) where matching phase conditions lead to trapped population, Fig. 5.6(b) exhibits population trapping while having opposite phases. This occurs because the initial conditions allow the first TLS to decay quickly while

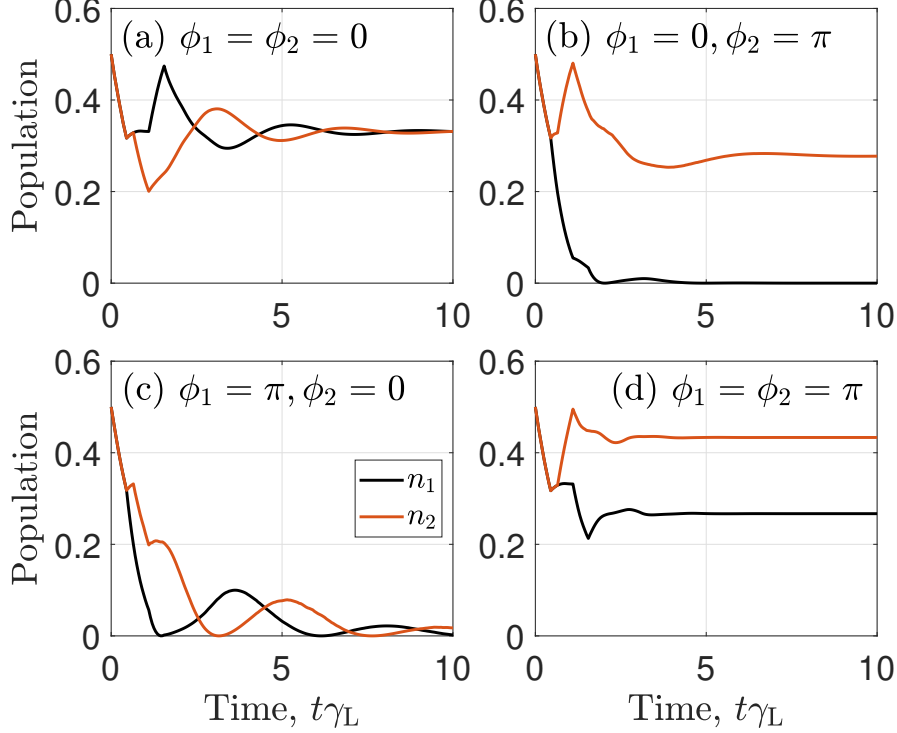


Figure 5.6: Population dynamics for the setup in 5.3(a) (a sub-radiant state) when feedback is introduced for a variety of choices for ϕ_1 and ϕ_2 when $\tau_1 = 1.5\gamma_L^{-1}$ and $\tau_2 = 0.5\gamma_L^{-1}$. Each set of results is the average of 5000 QTs.

the second TLS traps its initial population through the feedback loop. In Fig. 5.6(c) the sub-radiance is completely missing and the system relaxes to the ground state.

In Fig. 5.7, the population dynamics of a super-radiant state is shown for four choices of phases. This time the initial condition begins as $|\psi\rangle = 1/\sqrt{2}|e, g\rangle - 1/\sqrt{2}|g, e\rangle$, which without feedback would lead to super-radiance, and the system evolves and loses its super-radiance effect in all of the cases. For Figs. 5.7(a) and 5.7(c), the system still relaxes to its ground state but it does not occur faster than regular spontaneous emission for the system. Indeed, Figs. 5.7(b) and 5.7(d) show phase choices that lead to dynamics closer to a sub-radiant state where population is trapped in the system.

For an example of a non-linear response of the system we set an initial condition of $\psi = |e, e\rangle$, which explicitly is a two photon state, and thus requires a limit of

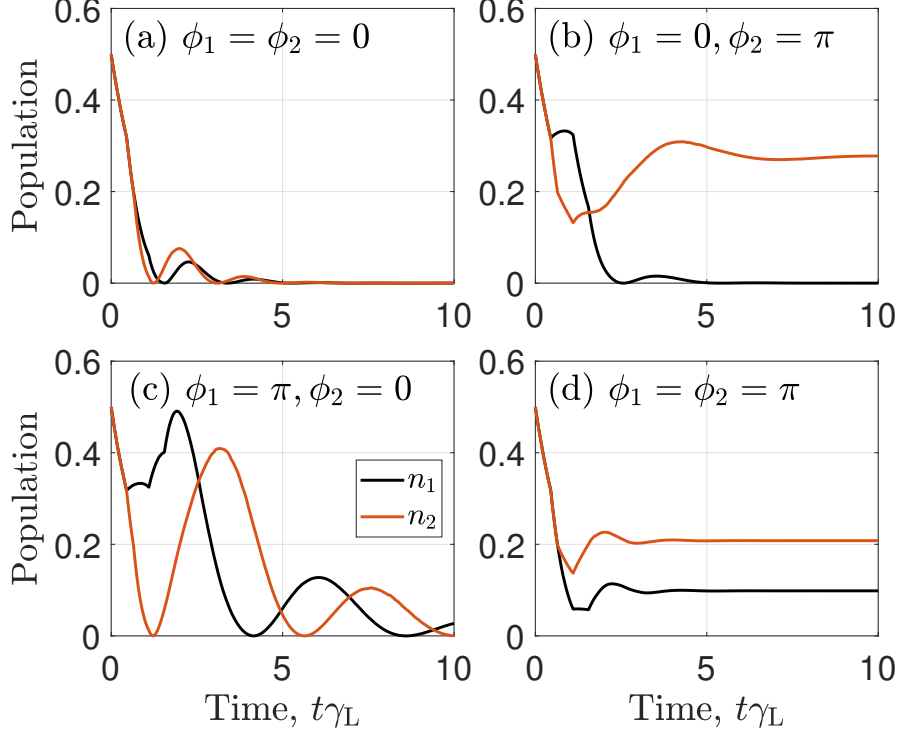


Figure 5.7: Population dynamics for the setup in 5.3(b) (a super-radiant state) when feedback is introduced for a variety of choices for ϕ_1 and ϕ_2 when $\tau_1 = 1.5\gamma_L^{-1}$ and $\tau_2 = 0.5\gamma_L^{-1}$. Each set of results is the average of 5000 QTs.

two photons in the loop. The system dynamics with and without feedback for two choices of phase change are presented in Fig. 5.8. For the system without feedback, when $\phi = 0$ in Fig. 5.8(a) the system evolves to a weakly populated entangled state. This state takes a relatively long time to reach its trapped state compared to the sub-radiant state presented earlier. This is due to the photon blockade set up by having two photons initially in the system. When the phase change is changed to $\phi = \pi$, the population follows simple decay out of the system as shown in Fig. 5.8(b). Feedback is then introduced to the system and we simulate the same phase changes when $\phi_1 = \phi_2$. There is a small change in the dynamics when feedback is introduced for $\phi_1 = \phi_2 = 0$ in Fig. 5.8(c), but ultimately the system still evolves to a weakly populated entangled state. Interestingly though, when $\phi_1 = \phi_2 = \pi$ in Fig. 5.8(d) the system no longer just decays but evolves to an entangled state with a larger

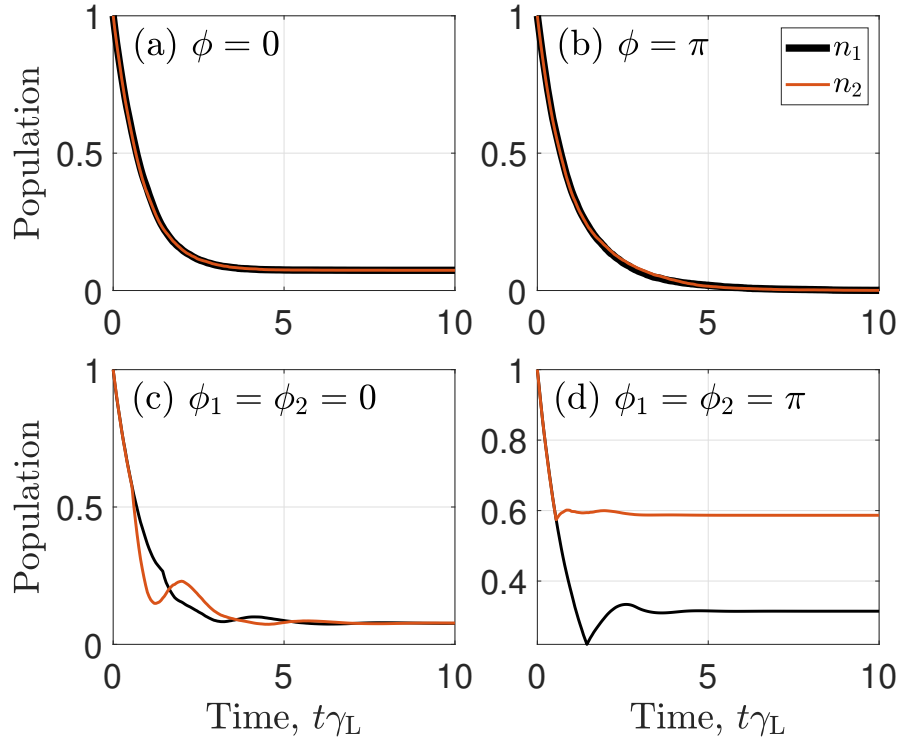


Figure 5.8: Population dynamics when the undriven system begins in the $\psi = |e, e\rangle$ state. The time delay between the two TLS's is $0.5\gamma_L^{-1}$ and when feedback is introduced in (c) and (d) the feedback loop has length $\tau_2 = 0.5\gamma_L^{-1}$. The dynamics are shown for (a) $\phi = 0$ and (b) $\phi = \pi$ for the system without feedback, and for (c) $\phi_1 = \phi_2 = 0$ and (d) $\phi_1 = \phi_2 = \pi$ for the system with feedback. Each simulation is an average of 5000 QTs.

population than either Figs. 5.8(a) or 5.8(c).

Chapter 6

Conclusions and Recommendations

6.1 Summary and Conclusions

In this thesis, we have developed two models for simulating cavity-QED systems with time-delayed coherent optical feedback. Results for both of these models, in a variety of parameter spaces, have been presented, verifying previous observations and demonstrating new results. In particular, we have used QT theory to develop a frequency mode representation (FMR) of feedback that was used to demonstrate how coherent feedback could be used to increase the photon lifetime of typical cavity-QED systems. We also presented nonlinear few-photon effects while in the “one photon in the loop” limit. In order to move beyond this approximation, the time discretized waveguide (TDW) model was developed in order to avoid the analytical pitfalls of the FMR model when moving to the two photon in the loop limit. Results comparing the one and two photon limits in the feedback loop were presented, as well as a comparison of the computational performance between the FMR and TDW models. The TDW model was then expanded to model two TLS’s separately coupled to a waveguide with feedback and initial results for this system were presented. Throughout this thesis, QT theory was harnessed as a platform to model non-Markovian dynamics. It also provided insight into the unique stochastic nature of individual trajectories, allowing for further analysis of how coherent feedback affects the systems of interest.

6.2 Suggestions for Future Work

After developing and testing these models, there are many potential avenues for future research modelling coherent feedback. With the relative flexibility of the TDW model, a variety of systems can be studied to quantify the system improvement with feedback present. For example, modelling the system response to various time-dependent pulses in the presence of feedback is of interest to identify possible improvements to single-photon sources or entangled-photon pairs. Finite-length pulses introduced down the waveguide are also of interest to model the reflection (and transmission) spectrum of various systems, and how it affects the photon statistics. Indeed this does not only apply to systems with coherent feedback. There is also interest in modelling the transmission and reflection spectra for long chains of cavity-QED systems. When these systems have a non-negligible photon travel time from start to end, non-Markovian effects are introduced which can be modelled with this technique.

Another potential area of research is to continue expanding and refining the model. For example, rarely do current approaches modelling coherent feedback allow for nonlinear dispersion in the waveguide. Indeed many models (both of ours included) rely on the assumption of linear dispersion to make the analytic simplifications that make the models tractable. It would be very interesting to expand the TDW model to allow for some nonlinear effects and see how the basic results of feedback, such as population trapping for the TLS, are affected by this change.

Lastly, it would be useful to the coherent feedback community at large to present a comparison between various feedback techniques. Matrix product states is one of the few other models able to move beyond the “one photon in the loop” approximation, so a computational comparison between it and the TDW model is of interest. Using matrix product states requires a significant amount of technical understanding to implement and so a computationally competitive, more intuitive approach, such as the TDW model would be helpful. Then, a detailed comparison between matrix products states and TDW models should prove to be extremely useful for the community.

Bibliography

- [1] A. V. Akimov, A. Mukherjee, C. L. Yu, D. E. Chang, A. S. Zibrov, P. R. Hemmer, H. Park, and M. D. Lukin, “Generation of single optical plasmons in metallic nanowires coupled to quantum dots”, [Nature](#) **450**, 402 (2007).
- [2] F. Albert, C. Hopfmann, S. Reitzenstein, C. Schneider, S. Höfling, L. Worschech, M. Kamp, W. Kinzel, A. Forchel, and I. Kanter, “Observing chaos for quantum-dot microlasers with external feedback”, [Nat. Commun.](#) **2**, 366 (2011).
- [3] F. Arute et al., “Quantum supremacy using a programmable superconducting processor”, [Nature](#) **574**, 505 (2019).
- [4] S. Ashhab, J. R. Johansson, and F. Nori, “Rabi oscillations in a qubit coupled to a quantum two-level system”, [New J. Phys.](#) **8**, 103 (2006).
- [5] A. Ashkin, “Acceleration and trapping of particles by radiation pressure”, [Phys. Rev. Lett.](#) **24**, 156 (1970).
- [6] A. Balouchi and K. Jacobs, “Coherent versus measurement-based feedback for controlling a single qubit”, [Quantum Science and Technology](#) **2**, 025001 (2017).
- [7] B. E. Billingham, J. C. Bergstrom, L. Dallin, M. de Jong, T. E. May, J. M. Vogt, and W. A. Wurtz, “Observation of superradiant synchrotron radiation in the terahertz region”, [Phys. Rev. ST Accel. Beams](#) **16**, 060702 (2013).
- [8] G. Binnig, C. F. Quate, and C. Gerber, “Atomic force microscope”, [Phys. Rev. Lett.](#) **56**, 930 (1986).
- [9] N. Bohr, “I. On the constitution of atoms and molecules”, [The London, Edinburgh, and Dublin Philosophical Magazine and Journal of Science](#) **26**, 1 (1913).
- [10] T. Brandes, “Feedback control of quantum transport”, [Phys. Rev. Lett.](#) **105**, 060602 (2010).
- [11] T. A. Brun, “A simple model of quantum trajectories”, [American Journal of Physics](#) **70**, 719 (2002).
- [12] J. C. Butcher, *Numerical methods for ordinary differential equations* (John Wiley & Sons, England, 2008).
- [13] A. Carmele, J. Kabuss, F. Schulze, S. Reitzenstein, and A. Knorr, “Single photon delayed feedback: a way to stabilize intrinsic quantum cavity electrodynamics”, [Phys. Rev. Lett.](#) **110**, 013601 (2013).

- [14] H. J. Carmichael, “Spectrum of squeezing and photocurrent shot noise: a normally ordered treatment”, *J. Opt. Soc. Am. B* **4**, 1588 (1987).
- [15] H. J. Carmichael, *Statistical Methods in Quantum Optics 1: master Equations and Fokker-Planck Equations* (Springer-Verlag, 2002) Chap. 1.
- [16] H. J. Carmichael, *Statistical Methods in Quantum Optics 2: non-classical fields* (Springer-Verlag, 2008).
- [17] M.-T. Cheng, J. Xu, and G. S. Agarwal, “Waveguide transport mediated by strong coupling with atoms”, *Physical Review A* **95**, 053807 (2017).
- [18] S. Chu, L. Hollberg, J. E. Bjorkholm, A. Cable, and A. Ashkin, “Three-dimensional viscous confinement and cooling of atoms by resonance radiation pressure”, *Physical Review Letters* **55**, 48 (1985).
- [19] J. Claudon, J. Bleuse, N. S. Malik, M. Bazin, P. Jaffrennou, N. Gregersen, C. Sauvan, P. Lalanne, and J.-M. Gérard, “A highly efficient single-photon source based on a quantum dot in a photonic nanowire”, *Nature Photonics* **4**, 174 (2010).
- [20] R. J. Coles, D. M. Price, J. E. Dixon, B. Royall, E. Clarke, P. Kok, M. S. Skolnick, A. M. Fox, and M. N. Makhonin, “Chirality of nanophotonic waveguide with embedded quantum emitter for unidirectional spin transfer”, *Nat. Commun.* **7**, 11183 (2016).
- [21] G. Conte and A. M. Perdon, “The disturbance decoupling problem for systems over a ring”, *SIAM J. Control Optim.* **33**, 750 (1995).
- [22] C. Cosentino and D. Bates, *Feedback control in systems biology* (CRC Press, 2011).
- [23] J. D. Cresser, “Micromaser cavity field spectrum by atomic beam measurements”, *Journal of Physics B: Atomic, Molecular and Optical Physics* **39**, S733 (2006).
- [24] G. Crowder, H. Carmichael, and S. Hughes, “Quantum trajectory theory of few-photon cavity-QED systems with a time-delayed coherent feedback”, *Phys. Rev. A* **101**, 023807 (2020).
- [25] J. Dalibard, Y. Castin, and K. Mølmer, “Wave-function approach to dissipative processes in quantum optics”, *Phys. Rev. Lett.* **68**, 580 (1992).
- [26] R. H. Dicke, “Coherence in spontaneous radiation processes”, *Phys. Rev.* **93**, 99 (1954).
- [27] F. Dinc and A. M. Brańczyk, “Non-Markovian super-superradiance in a linear chain of up to 100 qubits”, *Physical Review Research* **1**, 032042 (2019).
- [28] U. Dorner and P. Zoller, “Laser-driven atoms in half-cavities”, *Phys. Rev. A* **66**, 023816 (2002).

- [29] L. Droenner, N. L. Naumann, E. Schöll, A. Knorr, and A. Carmele, “Quantum pyragas control: selective control of individual photon probabilities”, *Phys. Rev. A* **99**, 023840 (2019).
- [30] L. Du, Y. Hu, Z.-W. Zhou, G.-C. Guo, and X. Zhou, “Integrated photonic qubit quantum computing on a superconducting chip”, *New Journal of Physics* **12**, 063015 (2010).
- [31] R. Dum, P. Zoller, and H. Ritsch, “Monte carlo simulation of the atomic master equation for spontaneous emission”, *Phys. Rev. A* **45**, 4879 (1992).
- [32] A. Einstein, “The Quantum Theory of Radiation”, *Physikalische Zeitschrift* **18** (1917).
- [33] G. F. Franklin, J. D. Powell, and A. Emami-Naeini, *Feedback control of dynamic systems* (Pearson, 2014).
- [34] A. Frees, S. Mehl, J. K. Gamble, M. Friesen, and S. N. Coppersmith, “Adiabatic two-qubit gates in capacitively coupled quantum dot hybrid qubits”, *npj Quantum Information* **5**, 1 (2019).
- [35] C. W. Gardiner and P. Zoller, *Quantum noise: a handbook of markovian and non-markovian quantum stochastic methods with applications to quantum optics* (Springer, Berlin, Germany, 2004).
- [36] B. M. Garraway, “The dicke model in quantum optics: dicke model revisited”, *Philosophical Transactions of the Royal Society A: Mathematical, Physical and Engineering Sciences* **369**, 1137 (2011).
- [37] G. G. Gillett, R. B. Dalton, B. P. Lanyon, M. P. Almeida, M. Barbieri, G. J. Pryde, J. L. O’Brien, K. J. Resch, S. D. Bartlett, and A. G. White, “Experimental feedback control of quantum systems using weak measurements”, *Phys. Rev. Lett.* **104**, 080503 (2010).
- [38] J. P. Gordon, H. J. Zeiger, and C. H. Townes, “Molecular microwave oscillator and new hyperfine structure in the microwave spectrum of NH_3 ”, *Phys. Rev.* **95**, 282 (1954).
- [39] P. Goy, J. M. Raimond, M. Gross, and S. Haroche, “Observation of cavity-enhanced single-atom spontaneous emission”, *Phys. Rev. Lett.* **50**, 1903 (1983).
- [40] A. L. Grimsmo, “Time-delayed quantum feedback control”, *Phys. Rev. Lett.* **115**, 060402 (2015).
- [41] P.-O. Guimond, M. Pletyukhov, H. Pichler, and P. Zoller, “Delayed coherent quantum feedback from a scattering theory and a matrix product state perspective”, *Quantum Science and Technology* **2**, 044012 (2017).
- [42] S. M. Hein, A. Carmele, and A. Knorr, “Creation and control of entanglement by time-delayed quantum-coherent feedback”, *Proc. SPIE* **9742**, 974216 (2016).

- [43] S. M. Hein, F. Schulze, A. Carmele, and A. Knorr, “Optical Feedback-Enhanced Photon Entanglement from a Biexciton Cascade”, [Physical Review Letters](#) **113**, 027401 (2014).
- [44] B. Hensen et al., “A silicon quantum-dot-coupled nuclear spin qubit”, en, [Nature Nanotechnology](#) **15**, 13 (2020).
- [45] D. R. Hjelm, A. R. Mickelson, and R. G. Beausoleil, “Semiconductor laser stabilization by external optical feedback”, [IEEE Journal of Quantum Electronics](#) **27**, 352 (1991).
- [46] T. B. Hoang, G. M. Akselrod, and M. H. Mikkelsen, “Ultrafast room-temperature single photon emission from quantum dots coupled to plasmonic nanocavities”, [Nano Letters](#) **16**, 270 (2016).
- [47] M. R. Hogan and H. Hogan, *A History of the Laser: 1960 - 2019*.
- [48] D. Huber, M. Reindl, S. F. Covre da Silva, C. Schimpf, J. Martín-Sánchez, H. Huang, G. Piredda, J. Edlinger, A. Rastelli, and R. Trotta, “Strain-tunable GaAs quantum dot: a nearly dephasing-free source of entangled photon pairs on demand”, [Phys. Rev. Lett.](#) **121**, 033902 (2018).
- [49] S. Hughes, “Coupled-cavity QED using planar photonic crystals”, [Phys. Rev. Lett.](#) **98**, 083603 (2007).
- [50] S. Hughes, “Modified spontaneous emission and qubit entanglement from dipole-coupled quantum dots in a photonic crystal nanocavity”, [Phys. Rev. Lett.](#) **94**, 227402 (2005).
- [51] S. Hughes and H. J. Carmichael, “Stationary inversion of a two level system coupled to an off-resonant cavity with strong dissipation”, [Phys. Rev. Lett.](#) **107**, 193601 (2011).
- [52] E. T. Jaynes and F. W. Cummings, “Comparison of quantum and semiclassical radiation theories with application to the beam maser”, [Proc. IEEE](#) **51**, 89 (1963).
- [53] J. Johansson, P. Nation, and F. Nori, “Qutip 2: a python framework for the dynamics of open quantum systems”, [Computer Physics Communications](#) **184**, 1234 (2013).
- [54] J. Kabuss, D. O. Krimer, S. Rotter, K. Stannigel, A. Knorr, and A. Carmele, “Analytical study of quantum-feedback-enhanced Rabi oscillations”, [Phys. Rev. A](#) **92**, 053801 (2015).
- [55] Y. Kaluzny, P. Goy, M. Gross, J. M. Raimond, and S. Haroche, “Observation of self-induced Rabi oscillations in two-level atoms excited inside a resonant cavity: the ringing regime of superradiance”, [Phys. Rev. Lett.](#) **51**, 1175 (1983).
- [56] E. Knill, R. Laflamme, and G. J. Milburn, “A scheme for efficient quantum computation with linear optics”, [Nature](#) **409**, 46 (2001).

- [57] V. B. Kolmanovskii, “On the liapunov-krasovskii functionals for stability analysis of linear delay systems”, *International Journal of Control* **72**, 374 (1999).
- [58] U. Koren, “Waveguide based photonic integrated circuits”, in *Optoelectronic integration: physics, technology and applications*, edited by O. Wada (Springer US, Boston, MA, 1994), pp. 233–272.
- [59] M. Kraft, S. M. Hein, J. Lehnert, E. Schöll, S. Hughes, and A. Knorr, “Time-delayed quantum coherent pyragas feedback control of photon squeezing in a degenerate parametric oscillator”, *Phys. Rev. A* **94**, 023806 (2016).
- [60] A. Kubanek, M. Koch, C. Sames, A. Ourjoumtsev, P. W. H. Pinkse, K. Murr, and G. Rempe, “Photon-by-photon feedback control of a single-atom trajectory”, *Nature* **462**, 898 (2009).
- [61] W. Kutta, “Bietrag zur näherungsweise integration totaler differentialgleichungen”, de, *Zeitschrift Für Mathematik Und Physik*, 435 (1901).
- [62] S. Lloyd, “Coherent quantum feedback”, *Phys. Rev. A* **62**, 022108 (2000).
- [63] P. Lodahl, S. Mahmoodian, and S. Stobbe, “Interfacing single photons and single quantum dots with photonic nanostructures”, *Rev. Mod. Phys.* **87**, 347 (2015).
- [64] P. Lodahl, S. Mahmoodian, S. Stobbe, A. Rauschenbeutel, P. Schneeweiss, J. Volz, H. Pichler, and P. Zoller, “Chiral quantum optics”, *Nature* **541**, 473 (2017).
- [65] Y. Lu, N. L. Naumann, J. Cerrillo, Q. Zhao, A. Knorr, and A. Carmele, “Intensified antibunching via feedback-induced quantum interference”, *Phys. Rev. A* **95**, 063840 (2017).
- [66] T. H. Maiman, “Stimulated Optical Radiation in Ruby”, *Nature* **187**, 493 (1960).
- [67] T. Maka, D. N. Chigrin, S. G. Romanov, and C. M. Sotomayor Torres, “Three dimensional photonic crystals in the visible regime”, *Progress in Electromagnetics Research* **41**, 307 (2003).
- [68] D. Meschede, H. Walther, and G. Müller, “One-atom maser”, *Phys. Rev. Lett.* **54**, 551 (1985).
- [69] G. Milburn and D. Walls, “Production of squeezed states in a degenerate parametric amplifier”, *Optics Communications* **39**, 401 (1981).
- [70] D. A. B. Miller, “Quantum mechanics for scientists and engineers”, in (Cambridge University Press, 2008) Chap. 14.
- [71] Z. K. Mineev, S. O. Mundhada, S. Shankar, P. Reinhold, R. Gutiérrez-Jáuregui, R. J. Schoelkopf, M. Mirrahimi, H. J. Carmichael, and M. H. Devoret, “To catch and reverse a quantum jump mid-flight”, *Nature* **570**, 200 (2019).

- [72] M. Mirhosseini, E. Kim, X. Zhang, A. Sipahigil, P. B. Dieterle, A. J. Keller, A. Asenjo-Garcia, D. E. Chang, and O. Painter, “Cavity quantum electrodynamics with atom-like mirrors”, *Nature* **569**, 692 (2019).
- [73] N. Mohammadi Estakhri, B. Edwards, and N. Engheta, “Inverse-designed metastructures that solve equations”, *Science* **363**, 1333 (2019).
- [74] K. Mølmer, Y. Castin, and J. Dalibard, “Monte Carlo wave-function method in quantum optics”, *J. Opt. Soc. Am. B* **10**, 524 (1993).
- [75] L. N. Naumann, L. Droenner, S. M. Hein, A. Carmele, A. Knorr, and J. Kabuss, “Feedback control of optomechanical systems”, *Proc. SPIE* **9742**, 974216 (2016).
- [76] N. L. Naumann, S. M. Hein, M. Kraft, A. Knorr, and A. Carmele, “Feedback control of photon statistics”, *Proc. SPIE* **10098**, 100980N (2017).
- [77] N. Német, A. Carmele, S. Parkins, and A. Knorr, “Comparison between continuous- and discrete-mode coherent feedback for the jaynes-cummings model”, *Phys. Rev. A* **100**, 023805 (2019).
- [78] N. Német and S. Parkins, “Enhanced optical squeezing from a degenerate parametric amplifier via time-delayed coherent feedback”, *Phys. Rev. A* **94**, 023809 (2016).
- [79] M. Nomura, N. Kumagai, S. Iwamoto, Y. Ota, and Y. Arakawa, “Laser oscillation in a strongly coupled single-quantum-dot-nanocavity system”, *Nat. Phys.* **6**, 279 (2010).
- [80] K. C. Nowack, M. Shafiei, M. Laforest, G. E. D. K. Prawiroatmodjo, L. R. Schreiber, C. Reichl, W. Wegscheider, and L. M. K. Vandersypen, “Single-shot correlations and two-qubit gate of solid-state spins”, *Science* **333**, 1269 (2011).
- [81] A. W. Olbrot, “Algebraic criteria of controllability to zero function for linear constant time-lag systems”, *Control and Cybernetics* **2**, 59 (1984).
- [82] A. Orieux, M. A. M. Versteegh, K. D. Jöns, and S. Ducci, “Semiconductor devices for entangled photon pair generation: a review”, *Reports on Progress in Physics* **80**, 076001 (2017).
- [83] H. Pichler and P. Zoller, “Photonic circuits with time delays and quantum feedback”, *Phys. Rev. Lett.* **116**, 093601 (2016).
- [84] M. Planck, “On the Theory of the Energy Distribution Law of the Normal Spectrum”, *Verh. Dtsch. Phys. Ges.* **2** (1900).
- [85] M. B. Plenio and P. L. Knight, “The quantum-jump approach to dissipative dynamics in quantum optics”, *Rev. Mod. Phys.* **70**, 101 (1998).
- [86] E. M. Purcell, “Spontaneous emission probabilities at radio frequencies”, *Proc. Phys. Soc. America* **69**, 681 (1946).

- [87] J.-P. Richard, “Time-delay systems: an overview of some recent advances and open problems”, *Automatica* **39**, 1667 (2003).
- [88] A. Rivas and S. A. Huelga, “Open quantum systems. an introduction”, in (SpringerBriefs in Physics, 2012).
- [89] C. Runge, “Ueber die numerische Auflösung von Differentialgleichungen”, de, *Mathematische Annalen* **46**, 167 (1895).
- [90] L. Sapienza, H. Thyrestrup, S. Stobbe, P. D. Garcia, S. Smolka, and P. Lodahl, “Cavity quantum electrodynamics with anderson-localized modes”, *Science* **327**, 1352 (2010).
- [91] N. Shammah, N. Lambert, F. Nori, and S. De Liberato, “Superradiance with local phase-breaking effects”, *Phys. Rev. A* **96**, 023863 (2017).
- [92] K. Sinha, P. Meystre, E. A. Goldschmidt, F. K. Fatemi, S. L. Rolston, and P. Solano, “Non-Markovian Collective Emission from Macroscopically Separated Emitters”, *Physical Review Letters* **124**, 043603 (2020).
- [93] N. Somaschi et al., “Near-optimal single-photon sources in the solid state”, en, *Nature Photonics* **10**, 340 (2016).
- [94] A. Streltsov, G. Adesso, and M. B. Plenio, “Colloquium: quantum coherence as a resource”, *Rev. Mod. Phys.* **89**, 041003 (2017).
- [95] S. M. Tan, “A computational toolbox for quantum and atomic optics”, *Journal of Optics B: Quantum and Semiclassical Optics* **1**, 424 (1999).
- [96] L. Tian and H. J. Carmichael, “Quantum trajectory simulations of two-state behavior in an optical cavity containing one atom”, *Phys. Rev. A* **46**, R6801 (1992).
- [97] T. Tufarelli, F. Ciccarello, and M. S. Kim, “Dynamics of spontaneous emission in a single-end photonic waveguide”, *Phys. Rev. A* **87**, 013820 (2013).
- [98] P. Türschmann, H. L. Jeannic, S. F. Simonsen, H. R. Haakh, S. Götzinger, V. Sandoghdar, P. Lodahl, and N. Rotenberg, “Coherent nonlinear optics of quantum emitters in nanophotonic waveguides”, *Nanophotonics* **8**, 1641 (2019).
- [99] S. M. Ulrich, S. Ates, S. Reitzenstein, A. Löffler, A. Forchel, and P. Michler, “Dephasing of triplet-sideband optical emission of a resonantly driven InAs/GaAs quantum dot inside a microcavity”, *Phys. Rev. Lett.* **106**, 247402 (2011).
- [100] G. S. Virk, “Runge kutta method for delay-differential systems”, *IEE Proceedings D - Control Theory and Applications* **132**, 119 (1985).
- [101] S. J. Whalen, “Collision model for non-markovian quantum trajectories”, *Phys. Rev. A* **100**, 052113 (2019).

-
- [102] S. J. Whalen, A. L. Grimsmo, and H. J. Carmichael, “Open quantum systems with delayed coherent feedback”, [Quantum Sci. Technol. **2**, 044008 \(2017\)](#).
- [103] S. Whalen, “Open quantum systems with time-delayed interactions”, Thesis (ResearchSpace@Auckland, 2015).
- [104] H. M. Wiseman and G. J. Milburn, *Quantum Measurement and Control* (Cambridge University Press, Oxford, 2002), p. 231.
- [105] G. Xiu, A. F. Kockum, A. Miranowicz, Y.-X. Liu, and F. Nori, “Microwave photonics with superconducting quantum circuits”, [Phys. Rep. **718-719**, 1 \(2017\)](#).
- [106] P. Yao and S. Hughes, “Macroscopic entanglement and violation of Bell’s inequalities between two spatially separated quantum dots in a planar photonic crystal system”, [Opt. Express **17**, 11505 \(2009\)](#).
- [107] J. Yin et al., “Satellite-based entanglement distribution over 1200 kilometers”, [Science **356**, 1140 \(2017\)](#).
- [108] A. B. Young, A. C. T. Thijssen, D. M. Beggs, P. Androvitsaneas, L. Kuipers, J. G. Rarity, S. Hughes, and R. Oulton, “Polarization engineering in photonic crystal waveguides for spin-photon entanglers”, [Phys. Rev. Lett. **115**, 153901 \(2015\)](#).
- [109] I. E. Zadeh, A. W. Elshaari, K. D. Jöns, A. Fognini, D. Dalacu, P. J. Poole, M. E. Reimer, and V. Zwiller, “Deterministic integration of single photon sources in silicon based photonic circuits”, [Nano Letters **16**, 2289 \(2016\)](#).
- [110] X. Zhang, H.-O. Li, K. Wang, G. Cao, M. Xiao, and G.-P. Guo, “Qubits based on semiconductor quantum dots”, [Chinese Physics B **27**, 020305 \(2018\)](#).
- [111] Y. P. Zhong et al., “Violating Bell’s inequality with remotely connected superconducting qubits”, [Nature Physics **15**, 741 \(2019\)](#).